

# Spatiotemporal Besov Priors for Bayesian Inverse Problems

Shiwei Lan<sup>\*1</sup>, Mirjeta Pasha<sup>2</sup>, Shuyi Li<sup>1</sup>, and Weining Shen<sup>3</sup>

<sup>1</sup>*School of Mathematical & Statistical Sciences, Arizona State University, 901 S Palm Walk, Tempe, AZ 85287*

<sup>2</sup>*Laboratory for Decision and Information System, Massachusetts Institute of Technology, 77 Massachusetts Avenue, Cambridge, MA 02139*

<sup>3</sup>*Department of Statistics, University of California - Irvine, Donald Bren Hall, Irvine, CA 92697*

## Abstract

Fast development in science and technology has driven the need for proper statistical tools to capture special data features such as abrupt changes or sharp contrast. Many inverse problems in data science require spatiotemporal solutions derived from a sequence of time-dependent objects with these spatial features, e.g. dynamic reconstruction of computerized tomography (CT) images with edges. Conventional methods based on Gaussian processes (GP) often fall short in providing satisfactory solutions since they tend to offer over-smooth priors. Recently, the Besov process (BP), defined by wavelet expansions with random coefficients, has emerged as a more suitable prior for Bayesian inverse problems of this nature. While BP excels in handling spatial inhomogeneity, it does not automatically incorporate temporal correlation inherited in the dynamically changing objects. In this paper, we generalize BP to a novel spatiotemporal Besov process (STBP) by replacing the random coefficients in the series expansion with stochastic time functions as Q-exponential process (Q-EP) which governs the temporal correlation structure. We thoroughly investigate the mathematical and statistical properties of STBP. A white-noise representation of STBP is also proposed to facilitate the inference. Simulations, two limited-angle CT reconstruction examples and a highly non-linear inverse problem involving Navier-Stokes equation are used to demonstrate the advantage of the proposed STBP in preserving spatial features while accounting for temporal changes compared with the classic STGP and a time-uncorrelated approach.

**Keywords:** Spatiotemporal functional data analysis, Inhomogeneous data,  $L_q$  regularization, Q-Exponential process, Edge-preserving priors

## 1 Introduction

Many modern science and engineering applications are presented as inverse problems whose main goal is to recover parameters of interest from observed data. These data may possess inhomogeneity in the sense that certain portions differs from others significantly. For example, some medical images exhibit sharp edges where properties undergo dramatic changes. Furthermore, these complex datasets may be spatiotemporal, with solutions extending across both space and time. One of the key challenges in these types of inverse problems is to

---

<sup>\*</sup>slan@asu.edu

effectively capture the distinctive characteristics of high-dimensional (potentially infinite-dimensional) objects using limited data. Surging need has been posed for statistical methodology to appropriately impose regularization or fill in prior information for these ill-posed inverse problems in order to construct meaningful solutions [17].

In the literature of optimization, deterministic regularization methods for inverse problems date back to 1943 with the seminal work by Tikhonov [69], followed by Ivanov [32]. A regularization term reflecting properties of the target solution is typically added to a pre-determined energy function that depends on the forward model and the statistical assumptions of the observational noise. More recent methods and algorithms developed in this class have been applied in signal and image processing [36], geophysics and seismic monitoring [66], tomography reconstruction [56], etc. In statistics, there is also a long history of developing models with penalty based on the prior knowledge of unknown parameters including but not limited to Bayesian Lasso [55, 12] and bridge [59], spike-and-slab [52, 49, 31, 3], and horseshoe [11, 57] priors. If we view the Bayesian regression model as an inverse problem, there is a natural analogy between the likelihood (prior) and the energy (regularization) function.

In nonparametric modeling, GP [61] has been widely used as an  $L_2$  penalty (negative log-density as a quadratic form) or a prior on the function space. However, despite the flexibility, random functions generated from GPs often exhibit excessive smoothing, which is not ideal for modeling inhomogeneous objects such as images with sharp edges (See Figure 10 for illustration). To address this issue, researchers have proposed a class of  $L_1$  penalty based priors including Laplace random field [58, 39, 2] and Besov process (BP) [42, 14, 33, 15]. There are also many heavy-tailed priors based on Markov random fields such as Cauchy [50, 68] and total variation (TV) [45, 78], and data-informed priors based on level set functions [16, 30] proposed for handling inhomogeneity. These approaches have found significant applications in spatial modeling [58], signal processing [39], imaging analysis [56], and inverse problems [14].

Most of these sparsity-promoting and edge-preserving priors in the literature work well in characterizing spatial inhomogeneity, but few of them are tailored to specially address spatiotemporal targets and their temporal correlations. In this paper, we focus on BP proposed by [42] for imaging analysis and generalize it to the spatiotemporal domain. Historically, [43] discovered that the TV prior degenerates to a Gaussian prior as the discretization mesh becomes denser and loses the edge-preserving properties in high-dimensional applications. Therefore, [42] proposed the BP prior defined using wavelet basis and random coefficients following a (univariate)  $q$ -exponential distribution and proved its discretization-invariant property. Recently, [47] introduced a stochastic process based on a consistent multivariate generalization of the  $q$ -exponential distribution, hence named  $Q$ -exponential process (Q-EP). The Q-EP can be viewed as an explicit probabilistic definition of BP with direct control on the correlation structure and tractable prediction formula. In this paper, we propose a novel *spatiotemporal Besov process (STBP)* by replacing the (univariate)  $q$ -exponential random coefficients in the series definition of BP with stochastic time functions as Q-EP. The proposed STBP offers a flexible prior in modeling functional data with spatial features while controlling the temporal correlations explicitly through a covariance kernel. Similarly as BP, STBP also includes spatiotemporal GP (STGP) as a special case for  $q = 2$  (See Figure 1 for their relationship). Since our motivation is to model inhomogeneous data with priors imposing sharp  $L_q$  regularization, we focus on  $1 \leq q \leq 2$  in this paper (See Figure 10 for the regularization effect of parameter  $q$ ). To the best of our knowledge, this is by far the first spatiotemporal generalization of BP.

To justify STBP as a working prior for spatiotemporal inverse problems, Bayes theorem in this setting is re-examined based on [14, 15]. With proper assumptions on the likelihood,

the posterior contraction theorems for Bayesian inverse models with STBP priors are established based on [21, 72, 1]. Posterior contraction properties with Gaussian priors have been extensively studied by [72–74, 22] for regression and classification, density estimation, white noise models, and Bayesian linear inverse problems [37] and nonlinear inverse problems [76]. [23] also studied the posterior contraction of density estimation for a class of  $L^r$ -metrics ( $1 \leq r \leq \infty$ ) based priors including GP, wavelet series and normal mixture. [1] studied the posterior contraction theorems for a re-branded BP named  $p$ -exponential process (which only differs from BP by a constant in the univariate  $q$ -exponential distribution) for density estimation and white noise model. Other works on the posterior contraction of Besov-type priors include [62, 20, 24]. Compared with the existing literature, our theoretic results are novel in terms of: 1) generalization to spatiotemporal models for inverse problems; 2) simplified contraction rates given in a class of Besov-type spaces contained in  $L^q$  spaces.

To facilitate Bayesian inference for models with STBP priors, we introduce a novel white-noise representation [13] of the random function drawn from STBP and take advantage of the dimension-independent MCMC algorithms [8] for efficient implementation. The numerical advantages of the proposed STBP over STGP have been supported by multiple experiments in dynamic CT reconstruction and inverse problems constrained by highly nonlinear differential equation. Our proposed work on STBP has multiple contributions to the literature of spatiotemporal inverse problems:

1. It generalizes BP to the spatiotemporal domain to simultaneously model the spatial inhomogeneity and the temporal correlations.
2. It provides theoretic characterization on the posterior contraction in the infinite data limit, justifying its validity as a nonparametric learning tool.
3. It demonstrates utility in dynamic CT reconstruction and indicates potential impact on medical imaging analysis.

The rest of the paper is organized as follows. Section 2 provides a background review on the Bayesian inverse problems and BP used as a flexible edge-preserving prior. Section 3 introduces Q-EP as random coefficient functions on the time domain. We then formally define STBP and study its theoretic properties in Section 4. In Section 5 we describe a white-noise representation of STBP that facilitates the inference for models with STBP prior. In Section 6 we demonstrate the advantage of the proposed STBP prior in retaining spatial features and capturing temporal correlations for the spatiotemporal inverse problems using a simulated regression, two dynamic CT reconstruction examples and a nonlinear inverse problem involving Navier-Stokes equation. Finally we conclude with some discussion on future research in Section 7.

## 2 Background on Besov priors for Bayesian Inverse Problems

The Bayesian approach to inverse problems [15] has recently gained increasing popularity because it provides a natural framework for model calibration and uncertainty quantification (UQ) as well. In this section, we review some background about the set up of Bayesian inverse problems and the definition of BP as a flexible prior for modeling objects with spatial features.

### 2.1 Bayesian Inverse Problems

We consider the inverse problem of recovering an unknown parameter  $u \in \mathbb{X}$  from a noisy observation  $y \in \mathbb{Y}$  based on the following Bayesian model

$$\begin{aligned} y &= \mathcal{G}(u) + \eta, & \eta &\sim \mathbb{Q}_0, \\ u &\sim \Pi, \end{aligned} \tag{1}$$

where both  $\mathbb{X}$  and  $\mathbb{Y}$  are separable Banach spaces,  $\mathcal{G} : \mathbb{X} \rightarrow \mathbb{Y}$  is a forward mapping from the parameter space  $\mathbb{X}$  to the data space  $\mathbb{Y}$ , and  $\eta \in \mathbb{Y}$  denotes the random noise whose distribution  $\mathbb{Q}_0$  is independent from the prior  $\Pi$ . We assume the conditional  $y|u$  is distributed according to the measure  $\mathbb{Q}_u \ll \mathbb{Q}_0$  for  $u$   $\Pi$ -almost surely (a.s.), and hence define the potential (negative log-likelihood) function  $\Phi : \mathbb{X} \times \mathbb{Y} \rightarrow \mathbb{R}$ :

$$\frac{d\mathbb{Q}_u}{d\mathbb{Q}_0}(y) = \exp(-\Phi(u; y)). \quad (2)$$

The objective of Bayesian inverse problem is to seek the posterior solution of  $u|y$  whose distribution, denoted as  $\Pi^y$ , according to the Bayes' theorem [67, 15], satisfies the requirement that if  $0 < Z := \int_{\mathbb{X}} \exp(-\Phi(u; y))\Pi(du) < +\infty$  for  $y$   $\mathbb{Q}_0$ -a.s., then

$$\frac{d\Pi^y}{d\Pi}(u) = \frac{1}{Z} \exp(-\Phi(u; y)). \quad (3)$$

The forward operator  $\mathcal{G}$  could be linear or nonlinear, possibly encoding physical information represented by a system of ordinary or partial differential equations (ODE/PDE). The resulted posterior  $\Pi^y$  is usually non-Gaussian with a complicated geometric structure even if a Gaussian prior  $\Pi = \mathcal{GP}(0, \mathcal{C})$  is adopted.

When there are sparse data but the targets are high-dimensional, the inverse problems are ill-posed. Proper prior information is crucial to induce well-defined solutions [17]. In a plethora of applications such as image deblurring [63] and CT reconstruction [56], methods are developed with priors that are sparse [9], and/or have sparse gradients [42, 15] to preserve the sharp edge features. In this work we focus on Besov-type priors [42].

## 2.2 Besov Process

Let  $\mathcal{X} \subset \mathbb{R}^d$  be the spatial domain, e.g.  $d$ -dimensional torus,  $\mathcal{X} = \mathbb{T}^d = (0, 1]^d$  for  $d \leq 3$ . Consider a separable Banach space  $(\mathbb{X}, \|\cdot\|)$  with a Schauder basis  $\{\phi_\ell\}_{\ell=1}^\infty$ , e.g. square integrable function  $L^2(\mathcal{X}) := \{u : \mathcal{X} \rightarrow \mathbb{R} \mid \int_{\mathcal{X}} |u(\mathbf{x})|^2 d\mathbf{x} < \infty\}$  with Fourier basis. Any function  $u \in \mathbb{X}$  can then be represented by the following series:

$$u(\mathbf{x}) = \sum_{\ell=1}^{\infty} u_\ell \phi_\ell(\mathbf{x}) \quad (4)$$

Based on (4), we consider a norm  $\|\cdot\|_{s,q}$  defined with a smoothness parameter  $s > 0$  and an integrability parameter  $q \geq 1$  [42, 14]:

$$\|u(\cdot)\|_{s,q} = \left( \sum_{\ell=1}^{\infty} \ell^{\tau_q(s)q} |u_\ell|^q \right)^{\frac{1}{q}}, \quad \tau_q(s) = \frac{s}{d} + \frac{1}{2} - \frac{1}{q}. \quad (5)$$

We define the Banach space  $B^{s,q}(\mathcal{X}) := \{u : \mathcal{X} \rightarrow \mathbb{R} \mid \|u(\cdot)\|_{s,q} < \infty\}$ . If  $\{\phi_\ell\}_{\ell=1}^\infty$  is an  $r$ -regular wavelet basis for  $r > s$ , then  $B^{s,q}(\mathcal{X})$  becomes the Besov space  $B_{qq}^s$  [70]. In particular, if  $q = 2$  and  $\{\phi_\ell\}_{\ell=1}^\infty$  form the Fourier basis, then  $B^{s,2}(\mathcal{X})$  reduces to the Sobolev space  $H^s(\mathcal{X})$  with the special case  $B^{0,2}(\mathcal{X}) = L^2(\mathcal{X})$  assuming  $s = 0$ .

For a given basis  $\{\phi_\ell\}_{\ell=1}^\infty$ , based on the the series expansion (4), there is a one-to-one correspondence between the  $B^{s,q}(\mathcal{X})$  function  $u(\cdot)$  and the infinite sequence  $u := \{u_\ell\}_{\ell=1}^\infty$  in a weighted  $\ell^q$  space,  $\ell^{q,\tau} := \{u \in \mathbb{R}^\infty \mid \|u\|_{\tau,q} = (\sum_{\ell=1}^{\infty} \ell^{\tau q} |u_\ell|^q)^{\frac{1}{q}} < \infty\}$ , which reduces to the regular  $\ell^q$  space when  $\tau = 0$ . Hence  $\|u(\cdot)\|_{s,q} = \|u\|_{\tau_q(s),q}$ . In the following, we will use  $u$  to refer to both notations under such correspondence when there is no confusion.

Now we define *Besov process (BP)*  $u(\cdot)$  in (4) by randomizing the coefficients  $\{u_\ell\}_{\ell=1}^\infty$ . More specifically, we set for  $\ell \in \mathbb{N}$

$$u_\ell := \gamma_\ell \xi_\ell, \quad \gamma_\ell = \kappa^{-\frac{1}{q}} \ell^{-\tau_q(s)}, \quad \xi_\ell \stackrel{i.i.d.}{\sim} \pi_\xi(\cdot) \propto \exp\left(-\frac{1}{2} |\cdot|^q\right), \quad (6)$$

where  $\kappa > 0$  is a scaling factor, and  $\pi_\xi$  denotes the probability density function of the  $q$ -*exponential distribution* [14, 15]. Though not spelled out, such  $q$ -exponential distribution is actually a special case of the following exponential power (EP, a.k.a generalized normal) distribution  $\text{EP}(\mu, \sigma, q)$  with  $\mu = 0$ ,  $\sigma = 1$ :

$$p(\xi|\mu, \sigma, q) = \frac{q}{2^{1+1/q} \sigma \Gamma(1/q)} \exp\left\{-\frac{1}{2} \left|\frac{\xi - \mu}{\sigma}\right|^q\right\}. \quad (7)$$

When  $q = 2$ , this is just a normal distribution  $\mathcal{N}(\mu, \sigma^2)$ . When  $q = 1$ , it becomes a Laplace distribution  $L(\mu, b)$  with  $\sigma = 2^{-1/q} b$ .

Denote infinite sequences  $\gamma = \{\gamma_\ell\}_{\ell=1}^\infty$  and  $\xi = \{\xi_\ell\}_{\ell=1}^\infty$ . Then  $\xi$  is a random element of the probability space  $(\Omega, \mathcal{B}(\Omega), \mathbb{P})$  with  $\Omega = \mathbb{R}^\infty$ , product  $\sigma$ -algebra  $\mathcal{B}(\Omega)$  and probability measure  $\mathbb{P}$  defined by extending the finite product of  $\pi_\xi$  to the infinite product by the Kolmogorov extension theorem [c.f. Theorem 29 in section A.2.1 of 15]. Then we define *Besov measure* as the pushforward of  $\mathbb{P}$  as follows.

**Definition 1** (Besov Measure). *Let  $\mathbb{P}$  be the measure of random sequences  $\xi \in \Omega$ . Suppose we have the following map*

$$f_\gamma : \Omega \rightarrow B^{s,q}(\mathcal{X}), \quad \xi \mapsto u = \sum_{\ell=1}^{\infty} u_\ell \phi_\ell = \sum_{\ell=1}^{\infty} \gamma_\ell \xi_\ell \phi_\ell, \quad (8)$$

where  $\gamma_\ell$  and  $\xi_\ell$  are defined in (6). Then the pushforward  $f_\gamma^\# \mathbb{P}$  is Besov measure on  $B^{s,q}(\mathcal{X})$ , denoted as  $\mathcal{B}(\kappa, B^{s,q}(\mathcal{X}))$ , and we say BP  $u$  follows the Besov measure, i.e.,  $u \sim \mathcal{B}(\kappa, B^{s,q}(\mathcal{X}))$ .

**Remark 1.** *If  $q = 2$  and  $\{\phi_\ell\}_{\ell=1}^\infty$  is either a wavelet or Fourier basis, we obtain a Gaussian measure with the Cameron-Martin space  $B_{22}^{s,2}$  [70], which is the Hilbert space  $H^s(\mathcal{X})$ . Indeed, we have (8) reduced to a zero mean Gaussian random element based on Karhunen-Lovève representation (refer to Figure 1):*

$$u(\mathbf{x}) = \kappa^{-\frac{1}{2}} \sum_{\ell=1}^{\infty} \ell^{-\frac{s}{d}} \xi_\ell \phi_\ell(\mathbf{x}), \quad \xi_\ell \stackrel{i.i.d.}{\sim} \mathcal{N}(0, 1).$$

Define  $\|\xi\|_q := (\sum_{\ell=1}^{\infty} |\xi_\ell|^q)^{\frac{1}{q}}$  for  $\xi \in \Omega$ . Then we have  $\|u\|_{s,q} = \kappa^{-\frac{1}{q}} \|\xi\|_q$ . The following formal Lebesgue density can be made rigorous by Fernique theorem [14] (Refer to Theorem 4.2):

$$\mathbb{P}(d\xi) = p(\xi) d\xi, \quad p(\xi) = \prod_{\ell=1}^{\infty} \pi_\xi(\xi_\ell) \propto \exp\left\{-\frac{1}{2} \|\xi\|_q^q\right\} = \exp\left\{-\frac{\kappa}{2} \|u\|_{s,q}^q\right\}. \quad (9)$$

When used in the optimization to obtain a parameter estimate, the logarithm of Besov prior density (9) serves as an  $L_q$  regularization term. Larger regularization parameter ( $q > 0$ ) promotes smoother solutions, as demonstrated in a simulated regression example in Figure 10. In practice, Besov prior is often adopted for  $q = 1$  to preserve edges in imaging analysis.

Define the Banach space of  $q$ -integrable functions in  $(\Omega, \mathcal{B}(\Omega), \mathbb{P})$  as  $L_{\mathbb{P}}^q(\Omega; B^{s,q}(\mathcal{X})) = \{u : \mathcal{X} \times \Omega \rightarrow \mathbb{R} | \mathbb{E}(\|u\|_{s,q}^q) < \infty\}$ . We notice that for  $u \sim \mathcal{B}(\kappa, B^{s,q}(\mathcal{X}))$ ,  $u \notin L_{\mathbb{P}}^q(\Omega; B^{s,q}(\mathcal{X}))$  because  $\mathbb{E}(\|u\|_{s,q}^q) = \kappa^{-1} \mathbb{E}(\|\xi\|_q^q) = \infty$  due to the iid assumption on  $\xi$  in (6). However, the following theorem states that Besov random draw as in (8) has limit in a proper  $q$ -integrable function space [Theorem 4 of 15] and hence in a subset of  $L^q(\mathcal{X})$  in probability (almost surely).

**Theorem 2.1.** *If  $u \sim \mathcal{B}(\kappa, B^{s,q}(\mathcal{X}))$  as in (8), then  $u \in L_{\mathbb{P}}^q(\Omega; B^{s',q}(\mathcal{X}))$  for all  $s' < s - \frac{d}{q}$ .*

*Proof.* See Appendix A.1. □

**Remark 2.** *This theorem implies that for any random draw from  $\mathcal{B}(\kappa, B^{s,q}(\mathcal{X}))$ , we need to consider its  $q$ -integrability in a larger ambient space  $B^{s',q}(\mathcal{X})$  for some  $s' < s - \frac{d}{q}$  ( $B^{s,q}(\mathcal{X}) \subset B^{s',q}(\mathcal{X})$ , refer to Proposition 4.1).*

Next, we generalize the series representation of a Besov random function (8) to a representation for STBP by replacing the random variable  $\xi_\ell$  with a stochastic process  $\xi_\ell(\cdot)$  on the temporal domain  $\mathcal{T} \subset \mathbb{R}_+$ . For this purpose, in the following we will first introduce a properly defined process Q-EP for  $\xi_\ell(\cdot)$  that generalizes the  $q$ -exponential random variable  $\xi_\ell$  and has the capability of capturing the temporal dependence in data.

### 3 Q-exponential Process Valued Random Coefficients

#### 3.1 Multivariate Generalization of Q-exponential Distribution

To generalize aforementioned  $q$ -exponential (6) (or univariate EP (7)) random variable,  $\xi_\ell$ , to a multivariate random vector,  $\boldsymbol{\xi}_\ell$ , and further a stochastic process,  $\xi_\ell(\cdot)$ , we have two important requirements by the Kolmogorov' extension theorem [54]: i) **exchangeability** of the joint distribution, i.e.  $p(\boldsymbol{\xi}_{1:J}) = p(\boldsymbol{\xi}_{\tau(1:J)})$  for any finite permutation  $\tau$ ; and ii) **consistency** of the marginalization, i.e.  $p(\boldsymbol{\xi}_1) = \int p(\boldsymbol{\xi}_1, \boldsymbol{\xi}_2) d\boldsymbol{\xi}_2$ .

Consider the process  $\xi_\ell(\cdot)$  defined in a finite temporal domain  $\mathcal{T} \subset \mathbb{R}_+$ , i.e., there exists  $T < \infty$  such that  $\mathcal{T} \subset [0, T]$ . Suppose we observe  $\xi_\ell(t)$  at  $J$  time points,  $t_1, \dots, t_J \in \mathcal{T}$ , then we need to define the distribution of  $\boldsymbol{\xi}_\ell = (\xi_\ell(t_1), \dots, \xi_\ell(t_J))$ . [47] investigate the family of elliptic contour distributions [34, 19] and propose the following consistent *multivariate  $q$ -exponential distribution* for  $\boldsymbol{\xi}_\ell$ .

**Definition 2.** *A multivariate  $q$ -exponential distribution, denoted as  $q\text{-ED}_J(\boldsymbol{\mu}, \mathbf{C})$ , has the following density*

$$p(\boldsymbol{\xi} | \boldsymbol{\mu}, \mathbf{C}, q) = \frac{q}{2} (2\pi)^{-\frac{J}{2}} |\mathbf{C}|^{-\frac{1}{2}} r^{\left(\frac{q}{2}-1\right)\frac{J}{2}} \exp\left\{-\frac{r^{\frac{q}{2}}}{2}\right\}, \quad r(\boldsymbol{\xi}) = (\boldsymbol{\xi} - \boldsymbol{\mu})^\top \mathbf{C}^{-1} (\boldsymbol{\xi} - \boldsymbol{\mu}). \quad (10)$$

**Remark 3.** *When  $q = 2$ ,  $q\text{-ED}_J(\boldsymbol{\mu}, \mathbf{C})$  reduces to MVN  $\mathcal{N}_J(\boldsymbol{\mu}, \mathbf{C})$ . When  $J = 1$ , if we let  $C = 1$ , then we have the density for  $\xi$  as  $p(\xi) \propto |\xi|^{\frac{q}{2}-1} \exp\left\{-\frac{1}{2}|\xi|^q\right\}$ , differing from the original setup (6) by a term  $|\xi|^{\frac{q}{2}-1}$ . This is needed for the consistency of temporal process generalization.*

Based on [Theorem 1 of 35], [47] prove the following theorem [Theorem 3.3 of 47] which states that the multivariate  $q$ -exponential random vector following distribution (10) satisfies the conditions of Kolmogorov's extension theorem hence can be generalized to a stochastic process.

**Theorem 3.1.** *The multivariate  $q$ -exponential distribution (10) is both **exchangeable** and **consistent**.*

To generate random vectors  $\boldsymbol{\xi} \sim q\text{-ED}_J(\boldsymbol{\mu}, \mathbf{C})$ , one can take advantage of the stochastic representation [64, 10, 34], as detailed in the following proposition [c.f. Theorem 2.1 and Proposition A.1 47]. This will be needed for the Bayesian inference in Section 5.

**Proposition 3.1.** *If  $\xi \sim \text{q-ED}_J(\boldsymbol{\mu}, \mathbf{C})$ , then we have*

$$\xi = \boldsymbol{\mu} + \mathbf{R}\mathbf{L}S \quad (11)$$

where  $S \sim \text{Unif}(\mathcal{S}^{J+1})$  uniformly distributed on the unit-sphere  $\mathcal{S}^{J+1}$ ,  $\mathbf{L}$  is the Cholesky factor of  $\mathbf{C}$  such that  $\mathbf{C} = \mathbf{L}\mathbf{L}^\top$ ,  $R \perp S$  and  $R^q \stackrel{d}{=} r^{\frac{q}{2}} \sim \Gamma(\alpha = \frac{J}{2}, \beta = \frac{1}{2}) = \chi^2(J)$ .

### 3.2 Q-exponential Process

With a covariance (symmetric and positive-definite) kernel  $\mathcal{C} : \mathcal{T} \times \mathcal{T} \rightarrow \mathbb{R}$ , we define  $q$ -exponential process (Q-EP) based on the multivariate  $q$ -exponential distribution (10).

**Definition 3.** *A (centered)  $q$ -exponential process  $\xi(t)$  with kernel  $\mathcal{C}$ ,  $\text{q-EP}(0, \mathcal{C})$ , is a collection of random variables such that any finite set,  $\boldsymbol{\xi} := (\xi(t_1), \dots, \xi(t_J))$ , follows a multivariate  $q$ -exponential distribution  $\text{q-ED}_J(\mathbf{0}, \mathbf{C})$ , where  $\mathbf{C} = [\mathcal{C}(t_j, t_{j'})]_{J \times J}$ .*

**Remark 4.** *When  $q = 2$ ,  $\text{q-EP}(0, \mathcal{C})$  becomes  $\mathcal{GP}(0, \mathcal{C})$ . When  $q \in [1, 2)$ ,  $\text{q-EP}(0, \mathcal{C})$  lends flexibility to modeling functional data with more regularization than GP. See Figures 1 and 10, and more details in Section 6.*

In the square-integrable function space over  $\mathcal{T}$ , i.e.  $L^2(\mathcal{T})$ , the covariance kernel  $\mathcal{C}$  is associated with a Hilbert-Schmidt (HS) integral operator  $T_{\mathcal{C}} : L^2(\mathcal{T}) \rightarrow L^2(\mathcal{T})$ ,  $\xi(\cdot) \mapsto \int_{\mathcal{T}} \mathcal{C}(\cdot, t') \xi(t') \mu(dt')$  which has eigen-pairs  $\{\lambda_\ell, \psi_\ell(\cdot)\}_{\ell=1}^\infty$  such that for  $\forall \ell \in \mathbb{N}$ ,  $T_{\mathcal{C}} \psi_\ell(t) = \psi_\ell(t) \lambda_\ell$  and  $\|\psi_\ell\|_2 = 1$ . Then  $\{\psi_\ell\}_{\ell=1}^\infty$  serves a basis of  $L^2(\mathcal{T})$ . Denote  $\lambda := \{\lambda_\ell\}_{\ell=1}^\infty$ . We assume  $T_{\mathcal{C}}$  is a trace-class operator, i.e.,  $\text{tr}(T_{\mathcal{C}}) := \|\lambda\|_1 = \sum_{\ell=1}^\infty \lambda_\ell < \infty$ . [Theorem 3.4 of 47] shows that we have a Karhunen-Loève type of theorem on the series representation of random function  $\xi(\cdot) \sim \text{q-EP}(0, \mathcal{C})$  drawn from Q-EP.

**Theorem 3.2** (Karhunen-Loève). *If  $\xi(\cdot) \sim \text{q-EP}(0, \mathcal{C})$  with a trace-class HS operator  $T_{\mathcal{C}}$  having eigen-pairs  $\{\lambda_\ell, \psi_\ell(\cdot)\}_{\ell=1}^\infty$ , then we have the following series representation for  $\xi(t)$ :*

$$\xi(t) = \sum_{\ell=1}^{\infty} \xi_\ell \psi_\ell(t), \quad \xi_\ell := \int_{\mathcal{T}} \xi(t) \psi_\ell(t) \mu(dt) \sim \text{q-ED}(0, \lambda_\ell), \quad (12)$$

where  $\mathbb{E}[\xi_\ell] = 0$  and  $\text{Cov}(\xi_\ell, \xi_{\ell'}) = \lambda_\ell \delta_{\ell\ell'}$  with Dirac function  $\delta_{\ell\ell'} = 1$  if  $\ell = \ell'$  and 0 otherwise. Moreover, we have

$$\mathbb{E}[\|\xi(\cdot)\|_2^2] = \sum_{\ell=1}^{\infty} \mathbb{E}[\xi_\ell^2] = \text{tr}(T_{\mathcal{C}}) < \infty.$$

**Remark 5.** *By re-scaling  $\xi_\ell$  in (12), we have the series representation of Q-EP  $\xi(\cdot)$  in the same format as BP in (6):*

$$\xi_\ell := \gamma_\ell \xi_\ell^*, \quad \gamma_\ell = \sqrt{\lambda_\ell}, \quad \xi_\ell^* \stackrel{iid}{\sim} \text{q-ED}(0, 1) \sim \pi_\xi(\cdot). \quad (13)$$

If we choose  $\sqrt{\lambda_\ell} = \ell^{-\tau_q(s)}$  as in (13), then  $\text{q-EP}(0, \mathcal{C})$  process becomes equivalent to  $\mathcal{B}(1, B^{s,q}(\mathcal{T}))$  process. From this perspective, we can view Q-EP as a probabilistic definition of BP (See Figure 1).

The above Theorem 3.2 states that for the given basis  $\{\psi_\ell\}_{\ell=1}^\infty$  on the time domain  $\mathcal{T}$ , we can identify any random draw  $\xi(\cdot) \sim \text{q-EP}(0, \mathcal{C})$  with the associated infinite sequence  $\xi = \{\xi_\ell\}_{\ell=1}^\infty$  as in (12). Similarly as in Section 2.2, we can define  $\|\xi(\cdot)\|_{s,q} = \|\xi\|_{\tau_q(s),q} = (\sum_{\ell=1}^\infty \ell^{\tau_q(s)q} |\xi_\ell|^q)^{\frac{1}{q}}$  and  $B^{s,q}(\mathcal{T}) = \{\xi : \mathcal{T} \rightarrow \mathbb{R} \mid \|\xi(\cdot)\|_{s,q} < \infty\}$ .

In the probability space  $(\Omega, \mathcal{B}(\Omega), \mathbb{P})$  with  $\Omega = \mathbb{R}$  and  $\mathbb{P}$  defined by  $q$ - $\mathcal{EP}(0, \mathcal{C})$ , we consider a Banach space defined as  $L_{\mathbb{P}}^p(\Omega, L^p(\mathcal{T})) = \{\xi : \mathcal{T} \times \Omega \rightarrow \mathbb{R} \mid \mathbb{E}(\|\xi\|_p^p) < \infty\}$ . From Theorem 3.2, we immediately have that if  $\xi(\cdot) \sim q$ - $\mathcal{EP}(0, \mathcal{C})$  with a trace-class HS operator  $T_{\mathcal{C}}$ , then  $\xi(\cdot) \in L_{\mathbb{P}}^2(\Omega, L^2(\mathcal{T}))$ . More general integrability of  $\xi(\cdot)$  relates to the summability of eigenvalues  $\lambda$  of the HS operator  $T_{\mathcal{C}}$ , as expressed in the following assumption.

**Assumption 1.** Suppose  $\lambda = \{\lambda_\ell\}_{\ell=1}^\infty$  are eigenvalues of HS operator  $T_{\mathcal{C}}$  for the kernel  $\mathcal{C}$  in Definition 3.

(i) We assume for  $s' < s - \frac{d}{q}$ ,

$$\sqrt{\lambda} \in \ell^{q, \tau_q(s')}, \quad \text{i.e.,} \quad \|\sqrt{\lambda}\|_{\tau_q(s'), q}^q = \sum_{\ell=1}^{\infty} \ell^{\tau_q(s')q} \lambda_\ell^{\frac{q}{2}} < \infty.$$

(ii) In particular when  $\tau_q(s') = 0$ , i.e.  $s' = \frac{d}{2} - \frac{d}{q}$ , we assume

$$\lambda \in \ell^{\frac{q}{2}}, \quad \text{i.e.,} \quad \|\lambda\|_{\frac{q}{2}}^{\frac{q}{2}} = \sum_{\ell=1}^{\infty} \lambda_\ell^{\frac{q}{2}} < \infty.$$

**Theorem 3.3.** If  $\xi(\cdot) \sim q$ - $\mathcal{EP}(0, \mathcal{C})$  with a trace-class HS operator  $T_{\mathcal{C}}$  satisfying Assumption 1-(i), then  $\xi(\cdot) \in L_{\mathbb{P}}^q(\Omega, B^{s', q}(\mathcal{T}))$ . If Assumption 1-(ii) holds instead, then  $\xi(\cdot) \in L_{\mathbb{P}}^q(\Omega, L^q(\mathcal{T}))$  and in particular  $\mathbb{E}[\|\xi(\cdot)\|_q^q] = \|\lambda\|_{\frac{q}{2}}^{\frac{q}{2}} < \infty$ .

*Proof.* See Appendix A.1 □

Under Assumption 1-(i), e.g.  $\sqrt{\lambda}_\ell = \ell^{-\tau_q(s)}$ ,  $q$ - $\mathcal{EP}(0, \mathcal{C})$  process becomes equivalent to the BP,  $\mathcal{B}(1, B^{s, q}(\mathcal{T}))$ , which only differs from the  $p$ -exponential process [1] by a constant in the definition  $\pi_\xi(\cdot) \propto \exp\left(-\frac{1}{p}|\cdot|^p\right)$ . See Figure 1 for more illustration of their relationship. Therefore, the posterior concentration theory developed by [1] for the  $p$ -exponential process applies to the  $q$ - $\mathcal{EP}(0, \mathcal{C})$  process. For  $\xi(\cdot) \in B^{s', q}(\mathcal{T})$  with  $s' < s - \frac{d}{q}$ , we define the concentration function of the  $q$ -exponential measure  $\mu$  (hence  $\mathcal{B}(1, B^{s, q}(\mathcal{T}))$ ) at  $\xi = \xi^\dagger$  as follows.

$$\varphi_{\xi^\dagger}(\varepsilon) = \inf_{h \in B^{s, q}(\mathcal{T}) : \|h - \xi^\dagger\|_{s', q} \leq \varepsilon} \frac{1}{2} \|h\|_{s, q}^q - \log \mu(\|\xi\|_{s', q} \leq \varepsilon). \quad (14)$$

Quoted from [Theorem 3.1 and Lemma 5.14 of 1], the following general contraction theorem for  $p$ -exponential process (also BP, and hence Q-EP) priors will be used in the proof of posterior contraction Theorem 4.7 for STBP priors.

**Theorem 3.4.** Let  $\mu$  be a  $q$ - $\mathcal{EP}(0, \mathcal{C})$  measure satisfying Assumption 1-(i) in the separable Banach space  $(B^{s', q}(\mathcal{T}), \|\cdot\|_{s', q})$ , where  $q \in [1, 2]$ . Let  $\xi \sim \mu$  and the true parameter  $\xi^\dagger \in B^{s', q}(\mathcal{T})$ . Assume  $\varepsilon_n > 0$  such that  $\varphi_{\xi^\dagger}(\varepsilon_n) \leq n\varepsilon_n^2$ , where  $n\varepsilon_n^2 \gtrsim 1$ . Then for any  $C > 1$ , there exists a measurable set  $B_n \subset B^{s', q}(\mathcal{T})$  and a constant  $R > 0$  depending on  $C$  and  $q$ , such that

$$\log N(4\varepsilon_n, B_n, \|\cdot\|_{s', q}) \leq Rn\varepsilon_n^2, \quad (15)$$

$$\mu(\xi \notin B_n) \leq \exp(-Cn\varepsilon_n^2), \quad (16)$$

$$\mu(\|\xi - \xi^\dagger\|_{s', q} < 2\varepsilon_n) \geq \exp(-n\varepsilon_n^2). \quad (17)$$

where  $N(4\varepsilon_n, B_n, \|\cdot\|_{s', q})$  is the minimal number of  $\|\cdot\|_{s', q}$ -balls of radius  $4\varepsilon_n$  to cover  $B_n$ .

## 4 Spatiotemporal Besov Process

Now we generalize the Banach space  $B^{s,q}(\mathcal{X})$  to include the temporal domain. Let the coefficients  $\{u_\ell\}_{\ell=1}^\infty$  in (4) be  $L^p(\mathcal{T})$  functions over some bounded temporal domain  $\mathcal{T} \subset \mathbb{R}_+$ . Denote  $\mathcal{Z} = \mathcal{X} \times \mathcal{T}$  and  $\mathbf{z} = (\mathbf{x}, t)$ . Then we obtain a spatiotemporal function  $u(\mathbf{z}) = u(\mathbf{x}, t)$  on  $\mathcal{Z}$  by the following series expansion with an infinite sequence of  $L^p(\mathcal{T})$  functions:

$$u(\mathbf{z}) = \sum_{\ell=1}^{\infty} u_\ell(t) \phi_\ell(\mathbf{x}), \quad u_\ell(\cdot) \in L^p(\mathcal{T}), \quad \forall \ell \in \mathbb{N}. \quad (18)$$

Denote the infinite sequence  $u_{\mathcal{T}} := \{u_\ell(\cdot)\}_{\ell=1}^\infty$ . We define the following norm  $\|\cdot\|_{\tau,q,p}$  for  $u_{\mathcal{T}}$  with a spatial (BP) index  $q \geq 1$  and a temporal (Q-EP) index  $p \geq 1$ :

$$\|u_{\mathcal{T}}\|_{\tau,q,p} = \left( \sum_{\ell=1}^{\infty} \ell^{\tau q} \|u_\ell(\cdot)\|_p^q \right)^{\frac{1}{q}}. \quad (19)$$

Denote the space of such infinite sequences as  $\ell^{q,\tau}(L^p(\mathcal{T})) := \{u_{\mathcal{T}} \mid \|u_{\mathcal{T}}\|_{\tau,q,p} < \infty\}$ . For a fixed spatial basis  $\{\phi_\ell(\mathbf{x})\}_{\ell=1}^\infty$ , we can identify  $u$  with  $u_{\mathcal{T}}$  based on the series representation (18). Let  $\|u\|_{s,q,p} = \|u_{\mathcal{T}}\|_{\tau_q(s),q,p}$  with  $\tau_q(s) = \frac{s}{d} + \frac{1}{2} - \frac{1}{q}$  as in (5). Then we define the Banach space of spatiotemporal functions  $B^{s,q,p}(\mathcal{Z}) := \{u : \mathcal{Z} \rightarrow \mathbb{R} \mid \|u\|_{s,q,p} < \infty\}$ .

Next we generalize BP  $u(\mathbf{x}) \sim \mathcal{B}(\kappa, B^{s,q}(\mathcal{X}))$  as in (8) to be spatiotemporal by letting random coefficients  $\{\xi_\ell\}_{\ell=1}^\infty$  vary in time domain according to  $\mathfrak{q}\text{-}\mathcal{EP}(0, \mathcal{C})$ . For this purpose, we make the following assumption.

**Assumption 2.** In (18) we let

$$u_\ell(t) = \gamma_\ell \xi_\ell(t), \quad \gamma_\ell = \kappa \ell^{-\tau_q(s)}, \quad \xi_\ell(\cdot) \stackrel{i.i.d.}{\sim} \mathfrak{q}\text{-}\mathcal{EP}(0, \mathcal{C}). \quad (20)$$

Compared with (6), we absorb the scaling factor  $\kappa > 0$  into the covariance kernel  $\mathcal{C}$  and set  $\kappa = 1$  for the most part. We only vary  $\kappa$  in the posterior contraction with adaptive priors in Section 4.2.2. Under Assumption 2, we have  $u$  in (18) as a stochastic process termed *spatiotemporal Besov process (STBP)*, denoted as  $\mathcal{STBP}(\mathcal{C}, B^{s,q,p}(\mathcal{Z}))$ . Similarly as in Section 2.2, the infinite random sequence  $\xi_{\mathcal{T}} := \{\xi_\ell(\cdot)\}_{\ell=1}^\infty$  is a random element of the probability space  $(\Omega, \mathcal{B}(\Omega), \mathbb{P})$  with  $\Omega = (L^p(\mathcal{T}))^\infty$ , product  $\sigma$ -algebra  $\mathcal{B}(\Omega)$  and probability measure  $\mathbb{P}$  defined by the infinite product of  $\mathfrak{q}\text{-}\mathcal{EP}(0, \mathcal{C})$  measures. Then we can define a spatiotemporal Besov measure on  $B^{s,q,p}(\mathcal{Z})$  as the law of STBP.

**Definition 4** (Spatiotemporal Besov Measure). Let  $\mathbb{P}$  be the measure of random sequences  $\xi_{\mathcal{T}} \in \Omega$ . Suppose we have the following map

$$f_\gamma : \Omega \rightarrow B^{s,q,p}(\mathcal{Z}), \quad \xi_{\mathcal{T}} \mapsto u(\mathbf{z}) = \sum_{\ell=1}^{\infty} u_\ell(t) \phi_\ell(\mathbf{x}) = \sum_{\ell=1}^{\infty} \gamma_\ell \xi_\ell(t) \phi_\ell(\mathbf{x}), \quad (21)$$

where  $\gamma_\ell$  and  $\xi_\ell(\cdot)$  are defined in (20). Then the pushforward  $f_\gamma^\# \mathbb{P}$  is spatiotemporal Besov measure  $\Pi$  on  $B^{s,q,p}(\mathcal{Z})$ .

Based on (21), we need to bound  $\|u_\ell(\cdot)\|_p^q$  (or  $\|\xi_\ell(\cdot)\|_p^q$ ) so the norm (19) is well defined. By Theorem 3.3,  $\|\xi_\ell(\cdot)\|_p^q$  has bounded mean for  $1 \leq p \leq q$ . For the convenience of exposition and theoretic development, in the following we only consider  $p = q \in [1, 2]$ . This is also when most interesting applications happen (See more details in Section 6). Denote  $\|u\|_{s,q} := \|u\|_{s,q,q} = \|\xi_{\mathcal{T}}\|_{q,q} = \left( \sum_{\ell=1}^{\infty} \|\xi_\ell(\cdot)\|_q^q \right)^{\frac{1}{q}}$  and  $B^{s,q,q}(\mathcal{Z}) := B^{s,q}(\mathcal{Z})$ . Figure 1 summarizes the relationship between GP, BP, Q-EP and their spatiotemporal variants.

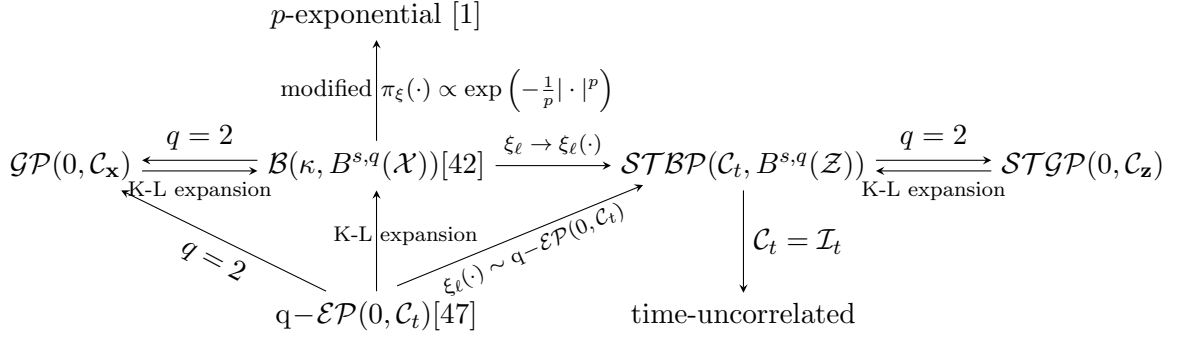


Figure 1: Relationship between GP, BP, Q-EP and their spatiotemporal variants.

#### 4.1 STBP as A Prior

In this section, we study multiple properties of STBP used as a prior. Similarly as in Section 2.2, for a given random draw  $u \sim \mathcal{STBP}(\mathcal{C}, B^{s,q}(\mathcal{Z}))$  as in (21), we have  $\mathbb{E}[\|u\|_{s,q}^q] = \mathbb{E}[\|\xi_{\mathcal{T}}\|_{q,q}^q] = \infty$  due to the iid assumption on  $\xi_{\mathcal{T}}$  in (20). However, we have the following integrability of STBP random sample in the ambient space  $B^{s',q}(\mathcal{Z})$  similar to Theorem 2.1.

**Theorem 4.1.** *If  $u \sim \mathcal{STBP}(\mathcal{C}, B^{s,q}(\mathcal{Z}))$  as in (21) satisfies both Assumptions 1-(ii) and 2, then  $u \in L_{\mathbb{P}}^q(\Omega; B^{s',q}(\mathcal{Z}))$  for all  $s' < s - \frac{d}{q}$ .*

The following (Fernique type) theorem enhances such result of well-definedness in the context of almost sure convergence for STBP random draws [42, 14, 15].

**Theorem 4.2.** *Let  $u \sim \mathcal{STBP}(\mathcal{C}, B^{s,q}(\mathcal{Z}))$  as in (21) satisfy both Assumptions 1-(ii) and 2. The following statements are equivalent:*

- (i)  $u \in B^{s',q}(\mathcal{Z})$   $\Pi$ -a.s.
- (ii)  $\mathbb{E}[\exp(\alpha \|u\|_{s',q}^q)] < \infty$  for any  $\alpha \in (0, (\sup_{\ell} \lambda_{\ell})^{-\frac{q}{2}}/2)$ .
- (iii)  $s' < s - \frac{d}{q}$ .

*Proof.* See Appendix A.1. □

**Remark 6.** *Fernique type result (ii) is important to make rigorous the formal Lebesgue density (9) and the conditions of similar format in Assumption 4 as well. The results (i) and (iii) immediately imply that the  $\mathcal{STBP}(\mathcal{C}, B^{s,q}(\mathcal{Z}))$  measure  $\Pi$  is supported on the ambient space  $B^{s',q}(\mathcal{Z})$  for  $s' < s - \frac{d}{q}$ , as stated in the following corollary.*

**Corollary 4.1.** *Let  $\Pi$  be an  $\mathcal{STBP}(\mathcal{C}, B^{s,q}(\mathcal{Z}))$  measure satisfying both Assumptions 1-(ii) and 2. Then  $\Pi(B^{s',q}(\mathcal{Z})) = 1$  for any  $s' < s - \frac{d}{q}$  and  $\Pi(B^{s',q}(\mathcal{Z})) = 0$  for any  $s' \geq s - \frac{d}{q}$ .*

It is known that  $B^{s,q}(\mathcal{Z}) \subset B^{s',q}(\mathcal{Z})$  for  $s' < s$ . More generally, we have the following continuous embeddings.

**Proposition 4.1.** *For  $q, q^{\dagger} \in [1, 2]$  and  $s' < s^{\dagger} - \left(\frac{d}{q^{\dagger}} - \frac{d}{q}\right)_{+}$  with  $x_{+} := \max\{x, 0\}$ , we have  $B^{s^{\dagger}, q^{\dagger} \wedge q, q}(\mathcal{Z}) \hookrightarrow B^{s',q}$ , where  $q^{\dagger} \wedge q := \min\{q^{\dagger}, q\}$ .*

*Proof.* See Appendix A.1. □

Similarly to Theorem 3.2, we have the Karhunen-Loève theorem for an STBP  $u(\cdot)$  as in (21) represented completely in the spatial  $(\{\phi_\ell\}_{\ell=1}^\infty)$  and temporal  $(\{\psi_{\ell'}\}_{\ell'=1}^\infty)$  bases.

**Theorem 4.3.** [Karhunen-Loève] *If  $u \sim \mathcal{STBP}(\mathcal{C}, B^{s,q}(\mathcal{Z}))$  as in (21) with a trace-class HS operator  $T_{\mathcal{C}}$  having eigen-pairs  $\{\lambda_\ell, \psi_\ell(\cdot)\}_{\ell=1}^\infty$ , then we have the following series representation for  $u(\mathbf{z})$ :*

$$u(\mathbf{z}) = \sum_{\ell=1}^{\infty} \sum_{\ell'=1}^{\infty} u_{\ell\ell'} \phi_\ell(\mathbf{x}) \psi_{\ell'}(t), \quad u_{\ell\ell'} := \int_{\mathcal{T}} u_\ell(t) \psi_{\ell'}(t) dt \sim \mathbf{q}\text{-ED}(0, \gamma_\ell^2 \lambda_{\ell'}). \quad (22)$$

Moreover, the spatiotemporal covariance of STBP bears a separable structure, i.e.,

$$\text{Cov}(u(\mathbf{z}), u(\mathbf{z}')) = \sum_{\ell=1}^{\infty} \gamma_\ell^2 \phi_\ell(\mathbf{x}) \phi_\ell(\mathbf{x}') \mathcal{C}(t, t'). \quad (23)$$

*Proof.* See Appendix A.1 □

**Remark 7.** *In practice (Section 6), we do not model with such pure series based representation (22) because it is not straightforward to specify correlations among sample functions which requires tweaking basis functions according to (23). Instead, it is our motivation to include a kernel  $\mathcal{C}$  in Definition 4 of STBP to directly model the temporal correlations through covariance functions, e.g. squared exponential, Matérn (See Section 5.3). In Section 6, we will also investigate the importance of temporal kernel  $\mathcal{C}$  by comparing against a time-uncorrelated method which sets it to be identity  $\mathcal{C} = \mathcal{I}$  (Refer to Figure 1).*

The regularity of an STBP random draw  $u(\mathbf{x}, t)$  as in (22) also depends on the properties of spatial  $(\{\phi_\ell\}_{\ell=1}^\infty)$  and temporal  $(\{\psi_{\ell'}\}_{\ell'=1}^\infty)$  bases. To study its Hölder continuity, we make the following assumption that mainly states that the bases are Hölder continuous with summable Lipschitz constants.

**Assumption 3.** *In the series expansion (22), we assume the spatial  $(\{\phi_\ell\}_{\ell=1}^\infty)$  and temporal  $(\{\psi_{\ell'}\}_{\ell'=1}^\infty)$  bases satisfy for  $\alpha > 0$  and  $s' < s - \frac{d}{q}$ :*

(i) *for  $\forall \mathbf{x}, \mathbf{x}' \in \mathcal{X}$ , the following holds*

$$|\phi_\ell(\mathbf{x}) - \phi_\ell(\mathbf{x}')| \leq L(\phi_\ell) |\mathbf{x} - \mathbf{x}'|^{\alpha + \frac{d}{q}}, \quad \sum_{\ell=1}^{\infty} \ell^{\frac{s'-s}{d}q} L(\phi_\ell) < \infty, \quad \sum_{\ell=1}^{\infty} \ell^{\frac{s'-s}{d}q} \|\phi_\ell(\cdot)\|_\infty^q < \infty;$$

(ii) *for  $\forall t, t' \in \mathcal{T}$ , the following holds*

$$|\psi_{\ell'}(t) - \psi_{\ell'}(t')| \leq L(\psi_{\ell'}) |t - t'|^{\alpha + \frac{d}{q}}, \quad \sum_{\ell'=1}^{\infty} \lambda_{\ell'}^{\frac{q}{2}} L(\psi_{\ell'}) < \infty.$$

The following theorem regarding the Hölder continuity of STBP random functions can be proved by the Kolmogorov continuity test [Theorem 30 in Section A.2.5 of 15].

**Theorem 4.4.** [Hölder Continuity] *Let  $u \sim \mathcal{STBP}(\mathcal{C}, B^{s,q}(\mathcal{Z}))$  as in (21) satisfy both Assumptions 1-(ii) and 2. Suppose the spatial  $(\{\phi_\ell\}_{\ell=1}^\infty)$  and temporal  $(\{\psi_{\ell'}\}_{\ell'=1}^\infty)$  bases in the series representation (22) satisfy Assumption 3. Then for any  $\beta < \alpha$ , there exists a version <sup>1</sup>  $\tilde{u}(\mathbf{z})$  of  $u(\mathbf{z})$  in  $C^{0,\beta}(\mathcal{Z}, B^{s',q}(\mathcal{Z}))$ .*

*Proof.* See Appendix A.1 □

<sup>1</sup>A version of stochastic process  $u(\mathbf{z})$  is  $\tilde{u}(\mathbf{z})$  such that  $\mathbb{P}[\tilde{u}(\mathbf{z}) = u(\mathbf{z})] = 1$  for  $\forall \mathbf{z} \in \mathcal{Z}$ .

## 4.2 Posterior Theorems for Inverse Problems with STBP Priors

In this section, we study the posterior properties of the Bayesian inverse model (1) with STBP priors. In particular, we set the separable Banach space  $\mathbb{X} = B^{s',q}(\mathcal{Z})$  for some  $s' < s - \frac{d}{q}$ , and let  $\mathbb{Y}$  be another separable Banach space, e.g.  $\mathbb{Y} = H^s(\mathcal{X})$  or  $\mathbb{Y} = \mathbb{R}^m$ , depending on the applications. Following [14], we also impose some conditions on the potential (negative log-likelihood) function  $\Phi : B^{s',q}(\mathcal{Z}) \times \mathbb{Y} \rightarrow \mathbb{R}$  as in (2) regarding its lower (i) and upper (ii) bounds, and the Lipschitz continuity in  $u$  (iii) and  $y$  (iv) in the following assumption.

**Assumption 4.** *The potential function  $\Phi : B^{s',q}(\mathcal{Z}) \times \mathbb{Y} \rightarrow \mathbb{R}$  satisfies:*

- (i) *there is an  $\alpha_1 > 0$  and for every  $r > 0$ , an  $M \in \mathbb{R}$ , such that for all  $u \in B^{s',q}(\mathcal{Z})$ , and for all  $y \in \mathbb{Y}$  such that  $\|y\|_{\mathbb{Y}} < r$ ,*

$$\Phi(u, y) \geq M - \alpha_1 \|u\|_{s',q};$$

- (ii) *for every  $r > 0$  there exists  $K = K(r) > 0$  such that for all  $u \in B^{s',q}(\mathcal{Z})$ ,  $y \in \mathbb{Y}$  with  $\max\{\|u\|_{s',q}, \|y\|_{\mathbb{Y}}\} < r$ ,*

$$\Phi(u, y) \leq K;$$

- (iii) *for every  $r > 0$  there exists  $L = L(r) > 0$  such that for every  $y \in \mathbb{Y}$  and for all  $u_1, u_2 \in B^{s',q}(\mathcal{Z})$  with  $\max\{\|u_1\|_{s',q}, \|u_2\|_{s',q}\} < r$ ,*

$$|\Phi(u_1, y) - \Phi(u_2, y)| \leq L \|u_1 - u_2\|_{s',q};$$

- (iv) *there is an  $\alpha_2 > 0$  and for every  $r > 0$  a  $C \in \mathbb{R}$  such that for all  $y_1, y_2 \in \mathbb{Y}$  with  $\max\{\|y_1\|_{\mathbb{Y}}, \|y_2\|_{\mathbb{Y}}\} < r$  and for every  $u \in B^{s',q}(\mathcal{Z})$ ,*

$$|\Phi(u, y_1) - \Phi(u, y_2)| \leq \exp(\alpha_2 \|u\|_{s',q} + C) \|y_1 - y_2\|_{\mathbb{Y}}.$$

### 4.2.1 Well-definedness and Well-posedness of Posteriors

Recall that  $\Pi$  is the STBP prior defined by (21) and  $\Pi^y$  is the resulting posterior measure in the model (1). We re-examine the well-definedness and well-posedness of the posterior measure based on Assumption 4.

**Theorem 4.5.** *[Well-definedness of Posterior] Let the potential function  $\Phi$  in (2) satisfy Assumption 4 (i)-(iii). If  $\Pi$  is an  $\mathcal{STBP}(\mathcal{C}, B^{s,q}(\mathcal{Z}))$  measure with  $s > s' + \frac{d}{q}$ , then  $\Pi^y \ll \Pi$  and satisfies*

$$\frac{d\Pi^y}{d\Pi}(u) = \frac{1}{Z(y)} \exp(-\Phi(u; y)), \quad (24)$$

with the normalizing factor  $0 < Z(y) = \int_{B^{s',q}(\mathcal{Z})} \exp(-\Phi(u; y)) \Pi(du) < \infty$ .

*Proof.* See Appendix A.2. □

Now we show the well-posedness of the posterior measure  $\Pi^y$  with respect to the data  $y$ . Define the Hellinger metric as  $d_H(\mu, \mu') = \sqrt{\frac{1}{2} \int \left( \sqrt{\frac{d\mu}{d\nu}} - \sqrt{\frac{d\mu'}{d\nu}} \right)^2 d\nu}$ . Note we require  $\mu, \mu' \ll \nu$ , but this definition is independent of the choice of the measure  $\nu$ . The following theorem states that the posterior measure is Lipschitz with respect to data  $y$ , in the Hellinger metric.

**Theorem 4.6.** [Well-posedness of Posterior] Let the potential function  $\Phi$  in (2) satisfy Assumption 4 (i)-(iv). If  $\Pi$  is an  $\mathcal{STBP}(\mathcal{C}, B^{s,q}(\mathcal{Z}))$  measure with  $s > s' + \frac{d}{q}$ , then

$$d_H(\Pi^y, \Pi^{y'}) \leq C \|y - y'\|_{\mathbb{Y}},$$

where  $C = C(r)$  is a constant depending on  $r$  such that  $\max\{\|y\|_{\mathbb{Y}}, \|y'\|_{\mathbb{Y}}\} \leq r$ .

*Proof.* See Appendix A.2. □

#### 4.2.2 Posterior Contraction of Bayesian Inverse Problems

In this section, we consider the concentration property of the posterior  $\Pi^y$  in the infinitely-informative data-limit. Unlike the Gaussian measure with reproducible kernel Hilbert space (RKHS), the lack of inner product structure on  $B^{s,q}(\mathcal{Z}) \subset B^{s',q}(\mathcal{Z})$  makes the posterior contraction theories more challenging [1]. We consider the separable Banach space  $(B^{s',q}(\mathcal{Z}), \|\cdot\|_{s',q})$ . Define the concentration function of STBP measure  $\Pi$  at  $u = u^\dagger$  as

$$\varphi_{u^\dagger}(\varepsilon) = \inf_{h \in B^{s,q}(\mathcal{Z}): \|h - u^\dagger\|_{s',q} \leq \varepsilon} \frac{1}{2} \|h\|_{s,q}^q - \log \Pi(\|u\|_{s',q} \leq \varepsilon). \quad (25)$$

Let  $n = I \wedge J = \min\{I, J\}$  with  $I, J$  being discrete spatial and temporal dimensions, respectively. We consider the inverse model (1) with observations  $Y^{(n)} := \{Y_j = y(\mathbf{X}, t_j)\}_{j=1}^n$  independent but not identically distributed (the mean  $\mathcal{G}(u)(\mathbf{X}, t_j)$  changes for different  $j$ ). Denote  $P_u^{(n)} := \bigotimes_{j=1}^n P_{u,j}$  as the product measure on  $\bigotimes_{j=1}^n (\mathbb{Y}_j, \mathcal{B}_j, \mu_j)$ . Each  $P_{u,j}$  has a density  $p_{u,j}$  with respect to the  $\sigma$ -finite reference measure  $\mu_j$ , which could be  $p_{\mathcal{N}(\mathcal{G}(u_j), \sigma_j^2)}$ . Define the average Hellinger distance as  $d_{n,H}^2(u, u') = \frac{1}{n} \sum_{j=1}^n \int (\sqrt{p_{u_j}} - \sqrt{p_{u'_j}})^2 d\mu_j$ . Then we have the following posterior contraction theorem.

**Theorem 4.7.** [Posterior Contraction] Let  $u$  be an  $\mathcal{STBP}(\mathcal{C}, B^{s,q}(\mathcal{Z}))$  random element as in (21) satisfying both Assumptions 1-(ii) and 2 in  $\Theta := B^{s',q}(\mathcal{Z})$  with  $s' < s - \frac{d}{q}$  and  $P_u^{(n)} := \bigotimes_{j=1}^n P_{u,j}$  be the product measure of  $Y^{(n)}$  parameterized by  $u$  with the potential function  $\Phi$  (2) satisfying Assumption 4 (i)-(iii). If the true value  $u^\dagger \in \Theta$  is in the support of  $u$ , and  $\varepsilon_n$  satisfies the rate equation  $\varphi_{u^\dagger}(\varepsilon_n) \leq n\varepsilon_n^2$  with  $\varepsilon_n \geq n^{-\frac{1}{2}}$ , then there exists  $\Theta_n \subset \Theta$  such that  $\Pi_n(u \in \Theta_n : d_{n,H}(u, u^\dagger) \geq M_n \varepsilon | Y^{(n)}) \rightarrow 0$  in  $P_{u^\dagger}^{(n)}$ -probability for every  $M_n \rightarrow \infty$ .

*Proof.* See Appendix A.2. □

Denote  $a \wedge b = \min\{a, b\}$ ,  $a \vee b = \max\{a, b\}$ , and  $x_+ = x \vee 0$ . By solving the inequality  $\varphi_{u^\dagger}(\varepsilon_n) \leq n\varepsilon_n^2$  for the minimal  $\varepsilon_n$ , we obtain the posterior contraction rate as follows.

**Theorem 4.8.** [Posterior Contraction Rate] Let  $u$  be an  $\mathcal{STBP}(\mathcal{C}, B^{s,q}(\mathcal{Z}))$  random element in  $\Theta := B^{s',q}(\mathcal{Z})$  with  $s' < s - \frac{d}{q}$ . The rest of the settings are the same as in Theorem 4.7. If the true value  $u^\dagger \in B^{s^\dagger, q^\dagger}(\mathcal{Z})$  with  $s^\dagger > s' + \left(\frac{d}{q^\dagger} - \frac{d}{q}\right)_+$  and  $q^\dagger, q \in [1, 2]$ , then

we have the rate of the posterior contraction as  $\varepsilon_n = n^{-\frac{\sigma(s,q,s^\dagger,q^\dagger) - s'}{2(\sigma(s,q,s^\dagger,q^\dagger) - s') + q(s - \sigma(s,q,s^\dagger,q^\dagger))}}$ , where  $\sigma(s, q, s^\dagger, q^\dagger) = \left(s - \frac{d}{q}\right) \wedge \left(s^\dagger - \left(\frac{d}{q^\dagger} - \frac{d}{q}\right)_+\right)$ .

*Proof.* See Appendix A.2. □

**Remark 8.** The contraction rate  $\varepsilon_n$  becomes optimal  $\varepsilon_n^* = n^{-\frac{1}{2 + \frac{d}{s^\dagger - s' - \left(\frac{d}{q^\dagger} - \frac{d}{q}\right)_+}}$  if  $s = s^\dagger + \frac{d}{q} - \left(\frac{d}{q^\dagger} - \frac{d}{q}\right)_+$ , which is further maximized as  $\varepsilon_n^\dagger = n^{-\frac{1}{2 + \frac{d}{s^\dagger - s'}}$  when  $q \leq q^\dagger$ . Note, such optimal rate is achieved regardless of the value of modeling regularization parameter  $q$  as long as  $q \leq q^\dagger$ . This implies that when modeling inhomogeneous data, under-smoothing (with smaller regularization parameter  $q$ ) is preferred to over-smoothing (with larger  $q$ , refer to Figure 10). This is also the reason why  $q = 1$  is often adopted – the posterior can contract the fastest if the true integrability  $q^\dagger$  is at least  $L_1$ .

**Remark 9.** Another observation is that the ambient space  $B^{s',q}(\mathcal{Z})$  can be chosen for the smoothness parameter  $s' < \sigma(s, q, s^\dagger, q^\dagger)$ . In particular, we consider two cases:

- (i) If we set  $\tau_q(s') = 0$ , i.e.  $s' = \frac{d}{q} - \frac{d}{2} \geq 0$ , then  $B^{s',q}(\mathcal{Z}) \cong \ell^q(L^q(\mathcal{T}))$ . For the Gaussian case ( $q^\dagger = 2$ ), if we adopt  $q = 2$  and hence  $s' = 0$  and  $B^{0,2}(\mathcal{Z}) \cong \ell^2(L^2(\mathcal{T})) \cong L^2(\mathcal{Z})$ , then the optimal rate  $\varepsilon_n^\dagger = n^{-\frac{s^\dagger}{2s^\dagger + d}}$  is minimax [72]. For other sub-Gaussian cases ( $q^\dagger < 2$ ), such optimal rate  $\varepsilon_n^\dagger = n^{-\frac{s^\dagger - s'}{2(s^\dagger - s') + d}}$  is not minimax [1] regardless of the choice of  $q \in [1, 2]$  because either  $s' > 0$  ( $q \leq q^\dagger < 2$ ) or such optimal rate is not attained ( $q > q^\dagger$ ).
- (ii) On the other hand, if we allow  $s' = 0$  and consider a larger ambient space  $B^{0,q}(\mathcal{Z}) \cong \ell^{q, \frac{1}{2} - \frac{1}{q}}(L^q(\mathcal{T})) \supset \ell^q(L^q(\mathcal{T}))$ , then the minimax rate  $\varepsilon_n^\dagger = n^{-\frac{s^\dagger}{2s^\dagger + d}}$  can be obtained for  $q \leq q^\dagger$ .

In general, the minimax posterior contraction rate is not achieved when  $q > q^\dagger$ . Therefore we typically rescale the prior to infuse additional regularity [73, 22, 1]. That is, we vary the scaling factor  $\kappa > 0$  as in (20) and rescale the Banach space  $(\kappa B^{s,q}(\mathcal{Z}), \|\cdot\|_{s,q}) \cong (B^{s,q}(\mathcal{Z}), \kappa^{-1} \|\cdot\|_{s,q})$ . Denote  $(B_\kappa^{s,q}(\mathcal{Z}), \|\cdot\|) := (B^{s,q}(\mathcal{Z}), \kappa^{-1} \|\cdot\|_{s,q})$  and the corresponding (rescaled) STBP measure as  $\Pi_\kappa$  in Definition 4. Now we redefine the posterior concentration function (25) to be

$$\varphi_{u^\dagger, \kappa}(\varepsilon) = \inf_{h \in B_\kappa^{s,q}(\mathcal{Z}) : \|h - u^\dagger\|_{s',q} \leq \varepsilon} \frac{\kappa^{-q}}{2} \|h\|_{s,q}^q - \log \Pi_\kappa(\|u\|_{s',q} \leq \varepsilon). \quad (26)$$

The following theorem regards the posterior contraction rate with rescaled STBP prior.

**Theorem 4.9.** [Adaptive Posterior Contraction Rate] Let  $u$  be an  $STBP(\mathcal{C}, B_\kappa^{s,q}(\mathcal{Z}))$  random element in  $\Theta := B_\kappa^{s',q}(\mathcal{Z})$  with  $s' < s - \frac{d}{q}$ . Suppose  $\varepsilon_n$  satisfies the rate equation  $\varphi_{u^\dagger, \kappa}(\varepsilon_n) \leq n\varepsilon_n^2$  with  $\varepsilon_n \geq n^{-\frac{1}{2}}$ . The rest of the settings are the same as in Theorem 4.7. If the true value  $u^\dagger \in B_\kappa^{s^\dagger, q^\dagger}(\mathcal{Z})$  with  $s^\dagger > s' + \left(\frac{d}{q^\dagger} - \frac{d}{q}\right)_+$  and  $1 \leq q^\dagger < q \leq 2$ , then the minimax posterior contraction rate  $\varepsilon_n^\dagger = n^{-\frac{s^\dagger}{2s^\dagger + d}}$  can be attained at  $s = \frac{s^\dagger(s^\dagger - s')}{s' + \left(\frac{d}{q^\dagger} - \frac{d}{q}\right)} + s'$  with

$$\text{the scaling factor } \kappa_n \asymp n^{-\frac{1}{2s^\dagger + d} \left[ -\frac{s^\dagger(s^\dagger - s')}{s' + \left(\frac{d}{q^\dagger} - \frac{d}{q}\right)} + \frac{d}{q} + s^\dagger \right]}.$$

*Proof.* See Appendix A.2. □

## 5 Bayesian Inference

In this section, we describe the inference of the Bayesian inverse problem (1) with spatiotemporal observations using an STBP prior. Assume the unknown function  $u$  is evaluated at  $I$  locations  $\mathbf{X} := \{\mathbf{x}_i\}_{i=1}^I$  and  $J$  time points  $\mathbf{t} := \{t_j\}_{j=1}^J$ , that is  $u(\mathbf{X}, \mathbf{t}) := \{u(\mathbf{x}_i, t_j)\}_{i,j=1}^{I,J}$ . The data  $\mathbf{Y} = \{\mathbf{y}_j\}_{j=1}^J$  with  $\mathbf{y}_j \in \mathbb{R}^m$  is observed through the forward operator  $\mathcal{G}$ , which could be a linear mapping or a nonlinear one governed by a PDE. Here we consider Gaussian noise and recap the model as follows:

$$\begin{aligned} \mathbf{y}_j &= \mathcal{G}(u)(\mathbf{X}, t_j) + \boldsymbol{\varepsilon}_j, \quad \boldsymbol{\varepsilon}_j \stackrel{iid}{\sim} \mathcal{N}_I(0, \Gamma_{\text{noise}}), \quad j = 1, 2, \dots, J, \\ u &\sim \text{STBP}(\mathcal{C}, B^{s,q}(\mathcal{Z})). \end{aligned} \quad (27)$$

In our applications of inverse problems, the spatial dimension  $I$  is usually tremendously higher than the temporal dimension ( $I \gg J$ ). Therefore we truncate  $u$  in (21) for the first  $L > 0$  terms:  $u(\mathbf{x}, t) \approx u^L(\mathbf{x}, t) = \sum_{\ell=1}^L \gamma_\ell \xi_\ell(t) \phi_\ell(\mathbf{x})$ , and choose  $L = 2000$  in the numerical experiments (Section 6). Denote  $\mathbf{u}_j = u(\mathbf{X}, t_j) \in \mathbb{R}^I$ , and  $\mathbf{U} = [\mathbf{u}_1, \dots, \mathbf{u}_J]_{I \times J} = u^L(\mathbf{X}, \mathbf{t}) = \boldsymbol{\Phi} \text{diag}(\boldsymbol{\gamma}) \boldsymbol{\Xi}^\top$  where  $\boldsymbol{\Phi} = [\phi_1(\mathbf{X}), \dots, \phi_L(\mathbf{X})]_{I \times L}$ ,  $\boldsymbol{\gamma} = (\gamma_1, \dots, \gamma_L)$ , and  $\boldsymbol{\Xi} = [\boldsymbol{\xi}_1, \dots, \boldsymbol{\xi}_L]_{J \times L}$  with  $\boldsymbol{\xi}_\ell = \xi_\ell(\mathbf{t})$ . Instead of the large dimensional matrix  $\mathbf{U}$ , we work with  $\boldsymbol{\Xi}$  of much smaller size. Let  $r_\ell = \boldsymbol{\xi}_\ell^\top \mathbf{C}_J^{-1} \boldsymbol{\xi}_\ell$ . The log-posterior for  $\boldsymbol{\Xi}$  is computed directly as

$$\begin{aligned} \log p(\boldsymbol{\Xi}, \theta | \mathbf{Y}) &= -\frac{J}{2} \log |\Gamma_{\text{noise}}| - \frac{1}{2} \sum_{j=1}^J \|\mathbf{y}_j - \mathcal{G}(\mathbf{u}_j)\|_{\Gamma_{\text{noise}}}^2 \\ &\quad - \frac{L}{2} \log |\mathbf{C}_J| + \frac{J}{2} \left(\frac{q}{2} - 1\right) \sum_{\ell=1}^L \log r_\ell - \frac{1}{2} \sum_{\ell=1}^L r_\ell^{\frac{q}{2}}. \end{aligned} \quad (28)$$

We optimize (28) to obtain the maximum a posteriori (MAP) estimate. To quantify the uncertainty efficiently, we need effective inference algorithms for high-dimensional models with non-Gaussian priors. We refer to the work of dimension-robust MCMC proposed by [13] based on the pushforward of Gaussian white noise which in turn takes advantage of the dimension-independent sampling algorithms for Gaussian priors [8]. For the convenience of application, in the following, we introduce a new white noise representation for STBP which is different from the one used in [13] for series based priors.

### 5.1 White Noise Representation

Recall we have the stochastic representation (11) of  $\boldsymbol{\xi} \sim \text{q-ED}_J(\mathbf{0}, \mathbf{C})$ :  $\boldsymbol{\xi} = \mathbf{R}\mathbf{L}\mathbf{S}$  with  $R^q \sim \chi^2(J)$  and  $S \sim \text{Unif}(\mathcal{S}^{J+1})$ . We can write

$$S = \frac{\boldsymbol{\zeta}}{\|\boldsymbol{\zeta}\|_2}, \quad R^q = \|\boldsymbol{\zeta}\|_2^2, \quad \text{for } \boldsymbol{\zeta} \sim \mathcal{N}_J(\mathbf{0}, \mathbf{I}_J).$$

Therefore,  $\boldsymbol{\xi}$  can be represented in terms of the white noise  $\boldsymbol{\zeta}$  by a pushforward mapping  $\Lambda: \mathbb{R}^J \rightarrow \mathbb{R}^J$  and vice versa with its inverse  $\Lambda^{-1}$ :

$$\boldsymbol{\xi} = \Lambda(\boldsymbol{\zeta}) = \mathbf{L}\boldsymbol{\zeta} \|\boldsymbol{\zeta}\|_2^{\frac{2}{q}-1}, \quad \boldsymbol{\zeta} = \Lambda^{-1}(\boldsymbol{\xi}) = \mathbf{L}^{-1}\boldsymbol{\xi} \|\mathbf{L}^{-1}\boldsymbol{\xi}\|_2^{\frac{q}{2}-1}. \quad (29)$$

For  $\zeta(\cdot) = \sum_{\ell'=1}^{\infty} \zeta_{\ell'} \psi_{\ell'}(\cdot)$ ,  $\xi(\cdot) = \sum_{\ell'=1}^{\infty} \xi_{\ell'} \psi_{\ell'}(\cdot) \in L^2(\mathcal{T})$ , we can extend  $\Lambda$  and its inverse  $\Lambda^{-1}$  to  $L^2(\mathcal{T})$  and have

$$\xi(\cdot) = \Lambda(\zeta(\cdot)) = \sum_{\ell'=1}^{\infty} \lambda_{\ell'}^{\frac{1}{2}} \zeta_{\ell'} \psi_{\ell'}(\cdot) \|\zeta(\cdot)\|_2^{\frac{2}{q}-1}, \quad \zeta(\cdot) = \Lambda^{-1}(\xi(\cdot)) = \sum_{\ell'=1}^{\infty} \lambda_{\ell'}^{-\frac{1}{2}} \xi_{\ell'} \psi_{\ell'}(\cdot) \|\xi(\cdot)\|_{2,\mathcal{C}}^{\frac{2}{q}-1},$$

where  $\|\zeta(\cdot)\|_2^2 = \sum_{\ell'=1}^{\infty} \zeta_{\ell'}^2$  and  $\|\xi(\cdot)\|_{2,C}^2 = \sum_{\ell'=1}^{\infty} \lambda_{\ell'}^{-1} \xi_{\ell'}^2$ . We propose the following representation of  $u(\mathbf{z})$  in terms of an infinite sequence of white noises, i.e.  $\zeta := \{\zeta_{\ell}(\cdot)\}_{\ell=1}^{\infty}$ :

$$u(\mathbf{z}) = T(\zeta) = \sum_{\ell=1}^{\infty} \gamma_{\ell} \Lambda(\zeta_{\ell}(t)) \phi_{\ell}(\mathbf{x}), \quad \zeta_{\ell}(\cdot) \stackrel{i.i.d.}{\sim} \mathcal{GP}(0, \mathcal{I}). \quad (30)$$

Denote  $\mathbf{Z} = [\zeta_1, \dots, \zeta_L]_{J \times L}$  with  $\zeta_{\ell} = \zeta_{\ell}(\mathbf{t})$ . From (30), we have  $\mathbf{U} = T(\mathbf{Z}) = \Phi \text{diag}(\gamma) \Lambda(\mathbf{Z})^{\top}$ . Then the log-posterior (28) can be rewritten in terms of  $\mathbf{Z}$ :

$$\begin{aligned} \log p(\mathbf{Z}, \theta | \mathbf{Y}) = & -\frac{J}{2} \log |\Gamma_{\text{noise}}| - \frac{1}{2} \sum_{j=1}^J \text{tr}((\mathbf{Y} - \mathcal{G}(T(\mathbf{Z})))^{\top} \Gamma_{\text{noise}}^{-1} (\mathbf{Y} - \mathcal{G}(T(\mathbf{Z})))) \\ & - \frac{L}{2} \log |\mathbf{C}_J| + \frac{J}{2} \left(\frac{q}{2} - 1\right) \sum_{\ell=1}^L \log r_{\ell} - \frac{1}{2} \sum_{\ell=1}^L r_{\ell}^{\frac{q}{2}}, \end{aligned} \quad (31)$$

where  $r_{\ell} = \Lambda(\zeta_{\ell})^{\top} \mathbf{C}_J^{-1} \Lambda(\zeta_{\ell})$ . Once the MAP  $\mathbf{Z}_{\text{MAP}}$  is obtained by maximizing the above log-posterior, we can obtain  $\mathbf{U}_{\text{MAP}} = T(\mathbf{Z}_{\text{MAP}})$ . We refer to this process as ‘‘optimization in the whitened space’’. The objective function can be explored more efficiently in the whitened space with variables de-correlated (See Figure 5).

## 5.2 White Noise MCMC

Denote the measure formed by infinite product of  $\mathcal{GP}(0, \mathcal{I})$  as  $\Pi_0$ . Then our STBP prior measure  $\Pi$  can be regained by the pushforward using  $T$ , i.e.  $\Pi = T^{\#} \Pi_0$ . A class of dimension-independent MCMC algorithms [8] for models with Gaussian prior  $\Pi_0$  can be reintroduced to posterior sampling with STBP prior  $\Pi$ .

Let  $u = T(\zeta)$  with  $\zeta \sim \Pi_0$ . Consider the following continuous-time Hamiltonian dynamics:

$$\frac{d^2 \zeta}{dt^2} + \mathcal{K}(\zeta) [\zeta + \nabla \Phi(\zeta)] = 0, \quad \left( \eta := \frac{d\zeta}{dt} \right) \Big|_{t=0} \sim \mathcal{N}(0, \mathcal{K}(\zeta)), \quad (32)$$

where  $\Phi(\zeta) := \Phi(T(\zeta)) - \log |dT(\zeta)|$ . More generally, we could set  $\mathcal{K}(\zeta)^{-1} = \mathcal{I} + \beta \mathcal{H}(\zeta)$  where  $\mathcal{H}(\zeta)$  can be chosen as Hessian, Gauss-Newton Hessian, or Fisher information operator [40]. For example, we can choose the Gauss-Newton Hessian computed as  $\mathcal{H}(\zeta) = dT^* \mathcal{H}(u) dT$  with  $dT$  being the Jacobian. Let  $g(\zeta) := -\mathcal{K}(\zeta) \{\alpha \nabla \Phi(\zeta) - \beta \mathcal{H}(\zeta) \zeta\}$  where  $\nabla_{\zeta} \Phi(\zeta) = dT^* \nabla_u \Phi(u) - \nabla_{\zeta} \log |dT(\zeta)|$ . The Hamiltonian Monte Carlo (HMC) algorithm [53] solves the dynamics (32) using the Störmer-Verlet symplectic (leapfrog) integrator with step size  $\varepsilon$ :

$$\begin{aligned} \eta^- &= \eta_0 + \frac{\varepsilon}{2} g(\zeta_0); \\ \begin{bmatrix} \zeta_{\varepsilon} \\ \eta^+ \end{bmatrix} &= \begin{bmatrix} \cos \varepsilon & \sin \varepsilon \\ -\sin \varepsilon & \cos \varepsilon \end{bmatrix} \begin{bmatrix} \zeta_0 \\ \eta^- \end{bmatrix}; \\ \eta_{\varepsilon} &= \eta^+ + \frac{\varepsilon}{2} g(\zeta_{\varepsilon}). \end{aligned} \quad (33)$$

Equation (33) gives rise to the leapfrog map  $\Psi_{\varepsilon} : (\zeta_0, \eta_0) \mapsto (\zeta_{\varepsilon}, \eta_{\varepsilon})$ . Given a time horizon  $\tau$  and current position  $\zeta$ , the MCMC mechanism proceeds by concatenating  $I = \lfloor \tau/\varepsilon \rfloor$  steps of leapfrog map consecutively,

$$\zeta' = \mathcal{P}_{\zeta} \{ \Psi_{\varepsilon}^I(\zeta, \eta) \}, \quad \eta \sim \mathcal{N}(0, \mathcal{K}(\zeta)),$$

where  $\mathcal{P}_\zeta$  denotes the projection onto the  $\zeta$ -argument. Then, the proposal  $\zeta'$  is accepted with probability  $a(\zeta, \zeta') = 1 \wedge \exp(-\Delta E(\zeta, \eta))$ , where

$$\begin{aligned} \Delta E(\zeta, \eta) &= E(\Psi_\varepsilon^I(\zeta, \eta)) - E(\zeta, \eta) \\ &= \Phi(\zeta_I) - \Phi(\zeta_0) + \frac{\beta}{2} \langle \eta_I, \mathcal{H}(\zeta_I) \eta_I \rangle - \frac{\beta}{2} \langle \eta_0, \mathcal{H}(\zeta_0) \eta_0 \rangle - \log |\mathcal{K}^{-\frac{1}{2}}(\zeta_I)| + \log |\mathcal{K}^{-\frac{1}{2}}(\zeta_0)| \\ &\quad - \frac{\varepsilon^2}{8} \{ \|g(\zeta_I)\|^2 - \|g(\zeta_0)\|^2 \} - \frac{\varepsilon}{2} \sum_{i=0}^{I-1} (\langle g(\zeta_i), \eta_i \rangle + \langle g(\zeta_{i+1}), \eta_{i+1} \rangle). \end{aligned} \quad (34)$$

At last we convert the sample  $\zeta$  back to  $u = T(\zeta)$ . This yields white-noise infinite-dimensional manifold HMC (wn- $\infty$ -mHMC) [8] which reduces to white-noise infinite-dimensional manifold Metropolis adjusted Langevin algorithm (wn- $\infty$ -mMALA) [7] when  $I = 1$ , and white-noise infinite-dimensional HMC (wn- $\infty$ -HMC) [6] when  $\beta = 0$ . We set  $\alpha = 1$  for both scenarios and summarize all these methods in Algorithm 1 of Appendix B named as *white-noise dimension-independent MCMC (wn- $\infty$ -MCMC)*.

### 5.3 Hyper-parameter Tuning

In Definitions 3 and 4, there is a temporal kernel  $\mathcal{C}$  that has not been specified. This is the key component to capture the temporal correlation which is absent in a pure series based approach (See Remark 7 and Section 6). There are hyper-parameters, denoted as  $\theta$ , in the covariance kernel  $\mathcal{C}$ , e.g. variance magnitude ( $\kappa$ ) and correlation length ( $\rho$ ), i.e.  $\theta = (\kappa, \rho)$ , that require careful adjustment and fine tuning as in, e.g., Matérn kernel:

$$\mathcal{C}(t, t') = \kappa \frac{2^{1-\nu}}{\Gamma(\nu)} w^\nu K_\nu(w), \quad w = \sqrt{2\nu} (\|t - t'\|/\rho)^\nu. \quad (35)$$

Unless we assume the likelihood in the Bayesian inverse model (1) to be another q-ED and the forward mapping is linear [c.f. Theorem 3.5 of 47], we do not have a tractable marginal likelihood to optimize for these hyper-parameters [61]. In general settings, e.g., in the model (27) with a Gaussian likelihood, we need to jointly update  $(\Xi, \theta)$  based on (28) or  $(\mathbf{Z}, \theta)$  according to (31). Denote  $\mathbf{C}_0 = \kappa^{-1} \mathbf{C}$  and  $r_{0,\ell} = \xi_\ell^\top \mathbf{C}_0^{-1} \xi_\ell$ . The following proposition permits conditional conjugacy for the variance magnitude ( $\kappa$ ) given an appropriate hyper-prior.

**Proposition 5.1.** *If we assume a inverse-gamma hyper-prior for the variance magnitude  $\kappa^{\frac{q}{2}} \sim \Gamma^{-1}(\alpha, \beta)$  such that  $\xi_\ell | \kappa \stackrel{iid}{\sim} \text{q-ED}_J(\mathbf{0}, \mathbf{C})$  in (27), then we have*

$$\kappa^{\frac{q}{2}} | \mathbf{u} \sim \Gamma^{-1}(\alpha', \beta'), \quad \alpha' = \alpha + \frac{JL}{2}, \quad \beta' = \beta + \frac{1}{2} \sum_{\ell=1}^L r_{0,\ell}^{\frac{q}{2}} \quad (36)$$

*Proof.* See Appendix B. □

Therefore, we could either update  $\kappa \leftarrow \left( \frac{\beta'}{\alpha'+1} \right)^{\frac{2}{q}}$  or sample  $\kappa$  according to (36). In general, there is no such conditional conjugacy for the correlation length ( $\rho$ ). We impose a hyper-prior for  $\rho$  and sample from  $p(\rho | \Xi)$ . Alternatively, one could also use Bayesian optimization methods [46, 18, 5] for tuning  $\rho$ .

## 6 Numerical Experiments

In this section, we compare the proposed STBP ( $\mathcal{STBP}(\mathcal{C}, B^{s,q}(\mathcal{Z}))$ ) with STGP (equivalent to  $\mathcal{STBP}(\mathcal{C}, B^{s,2}(\mathcal{Z}))$ ) and a time-uncorrelated prior ( $\mathcal{STBP}(\mathcal{I}, B^{s,q}(\mathcal{Z}))$ ) using a simulated regression, two dynamic tomography imaging examples and an inverse problem of recovering a spatiotemporal function. Since the main focus is to model inhomogeneous data such as images with edges, we tend to adopt sharper regularization and set  $q = 1$  for STBP throughout this section (See also Remark 8). Our numerical results demonstrate the advantage of Besov ( $L_1$ ) type priors over Gaussian ( $L_2$ ) type priors in modeling inhomogeneous data. Moreover, these examples highlight the importance of appropriately modeling temporal correlations in spatiotemporal inverse problems. All the computer codes are publicly available at <https://github.com/lanzithinking/Spatiotemporal-Besov-prior>.

In all these applications,  $u(\mathbf{x}_i, t_j)$  refers to the image pixel value of point  $\mathbf{x}_i$  at time  $t_j$  with resolution  $I = n_x \times n_y$ . To assess the quality of reconstructed images (viewed as inverse solutions  $u(\mathbf{x}, t)$  defined on 2d space, i.e.  $\mathcal{X} \subset \mathbb{R}^2$ ), we refer to several quantitative measures including the relative error,  $\text{RLE} = \frac{\|u^* - u^\dagger\|}{\|u^\dagger\|}$ , where  $u^\dagger$  denotes the reference/true image and  $u^*$  is its reconstruction. Additionally, we adopt the peak signal-to-noise ratio,  $\text{PSNR} = 10 * \log_{10}(\frac{\|u^\dagger\|_\infty^2}{\|u^* - u^\dagger\|_2^2})$ , by using the maximum possible pixel value as a reference point to normalise the MSE. We could also consider the structured similarity index [77],  $\text{SSIM}(u^*, u^\dagger) = \frac{(2\bar{u}^* \bar{u}^\dagger + c_1)(2s_{u^* u^\dagger} + c_2)}{(\bar{u}^{*2} + \bar{u}^{\dagger 2} + c_1)(s_{u^*}^2 + s_{u^\dagger}^2 + c_2)}$ , where  $\bar{u}$ ,  $s_u^2$  and  $s_{u_1 u_2}$  denote the sample mean, sample variance, and sample covariance respectively,  $c_i = (k_i L)^2$  for  $i = 1, 2$ ,  $k_1 = 0.01$ ,  $k_2 = 0.03$  and  $L$  is the dynamic range of the pixel values of the reference images. These image quality metrics are extensively used to benchmark algorithms in alignment with human perception, ensuring greater consistency.

### 6.1 Simulation

First, we consider a simulated regression problem of a rising and shrinking 2d annulus:

$$u(\mathbf{x}, t) = t\delta(\sin(\pi\|\mathbf{x}\|_2) \geq t), \quad \mathbf{x} \in \mathbb{R}^2 \text{ such that } \|\mathbf{x}\|_\infty \leq 1, \quad t \in (0, 1], \quad (37)$$

where  $\delta(\cdot)$  is the Dirac function returning 1 when the condition ( $\mathbf{x}$  is inside the 2d annulus) is met and 0 otherwise. The first column of Figure 2 plots this function at a few time points illustrating a 2d annulus forming and shrinking as time goes by. We simulate the data by discretizing the function  $u(\mathbf{x}, t)$  in (37) on a  $I = n_x \times n_y$  mesh (denoted as  $\mathbf{X}$ ) in the boxed spatial domain  $\mathcal{X} = [-1, 1]^2$  over a grid of  $J$  time points (denoted as  $\mathbf{t}$ ) in  $\mathcal{T} = (0, 1]$ , and adding some Gaussian noise with  $\sigma_\varepsilon = 0.1$ , i.e.

$$\mathbf{y}_j = u(\mathbf{X}, t_j) + \varepsilon_j, \quad \varepsilon_j \stackrel{iid}{\sim} \mathcal{N}_I(0, \sigma_\varepsilon^2 \mathbf{I}).$$

The noisy spatiotemporal data are demonstrated in the second column of Figure 2. Based on the observed data, the goal of this Bayesian inverse problem to recover the ground truth (37) using STBP, STGP and time-uncorrelated priors. We use this example to numerically investigate the posterior contraction studied in Section 4.2.2 as  $n = I \wedge J \rightarrow \infty$ . In particular, we will consider the problem with data observed at various spatiotemporal resolutions by combining  $I = 16 \times 16, 32 \times 32, 128 \times 128, 256 \times 256$  and  $J = 10, 20, 50, 100$  respectively.

Note, the spatial image of the function at each time point, when viewed as a picture, has clear edges. This imposes challenges for GP as it tends to over-smooth when modeling inhomogeneous objects while BP is more amenable. On the other hand, these sequential images are not isolated from each other in time, and the temporal kernel  $\mathcal{C}$  in STBP (STGP)

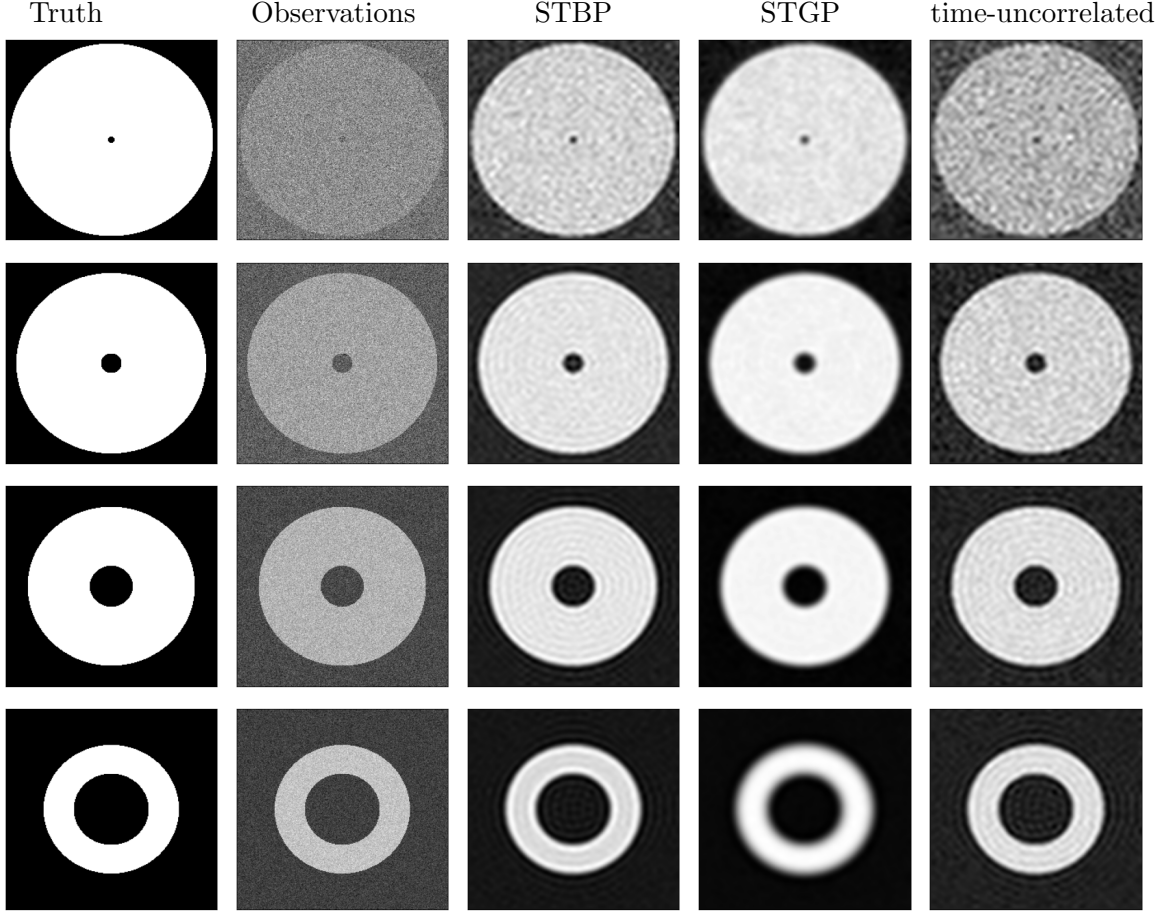


Figure 2: MAP reconstruction of simulated annulus with  $I = 256 \times 256$ ,  $J = 100$ . Columns from left to right: true images, observations, MAP estimates by STBP, STGP and time-uncorrelated models respectively. Rows from top to bottom: time step  $t_j = 0.1, 0.3, 0.6, 0.9$ .

can be well-used to capture such dependence. More specifically, we adopt the Matérn kernel (35) with  $\nu = \frac{1}{2}$ ,  $\sigma^2 = 1$ ,  $\rho = 0.1$  and  $s = 1$ . The MAP estimate for  $\mathbf{U} = u(\mathbf{X}, \mathbf{t})$  is obtained by minimizing the negative log-posterior (31) in the whitened space of  $\mathbf{Z}$  and converting  $\mathbf{Z}_{\text{MAP}}$  back to  $\mathbf{U}_{\text{MAP}} = T(\mathbf{Z}_{\text{MAP}})$ . The last three columns of Figure 2 compare the MAP estimates by STBP, STGP and time-uncorrelated models at  $I = 256 \times 256$ ,  $J = 100$ . The STGP model indeed returns an over-smoothed result; while the time-uncorrelated model yields a more noisy estimate due to the negligence of temporal correlation. Figure 10 also demonstrates different degrees of regularization interpolating with parameter  $q$  in the range of  $(0, 2]$  with  $q = 2$  (STGP) yielding the most blurry solution.

Next, we vary the spatiotemporal resolution by changing the mesh and the time interval for observations. Figure 3 investigates the MAP estimates by the STBP model with increasing data. They gradually approximate the true function (37) as the spatiotemporal resolution is refined. This verifies the posterior consistency described in Theorem 4.7 in terms of point estimation. Table 1 also shows an error reducing phenomenon with increasing data for all three models. To make a fair comparison across different resolutions, we adopt  $\|\mathbf{U}\|_{\infty, 1} = \max_{1 \leq i \leq I} \sum_{j=1}^J |u(\mathbf{x}_i, t_j)|$  in the RLE to focus on the pixel differences while averaging over the time domain. The STBP model outperforms the other two in most cases. Though not a direct verification of the posterior contraction rate Theorem 4.8, it shows that STBP reduces error with increasing data at rates not slower than STGP.

Table 1: Comparison of MAP estimates for simulated annulus generated by STBP, STGP and time-uncorrelated prior models in terms of RLE with increasing data. Standard deviations (in bracket) are obtained by repeating the experiments for 10 times with different random seeds for initialization.

$I = n_x \times n_y$	$J$	time-uncorrelated	STGP	STBP
16 × 16	10	0.2768 (5.32e-6)	0.2632 (7.91e-6)	0.2770 (4.14e-6)
	20	0.2399 (3.52e-6)	0.2063 (5.97e-6)	0.2421 (6.10e-6)
	50	0.2067 (1.02e-6)	0.1594 (1.08e-5)	0.1553 (1.07e-5)
	100	0.1850 (8.12e-7)	0.1217 (8.60e-6)	0.1211 (7.79e-6)
32 × 32	10	0.3677 (3.00e-6)	0.2465 (7.08e-6)	0.3672 (6.81e-6)
	20	0.2460 (1.49e-6)	0.1911 (4.88e-6)	0.2359 (5.02e-6)
	50	0.2236 (1.30e-6)	0.1464 (7.27e-6)	0.1662 (7.36e-6)
	100	0.1918 (9.90e-7)	0.1203 (7.73e-6)	0.1241 (9.31e-6)
128 × 128	10	0.1943 (1.57e-5)	0.2052 (4.51e-6)	0.1937 (1.36e-5)
	20	0.1474 (7.23e-6)	0.1497 (4.16e-6)	0.1399 (1.77e-5)
	50	0.1227 (4.95e-6)	0.1083 (1.03e-5)	0.1030 (1.51e-5)
	100	0.1146 (2.31e-6)	0.0934 (1.51e-5)	0.0909 (1.24e-5)
256 × 256	10	0.1635 (1.47e-5)	0.1970 (2.70e-6)	0.1633 (1.03e-5)
	20	0.1190 (7.24e-6)	0.1442 (7.18e-6)	0.1088 (1.24e-5)
	50	0.0966 (5.77e-6)	0.1012 (1.46e-5)	0.0858 (1.31e-5)
	100	0.0910 (3.89e-6)	0.0864 (6.68e-6)	0.0808 (1.36e-5)

## 6.2 Dynamic Tomography Reconstruction

In this section, we investigate the dynamic reconstruction of a simulated (STEMPO) and a real (emoji) tomography problems. Computed tomography (CT) is a medical imaging technique used to non-intrusively obtain detailed internal images of a subject such as human body [65, 28]. CT scanners project (Radon transformation) X-ray over the subject at different angles and measure the attenuated signals by an array of sensors recorded as sinograms. Reconstructing the (high-resolution) internal images from the limited observed sinograms is usually regarded as a linear inverse problem which is severely underdetermined (ill-posed). Therefore, appropriate (edge-preserving) priors are especially important for these tomography reconstruction problems.

### 6.2.1 STEMPO Tomography

In the first example, we consider a simulated dynamic tomography named Spatio-TEmporal Motor-POwered (STEMPO) ground truth phantom from [27]. The dataset contains 360 snapshots of CT images each of size  $I = 560 \times 560$  but we choose  $J = 20$  at equal time intervals. For each of  $J = 20$  snapshot, the ASTRA toolbox [See more details in 71] is used to generate the forward operators  $\mathcal{G}_j$ ,  $j = 1, 2, \dots, J$ . Each operator  $\mathcal{G}_j \in \mathbb{R}^{8701 \times 313600}$  then projects the true image  $u^\dagger(\mathbf{X}, t_j)$  to a sinogram  $\mathcal{G}_j(u^\dagger(\mathbf{X}, t_j)) \in \mathbb{R}^{791 \times 11}$  at  $n_a = 11$  angles ( $x$ -axis) with  $n_s = 791$  equally spaced X-ray detectors ( $y$ -axis) as shown in the second column of Figure 4. Finally, as in the model (27), Gaussian white noise  $\varepsilon_j \sim \mathcal{N}_{n_a n_s}(0, \sigma_j^2 \mathbf{I}_{n_a n_s})$  is added to the signogram to obtain the observation  $\mathbf{Y}_j = \mathcal{G}_j(u^\dagger(\mathbf{X}, t_j)) + \varepsilon_j$  such that the noise level  $\|\sigma_j\|_2 / \|\mathcal{G}_j(u^\dagger(\mathbf{X}, t_j))\|_2 = 0.01$ . The true images  $\{u^\dagger(\mathbf{X}, t_j)\}_{j=1}^J$  and the noisy observations  $\{\mathbf{Y}_j\}_{j=1}^J$  at time  $j = 0, 6, 13, 19$  are shown in the first two columns of Figure 4, respectively.

We minimize the negative log-posterior densities (31) in terms of the whitened coordinates

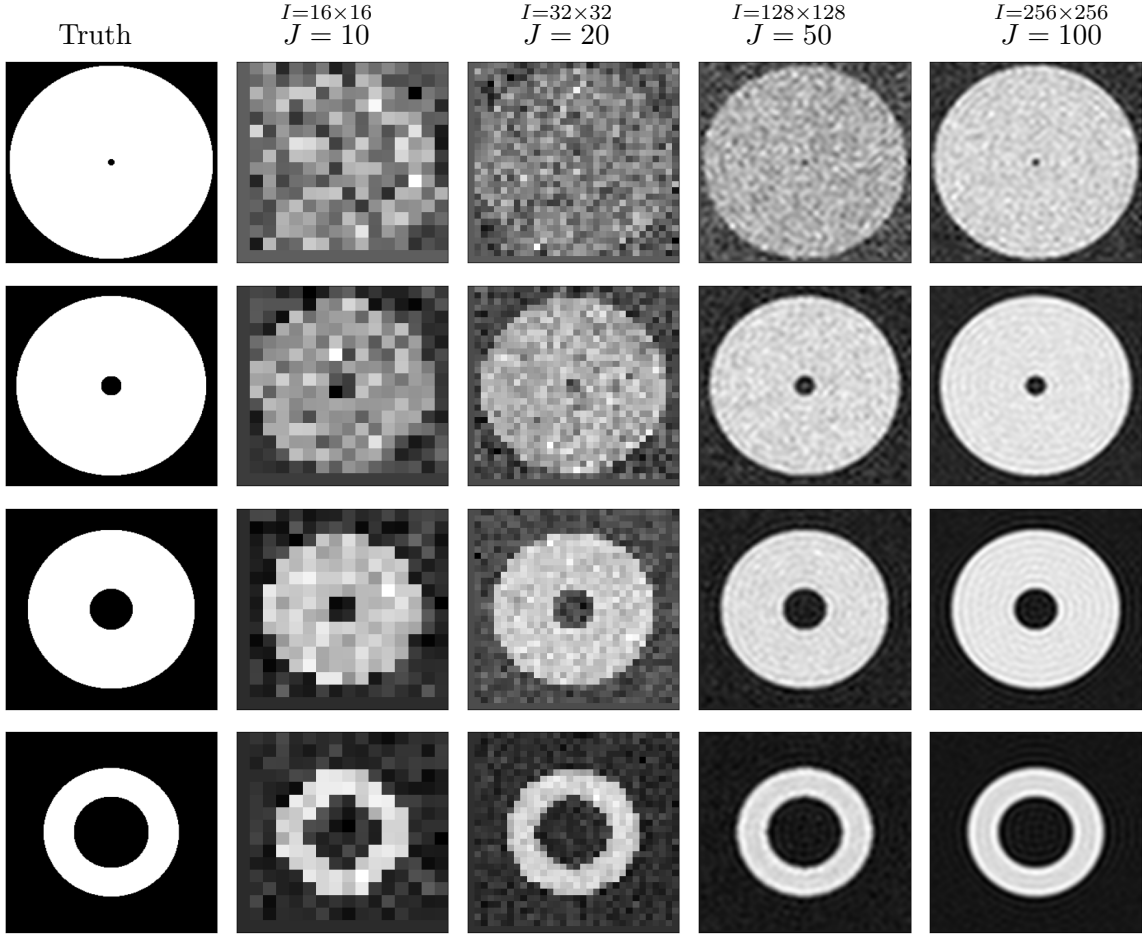


Figure 3: MAP reconstruction of simulated annulus by STBP model with increasing data. Columns from left to right: true images, MAP estimates obtained at different spatiotemporal resolutions. Rows from top to bottom: time step  $t_j = 0.1, 0.3, 0.6, 0.9$ .

$\mathbf{Z}$  for the three models with STBP, STGP and time-uncorrelated priors to obtain the MAP estimates. The rightmost three columns of Figure 4 compare these MAP estimates obtained in the whitened space and mapped to the original space. With STBP, we have the sharpest reconstruction on the third column that is the closest to the truth. However, the results by the other two models are either blurry (by STGP on the fourth column) or noisy (by the time-uncorrelated model on the last column). Table 2 confirms that the STBP model yields the reconstruction of the highest quality. Though their log-likelihood values are not comparable in the regularized optimization, the STBP model achieves the lowest  $\text{RLE} = 32.17\%$  on average in 10 experiments repeated with different random seeds. The same advantage is supported by high values in other image quality measures such as PSNR, and SSIM.

On the other hand, the MAP estimates generated by minimizing the negative log-posterior (28) in terms of the original parameters  $\mathbf{\Xi}$  are compared in Figure 11. They have more than 40% RLE's and are generally more blurry than those obtained in the whitened space (See Figure 4). Such difference is also observed in Figure 5 where the objective functions and RLE's are compared between optimization in the original space (w.r.t.  $\mathbf{\Xi}$ , left two panels) and optimization in the whitened space (w.r.t.  $\mathbf{Z}$ , right two panels) for these three models: the latter yields better results within fewer iterations bearing lower errors, possibly due to faster exploration in the whitened space with variables de-correlated. In general, STBP converges faster to the lowest error state among the three models.

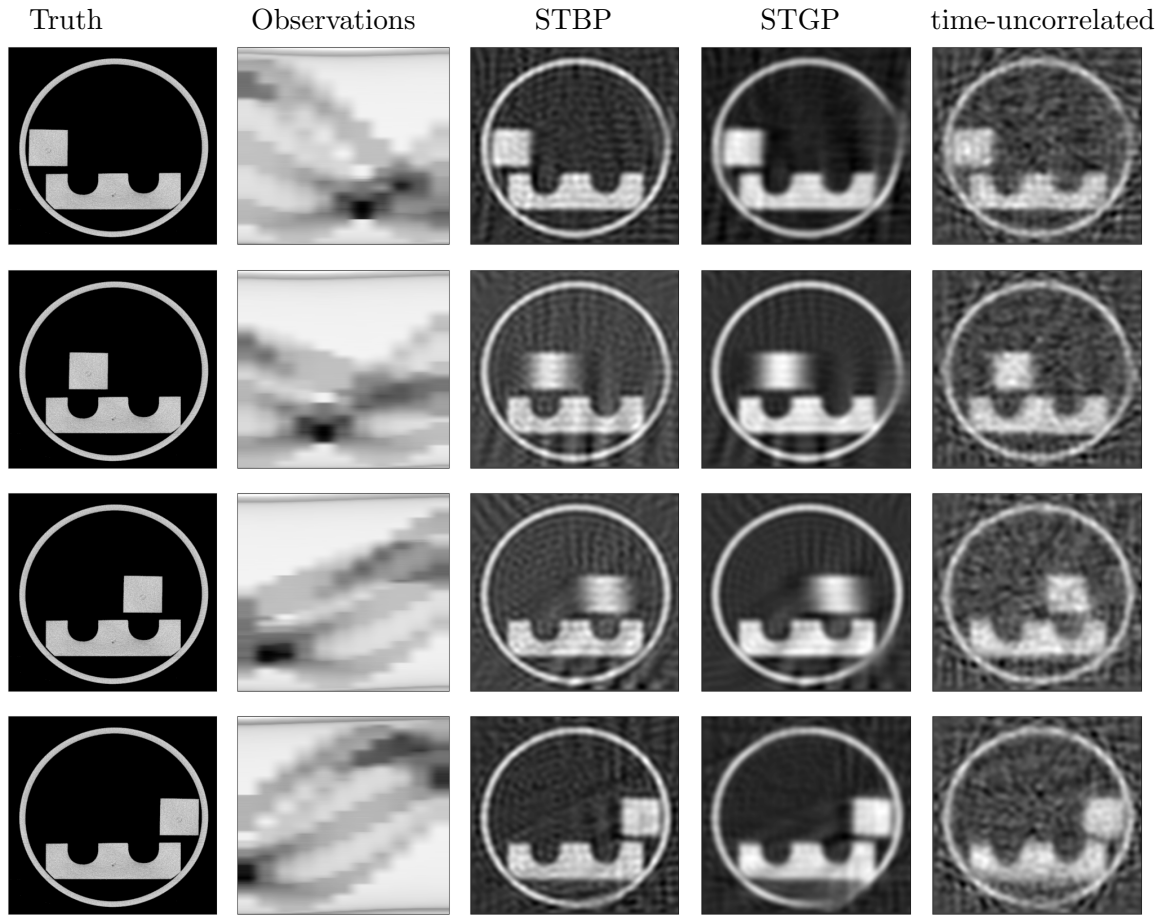


Figure 4: MAP reconstruction of dynamic STEMPO tomography in the whitened space. Columns from left to right: true images, sinograms, MAP estimates by STBP, STGP and time-uncorrelated models respectively. Rows from top to bottom: time step  $j = 0, 6, 13, 19$ .

Lastly, we apply the white-noise manifold infinite-dimensional MALA (wn- $\infty$ -mMALA) (Algorithm 1) to sample from the posterior distributions of the two models with STBP and STGP priors respectively (the result for time-uncorrelated prior is far worse and hence omitted) and compare their posterior estimates in Figure 6. We generate 3000 samples and discard the first 1000 samples. The remaining 2000 samples are used to estimate the posterior means (the second and the third columns) and posterior standard deviations (the last two columns). Due to the large dimensionality ( $560 \times 560 \times 20$ ) and limited number of samples, these posterior estimates tend to be noisy. The posterior mean estimates are not as good reconstructions as their MAP estimates. Yet the posterior standard deviations by STBP (the fourth column) provides uncertainty information with more clear spatial features than those by STGP model (the last column).

### 6.2.2 Emoji Tomography

Next, we test our methods on a real data of dynamic “emoji” phantom measured at the University of Helsinki [See more details in 51, about the machine (forward operator) set-up and data collection]. The available spatiotemporal data represent  $J = 33$  time steps of a series of the X-ray sinogram of emojis made of small ceramic stones obtained by shining  $n_s = 217$  X-ray projections from  $n_a = 10$  angles.

The inverse problem involves reconstructing a sequence of images  $u(\mathbf{X}, t_j)$ ,  $t = 1, 2, \dots, J$ ,

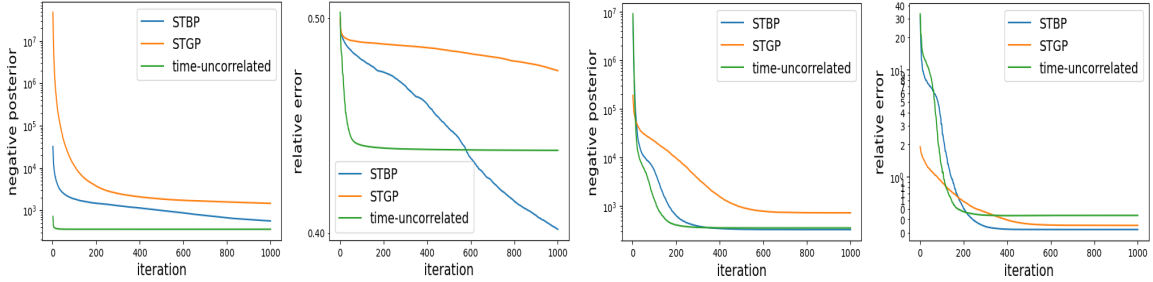


Figure 5: Dynamic STEMPO tomography reconstruction: negative posterior densities and relative errors for the optimization in the original space (left two) and in the whitened space (right two) as functions of iterations in the BFGS algorithm used to obtain MAP estimates. Early termination is implemented if the error falls below some threshold or the maximal iteration (1000) is reached.

Table 2: Comparison of MAP estimates for STEMPO tomography generated by STBP, STGP and time-uncorrelated prior models in terms of RLE, log-likelihood, PSNR, and SSIM measures. Standard deviations (in bracket) are obtained by repeating the experiments for 10 times with different random seeds for initialization.

	time-uncorrelated	STGP	STBP
RLE	0.4354 (2.91e-5)	0.3512(1.42e-4)	0.3217 (2.72e-5)
log-likelihood	-39190.72 (0.65)	-39085.37 (5.49)	-39697.93 (0.71)
PSNR	16.6235 (5.80e-4)	18.4896 (3.50e-3)	19.2532 (7.33e-4)
SSIM	0.1469 (3.50e-5)	0.3486 (3.47e-4)	0.2318 (7.10e-5)

each of size  $I = 128 \times 128$ , from low-dose observations measured at a limited number of  $n_a$  angles. Hence, the unknown images are collected in  $\mathbf{U} = u(\mathbf{X}, \mathbf{t}) \in \mathbb{R}^{16,384 \times 33}$ , representing the dynamic sequence of the emoji images changing from an expressionless face with closed eyes and a straight mouth to a face with smiling eyes and mouth, where the outmost circular shape does not change. We refer to Figure 7 for a sample of 4 setup images (first column) and sinograms (second column) at time steps  $t = 6, 14, 22, 30$ . The low-dose observations are modeled as in the model (27):  $\mathbf{Y}_j \sim \mathcal{N}_{2170}(\mathcal{G}_j(u^\dagger(\mathbf{X}, t_j)), \Gamma_{\text{noise}})$  with  $\Gamma_{\text{noise}}$  being the empirical covariance obtained from  $J = 33$  images, and measurement matrix  $\mathcal{G}_j$  being the result of the same Radon transform as above that represents line integrals [51]. Although the ground truth is not available, we can qualitatively compare the visual outputs from STBP, STGP and time-uncorrelated models.

Figure 7 compares the MAP estimates by STBP (the third column), STGP (the fourth row) and the time-uncorrelated (the last column) prior models in the whitened space. Again we observe similar advantage in reconstructing a sequence of sharper tomography images by STBP compared with those more blurry results by STGP. Note, due to the absence of temporal correlation, the time-uncorrelated prior model reconstructs images that are noisy and difficult to recognize. We also compare the UQ results generated by wn- $\infty$ -mMALA (See Algorithm 1) for the two models, STBP and STGP, respectively in Figure 13. Again we observe noisy posterior mean estimates (the second and the third columns) for both models. However, the posterior standard deviation estimates (the fourth column) by STBP are slightly clearer than those (the last column) by STGP in characterizing the uncertainty field representing the changing smiling faces.

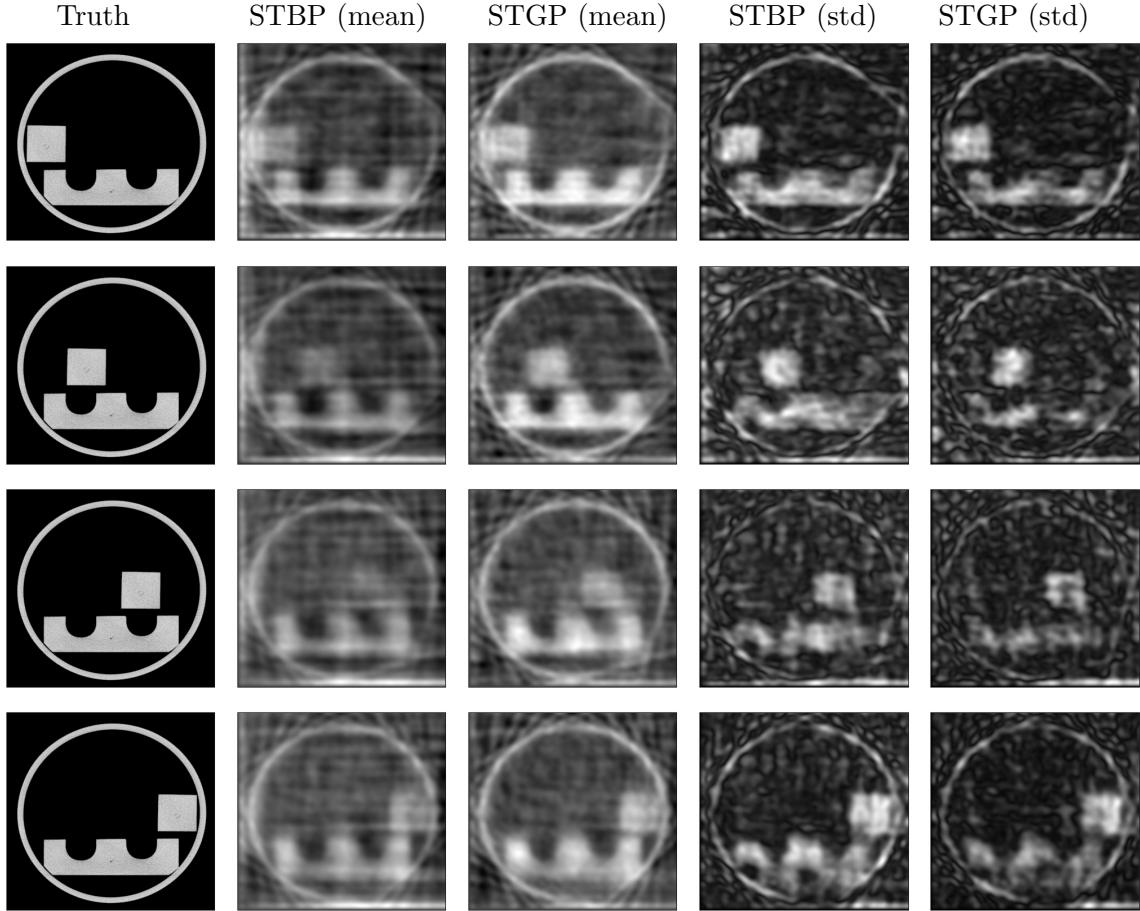


Figure 6: MCMC reconstruction of dynamic STEMPO tomography in the whitened space. Columns from left to right: true images, posterior mean estimates by STBP and STGP, posterior standard deviation estimates by STBP and STGP models respectively. Rows from top to bottom: time step  $j = 0, 6, 13, 19$ .

### 6.3 Navier-Stokes Inverse Problem

Lastly, we consider a complex non-linear inverse problem involving the following 2-d Navier-Stokes equation (NSE) for a viscous, incompressible fluid in vorticity form on the unit torus  $\mathbb{T}^2 = (0, 1)^2$ :

$$\begin{aligned}
\partial_t w(x, t) + u(x, t) \cdot \nabla w(x, t) &= \nu \Delta w(x, t) + f(x), & x \in (0, 1)^2, t \in (0, T], \\
\nabla \cdot u(x, t) &= 0, & x \in (0, 1)^2, t \in [0, T], \\
w(x, 0) &= w_0(x), & x \in (0, 1)^2.
\end{aligned}$$

where  $u \in C([0, T]; H^r(\mathbb{T}^2; \mathbb{R}^2))$  for any  $r > 0$  is the velocity field,  $w = \nabla \times u$  is the vorticity,  $w_0 \in L^2(\mathbb{T}^2; \mathbb{R})$  is the initial vorticity,  $\nu \in \mathbb{R}_+$  is the viscosity coefficient, and  $f \in L^2(\mathbb{T}^2; \mathbb{R})$  is the forcing function.

Because NSE is computationally intensive to solve, we build an emulator based on the Fourier operator neural network (FNO) [48, 38] that maps the vorticity up to time  $T_0 = 10$  to the vorticity up to some later time  $T > 10$ :

$$\mathcal{G} : C([0, T_0]; H^r(\mathbb{T}^2; \mathbb{R}^2)) \rightarrow C((T_0, T]; H^r(\mathbb{T}^2; \mathbb{R}^2)), \quad w|_{(0,1)^2 \times [0,10]} \mapsto w|_{(0,1)^2 \times (10,T]}$$

One of the attractive features of FNO is that the neural network is built to learn operators defined on function spaces. Compared with traditional neural networks for simulating PDE

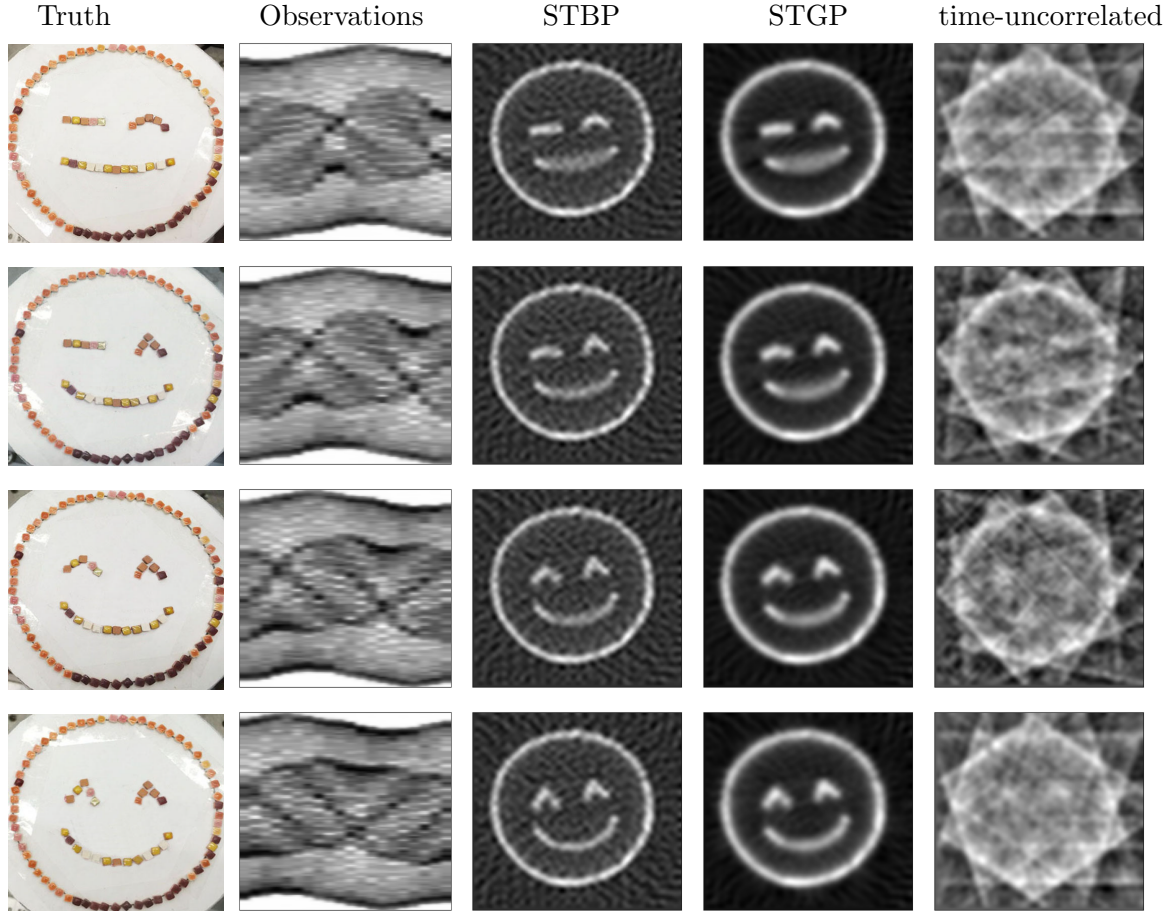


Figure 7: MAP reconstruction for the dynamic emoji tomography in the whitened space. Columns from left to right: true images, sinograms, MAP estimates by STBP, STGP and time-uncorrelated models respectively. Rows from top to bottom: time step  $j = 6, 14, 22, 30$ .

solutions including CNN [29, 75], PINNs [60], and ResNet [26], FNO is mesh-independent and very efficient for the inference of Bayesian inverse problem constrained by NSE.

In this example, we choose the viscosity  $\nu = 1e - 3$  and set  $T - T_0 = 30$ . Since the target operator,  $\mathcal{G}^\dagger$ , is time-dependent, we train a 3-d FNO (FNO-3d) based on 5000 pairs of input vorticity (for the first 10 unit time) and output vorticity (for the following 30 unit time) solved on  $I = 64 \times 64$  spatial mesh (denoted as  $\mathbf{X}$ ) using the network configuration the same as in [48]. We initialize the vorticity  $w_0$  with a (star-convex) polygon shown as in the top left of Figure 8 which also demonstrates a few snapshots of true vorticity trajectory,  $w^\dagger|_{(0,1)^2 \times [0,10]}(\mathbf{X}, t_j)$ , at  $j = 0, 3, 6, 9$  in the first column. We then observe data of vorticity  $w|_{(0,1)^2 \times (10,40]}(\mathbf{X}, t_j)$  with  $t_j \in (T_0, T]$  for  $j = 0, \dots, 29$  based on the true initial inputs  $w^\dagger|_{(0,1)^2 \times [0,10]}$ , with Gaussian noise contamination, i.e.,  $\mathbf{y}_j = \mathcal{G}(w^\dagger|_{(0,1)^2 \times [0,10]}(\mathbf{X}, t_j)) + \boldsymbol{\eta}_j$  with  $\boldsymbol{\eta}_j \sim N(0, \Gamma_{\text{noise}})$ , and  $\Gamma_{\text{noise}}$  empirically estimated as in the previous example. A few time snapshots of the observed vorticity are illustrated in the second column of Figure 8. Figure 14 compares the emulated NSE trajectory by the FNO network (lower row) against the true trajectory solved by the classical PDE solver (upper row) in the observation time window  $(T_0, T]$ . Their visual difference is hardly discernible.

Unlike the traditional time-dependent inverse problems seeking the solution of the initial condition  $w_0$  alone, we are interested in the inverse solution of vorticity for an initial period, i.e.,  $w|_{(0,1)^2 \times [0,10]}$ . What is more, we want to obtain UQ for such spatiotemporal object

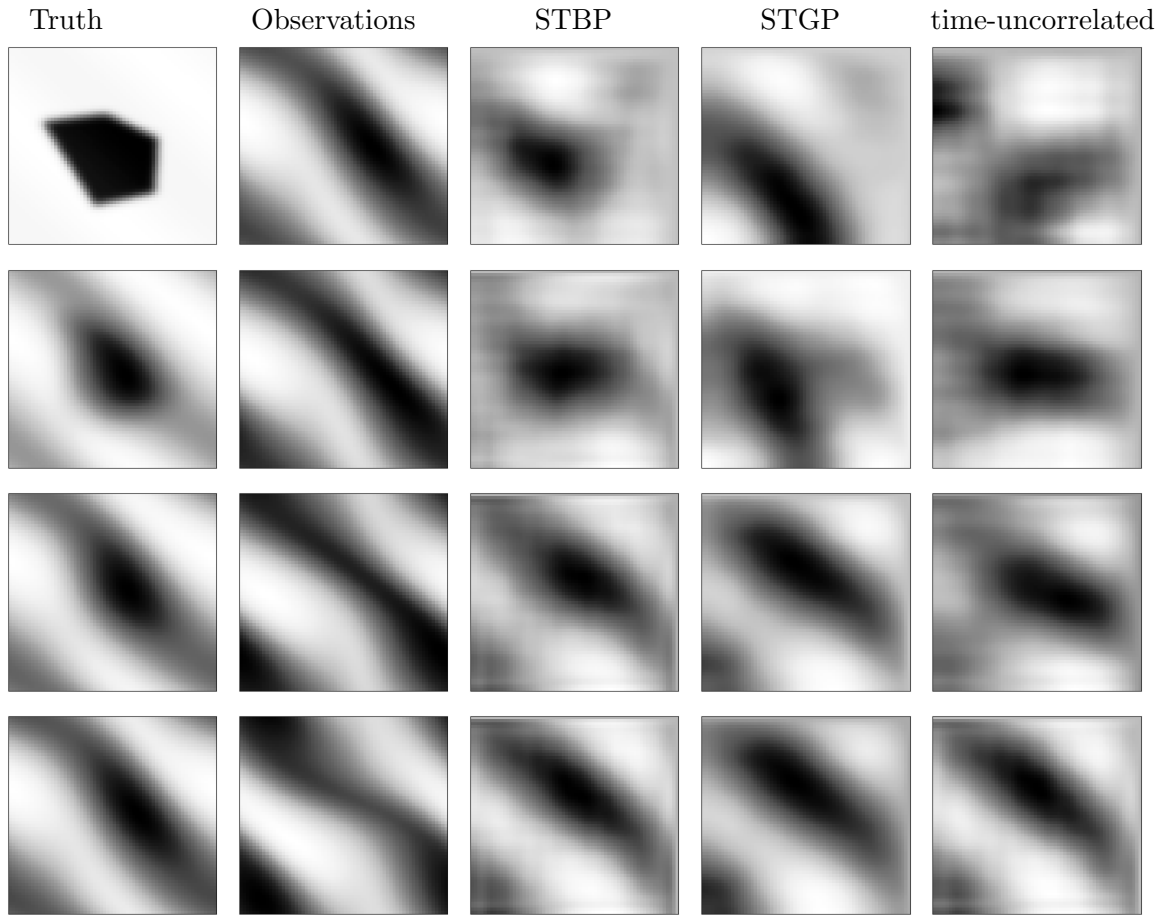


Figure 8: MAP inverse solutions of Navier-Stokes equation in the whitened space. Columns from left to right: true vorticity, observations, MAP estimates by STBP, STGP and time-uncorrelated models respectively. Rows from top to bottom: time step  $j = 0, 3, 6, 9$ .

in addition to its point estimate (MAP) using STBP, STGP and time-uncorrelated priors. Their MAP estimates are compared in the last three columns of Figure 8. Note, this inverse problem for a spatiotemporal solution is much more challenging than the traditional inverse problem for just the initial condition based on the same amount of downstream observations. STBP still yields the inverse solution (the third column) closest to the true trajectory (the first column) among the three models, especially the initial condition at  $t = 0$  (the first row) which is the most difficult because it is the farthest from the observation window  $(T_0, T]$ . Note, due to the lack of temporal correlation, the solution trajectory from the time-uncorrelated prior model appears excessively erratic. Table 3 further confirms that STBP prior model yields the best inverse solution with the lowest RLE, 66.18%, compared with the true trajectory, almost 10% lower than the other two methods. The high values of image reconstruction metrics also support the superiority of STBP model compared with the other two. Figure 9 compares the optimization objective (the negative log-posterior) and the relative error as functions of iterations. STBP converges to lower RLE value, while STGP terminates earlier at a higher RLE value.

Lastly, because of the computational cost, we apply white-noise infinite-dimensional HMC (wn- $\infty$ -HMC) (Algorithm 1) instead of wn- $\infty$ -mMALA for the UQ. We run 20,000 iterations, discard the first 5,000, and sub-sample one of every three. The remaining 5,000 samples are used to obtain posterior estimates illustrated in Figure 15 comparing STBP model (the

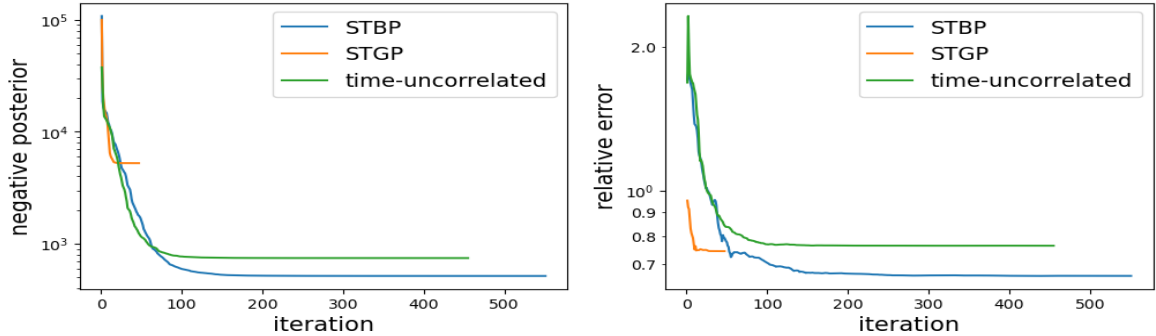


Figure 9: Navier-Stokes inverse problem: negative posterior densities (left) and relative errors (right) for the optimization in the whitened space as functions of iterations in the BFGS algorithm used to obtain MAP estimates. Early termination is implemented if the error falls below some threshold or the maximal iteration (1000) is reached.

Table 3: Comparison of MAP estimates of NSE trajectory generated by STBP, STGP and time-uncorrelated prior models in terms of RLE, log-likelihood, PSNR, and SSIM measures. Standard deviations (in bracket) are obtained by repeating the experiments for 10 times with different random seeds for initialization.

	time-uncorrelated	STGP	STBP
RLE	0.7656 (7.60e-5)	0.7457 (3.041e-5)	0.6618 (1.07e-4)
log-lik	-229.18 (0.21)	-1586.11 (0.47)	-173.33 (0.10)
PSNR	15.7267 (8.62e-4)	15.9555 (3.54e-4)	16.9921 (1.40e-3)
SSIM	0.1842 (7.84e-5)	0.2213 (5.68e-5)	0.3416 (1.67e-4)

second and the forth columns) against STGP model (the third and the last columns). The posterior mean by STBP (the second column) is more noisy compared with that by STGP (the third row). However the posterior standard deviation by STBP (the forth column) is more informative than that of STGP (the last column).

## 7 Conclusion

In this paper we propose a nonparametric Bayesian framework for spatiotemporal inverse problems with inhomogeneous data, such as sequential images with edges. Our proposed STBPs are generalizations of BP from spatial to spatiotemporal domain. The key idea is to replace the random coefficients (following a  $q$ -exponential distribution) in the series definition of BP with the recently proposed  $Q$ -EP [47] to account for the temporal correlations among spatial function images through a covariance kernel, similar to GP. Moreover, STBP controls the regularization of the posterior solutions through a parameter  $q \in [1, 2]$  and includes STGP as a special case ( $q = 2$ ).

We conduct a thorough theoretical investigation regarding well-definedness, Karhunen-Loève series representation of STBP priors and their posterior contraction property to justify the appropriateness and superiority of the proposed methodology. To address the challenges of posterior inference, we propose dimension-independent MCMC algorithms based on a new white-noise representation for series based priors [13]. Through extensive numerical experiments from various spatiotemporal inverse problems we demonstrate that STBP ( $q = 1$ ) has advantage in handling spatial inhomogeneity over STGP (which tends to be over-smooth) and

in capturing temporal correlations over a time-uncorrelated approach. These promising results from limited-angle CT reconstruction suggest potential applications in medical imaging analysis.

Several directions remain open for future research. Currently, the constraint of the STBP prior on a common spatial ( $q$ ) and temporal ( $p$ ) regularization parameter, i.e.,  $q = p$  (Section 4) can be relaxed to independently control the spatial and temporal regularities of the posterior solution – this might help with slow changing spatial data while  $L^2(\mathcal{T})$  ( $p = 2$ ) suffices the need for the temporal space. We also aim to extend the current work to the non-convex regime for  $q \in (0, 1)$ . It imposes more regularization than the adopted case ( $q = 1$ ) (refer to Figure 10) however the development is expected to be considerably more complex.

## Acknowledgments

SL is supported by NSF grant DMS-2134256. MP gratefully acknowledges support from the NSF award 2202846.

## References

- [1] Sergios Agapiou, Masoumeh Dashti, and Tapio Helin. Rates of contraction of posterior distributions based on p-exponential priors. *Bernoulli*, 27(3):1616 – 1642, 2021.
- [2] Yves A. Atchadaé. On the contraction properties of some high-dimensional quasi-posterior distributions. *The Annals of Statistics*, 45(5), October 2017.
- [3] Yves Atchade and Anwesha Bhattacharyya. An approach to large-scale quasi-bayesian inference with spike-and-slab priors. *arXiv:1803.10282*, 03 2018.
- [4] Frank Aurzada. On the lower tail probabilities of some random sequences in lp. *Journal of Theoretical Probability*, 20(4):843–858, Dec 2007.
- [5] Noor Awad, Neeratoy Mallik, and Frank Hutter. DEHB: Evolutionary hyperband for scalable, robust and efficient hyperparameter optimization. In *Proceedings of the Thirtieth International Joint Conference on Artificial Intelligence*. International Joint Conferences on Artificial Intelligence Organization, aug 2021.
- [6] A. Beskos, F. J. Pinski, J. M. Sanz-Serna, and A. M. Stuart. Hybrid Monte-Carlo on Hilbert spaces. *Stochastic Processes and their Applications*, 121:2201–2230, 2011.
- [7] Alexandros Beskos. A stable manifold MCMC method for high dimensions. *Statistics & Probability Letters*, 90:46–52, 2014.
- [8] Alexandros Beskos, Mark Girolami, Shiwei Lan, Patrick E. Farrell, and Andrew M. Stuart. Geometric MCMC for infinite-dimensional inverse problems. *Journal of Computational Physics*, 335, 2017.
- [9] Daniela Calvetti, Monica Pragliola, Erkki Somersalo, and Alexander Strang. Sparse reconstructions from few noisy data: analysis of hierarchical Bayesian models with generalized gamma hyperpriors. *Inverse Problems*, 36(2):025010, 2020.
- [10] Stamatis Cambanis, Steel Huang, and Gordon Simons. On the theory of elliptically contoured distributions. *Journal of Multivariate Analysis*, 11(3):368–385, 1981.
- [11] Carlos M Carvalho, Nicholas G Polson, and James G Scott. The horseshoe estimator for sparse signals. *Biometrika*, 97(2):465–480, 2010.

- [12] George Casella, Malay Ghosh, Jeff Gill, and Minjung Kyung. Penalized regression, standard errors, and Bayesian Lassos. *Bayesian analysis*, 5(2):369–411, 2010.
- [13] Victor Chen, Matthew M Dunlop, Omiros Papaspiliopoulos, and Andrew M Stuart. Dimension-robust mcmc in bayesian inverse problems. *arXiv preprint arXiv:1803.03344*, 2018.
- [14] Masoumeh Dashti, Stephen Harris, and Andrew Stuart. Besov priors for bayesian inverse problems. *Inverse Problems and Imaging*, 6(2):183–200, may 2012.
- [15] Masoumeh Dashti and Andrew M. Stuart. *The Bayesian Approach to Inverse Problems*, pages 311–428. Springer International Publishing, Cham, 2017.
- [16] Matthew M Dunlop and Andrew M Stuart. Map estimators for piecewise continuous inversion. *Inverse Problems*, 32(10):105003, 2016.
- [17] Heinz Werner Engl, Martin Hanke, and Andreas Neubauer. *Regularization of inverse problems*, volume 375. Springer Science & Business Media, 1996.
- [18] Stefan Falkner, Aaron Klein, and Frank Hutter. BOHB: Robust and efficient hyperparameter optimization at scale. In Jennifer Dy and Andreas Krause, editors, *Proceedings of the 35th International Conference on Machine Learning*, volume 80 of *Proceedings of Machine Learning Research*, pages 1437–1446. PMLR, 10–15 Jul 2018.
- [19] K. Fang and Y.T. Zhang. *Generalized Multivariate Analysis*. Science Press, 1990.
- [20] Chao Gao, Aad W. van der Vaart, and Harrison H. Zhou. A general framework for bayes structured linear models. *The Annals of Statistics*, 48(5), October 2020.
- [21] S. Ghosal and A.W. van der Vaart. Convergence rates of posterior distributions for non-i.i.d. observations. *Annals of Statistics*, 35(1):192–223, 2007. MR2332274.
- [22] Subhashis Ghosal and Aad van der Vaart. Fundamentals of nonparametric bayesian inference. 2017.
- [23] Evarist Giné and Richard Nickl. Rates of contraction for posterior distributions in  $L^r$ -metrics,  $1 \leq r \leq \infty$ . *The Annals of Statistics*, 39(6), December 2011.
- [24] Matteo Giordano. Besov-laplace priors in density estimation: optimal posterior contraction rates and adaptation. *Electronic Journal of Statistics*, 17(2), January 2023.
- [25] M. Hairer, A. M. Stuart, and J. Voss. Analysis of spdes arising in path sampling part ii: The nonlinear case. *The Annals of Applied Probability*, 17(5–6), October 2007.
- [26] Kaiming He, Xiangyu Zhang, Shaoqing Ren, and Jian Sun. *Deep Residual Learning for Image Recognition*. 2015.
- [27] Tommi Heikkilä. Stempo–dynamic X-ray tomography phantom. *arXiv preprint arXiv:2209.12471*, 2022.
- [28] Young M. Hermena S. Ct-scan image production procedures. StatPearls Publishing, August 2023.
- [29] Geoffrey Hinton. Imagenet classification with deep convolutional neural networks. *NIPS’12: Proceedings of the 25th International Conference on Neural Information Processing Systems - Volume 1*, 1:1097–1105, 2012.

- [30] Marco A Iglesias, Yulong Lu, and Andrew M Stuart. A bayesian level set method for geometric inverse problems. *Interfaces and free boundaries*, 18(2):181–217, 2016.
- [31] Hemant Ishwaran and J. Sunil Rao. Spike and slab variable selection: Frequentist and bayesian strategies. *The Annals of Statistics*, 33(2), April 2005.
- [32] Valentin Konstantinovich Ivanov. On linear problems which are not well-posed. In *Doklady akademii nauk*, volume 145, pages 270–272. Russian Academy of Sciences, 1962.
- [33] Junxiong Jia, Jigen Peng, and Jinghuai Gao. Bayesian approach to inverse problems for functions with a variable-index Besov prior. *Inverse Problems*, 32(8):085006, 2016.
- [34] Mark E. Johnson. *Multivariate Statistical Simulation*, chapter 6 Elliptically Contoured Distributions, pages 106–124. Probability and Statistics. John Wiley & Sons, Ltd, 1987.
- [35] Y. Kano. Consistency property of elliptic probability density functions. *Journal of Multivariate Analysis*, 51(1):139–147, 1994.
- [36] W Clem Karl. Regularization in image restoration and reconstruction. In *Handbook of Image and Video Processing*, pages 183–V. Elsevier, 2005.
- [37] Bartek T Knapik, Aad W Van Der Vaart, and J Harry van Zanten. Bayesian inverse problems with gaussian priors. *The Annals of Statistics*, 39(5):2626–2657, 2011.
- [38] Nikola Kovachki, Zongyi Li, Burigede Liu, Kamyar Azizzadenesheli, Kaushik Bhattacharya, Andrew Stuart, and Anima Anandkumar. Neural operator: Learning maps between function spaces with applications to pdes. *Journal of Machine Learning Research*, 24(89):1–97, 2023.
- [39] Tomasz J. Kozubowski, Krzysztof Podgórski, and Igor Rychlik. Multivariate generalized laplace distribution and related random fields. *Journal of Multivariate Analysis*, 113:59–72, 2013. Special Issue on Multivariate Distribution Theory in Memory of Samuel Kotz.
- [40] Shiwei Lan. Adaptive dimension reduction to accelerate infinite-dimensional geometric markov chain monte carlo. *Journal of Computational Physics*, 392:71 – 95, September 2019.
- [41] Shiwei Lan. Learning temporal evolution of spatial dependence with generalized spatiotemporal gaussian process models. *Journal of Machine Learning Research*, 23(259):1–53, 2022.
- [42] Matti Lassas, Eero Saksman, and Samuli Siltanen. Discretization-invariant bayesian inversion and besov space priors. *Inverse Problems and Imaging*, 3(1):87–122, 2009.
- [43] Matti Lassas and Samuli Siltanen. Can one use total variation prior for edge-preserving Bayesian inversion? *Inverse Problems*, 20(5):1537, 2004.
- [44] L. LeCam. Convergence of estimates under dimensionality restrictions. *The Annals of Statistics*, 1(1):38–53, Jan 1973.
- [45] J Lee and PK Kitanidis. Bayesian inversion with total variation prior for discrete geologic structure identification. *Water Resources Research*, 49(11):7658–7669, 2013.
- [46] Lisha Li, Kevin Jamieson, Giulia DeSalvo, Afshin Rostamizadeh, and Ameet Talwalkar. Hyperband: A novel bandit-based approach to hyperparameter optimization. *J. Mach. Learn. Res.*, 18(1):6765–6816, jan 2017.

- [47] Shuyi Li, Michael O’Connor, and Shiwei Lan. Bayesian learning via q-exponential process. In *Proceedings of the 37th Conference on Neural Information Processing Systems*. NeurIPS, 12 2023.
- [48] Zongyi Li, Nikola Borislavov Kovachki, Kamyar Azizzadenesheli, Burigede liu, Kaushik Bhattacharya, Andrew Stuart, and Anima Anandkumar. Fourier neural operator for parametric partial differential equations. In *International Conference on Learning Representations*, 2021.
- [49] David Madigan and Adrian E. Raftery. Model selection and accounting for model uncertainty in graphical models using occam’s window. *Journal of the American Statistical Association*, 89(428):1535–1546, December 1994.
- [50] Markku Markkanen, Lassi Roininen, Janne MJ Huttunen, and Sari Lasanen. Cauchy difference priors for edge-preserving Bayesian inversion. *Journal of Inverse and Ill-posed Problems*, 27(2):225–240, 2019.
- [51] Alexander Meaney, Zenith Purisha, and Samuli Siltanen. Tomographic x-ray data of 3d emoji. *arXiv preprint arXiv:1802.09397*, 2018.
- [52] T. J. Mitchell and J. J. Beauchamp. Bayesian variable selection in linear regression. *Journal of the American Statistical Association*, 83(404):1023–1032, December 1988.
- [53] R. M. Neal. MCMC using Hamiltonian dynamics. In S. Brooks, A. Gelman, G. Jones, and X. L. Meng, editors, *Handbook of Markov Chain Monte Carlo*. Chapman and Hall/CRC, 2010.
- [54] Bernt Øksendal. *Stochastic Differential Equations*. Springer Berlin Heidelberg, 2003.
- [55] Trevor Park and George Casella. The Bayesian Lasso. *Journal of the American Statistical Association*, 103(482):681–686, 2008.
- [56] Mirjeta Pasha, Arvind K. Saibaba, Silvia Gazzola, Malena I. Espa nol, and Eric de Sturler. A computational framework for edge-preserving regularization in dynamic inverse problems. *Electron. Trans. Numer. Anal.*, 58:486–516, 2023.
- [57] Juho Piironen and Aki Vehtari. Sparsity information and regularization in the horseshoe and other shrinkage priors. *Electronic Journal of Statistics*, 11(2), January 2017.
- [58] Krzysztof Podgórski and Jörg Wegener. Estimation for stochastic models driven by laplace motion. *Communications in Statistics - Theory and Methods*, 40(18):3281–3302, sep 2011.
- [59] Nicholas G. Polson, James G. Scott, and Jesse Windle. The Bayesian Bridge. *Journal of the Royal Statistical Society Series B: Statistical Methodology*, 76(4):713–733, 11 2013.
- [60] M. Raissi, P. Perdikaris, and G.E. Karniadakis. Physics-informed neural networks: A deep learning framework for solving forward and inverse problems involving nonlinear partial differential equations. *Journal of Computational Physics*, 378:686–707, 2019.
- [61] Carl Edward Rasmussen and Christopher K. I. Williams. *Gaussian Processes for Machine Learning*. The MIT Press, 2005.
- [62] Vincent Rivoirard and Judith Rousseau. Posterior concentration rates for infinite dimensional exponential families. *Bayesian Analysis*, 7(2), June 2012.

- [63] Uwe Schmidt, Kevin Schelten, and Stefan Roth. Bayesian deblurring with integrated noise estimation. In *CVPR 2011*, pages 2625–2632. IEEE, 2011.
- [64] I. J. Schoenberg. Metric spaces and completely monotone functions. *Annals of Mathematics*, 39:811–841, 1938.
- [65] L. A. Shepp and B. F. Logan. The fourier reconstruction of a head section. *IEEE Transactions on Nuclear Science*, 21(3):21–43, 1974.
- [66] Roel Snieder and Jeannot Trampert. Inverse problems in geophysics. In *Wavefield inversion*, pages 119–190. Springer, 1999.
- [67] Andrew M Stuart. Inverse problems: a Bayesian perspective. *Acta Numerica*, 19:451–559, 2010.
- [68] Jarkko Suuronen, Neil K. Chada, and Lassi Roininen. Cauchy markov random field priors for bayesian inversion. *Statistics and Computing*, 32(2):33, Mar 2022.
- [69] Andrey Nikolayevich Tikhonov. On the stability of inverse problems. In *Dokl. Akad. Nauk SSSR*, volume 39, pages 195–198, 1943.
- [70] Hans Triebel. *Theory of Function Spaces*. Springer Basel, 1983.
- [71] Wim Van Aarle, Willem Jan Palenstijn, Jan De Beenhouwer, Thomas Altantzis, Sara Bals, K Joost Batenburg, and Jan Sijbers. The ASTRA Toolbox: A platform for advanced algorithm development in electron tomography. *Ultramicroscopy*, 157:35–47, 2015.
- [72] A. W. van der Vaart and J. H. van Zanten. Rates of contraction of posterior distributions based on gaussian process priors. *The Annals of Statistics*, 36(3):1435–1463, 2008.
- [73] A. W. van der Vaart and J. H. van Zanten. Adaptive bayesian estimation using a gaussian random field with inverse gamma bandwidth. *Ann. Statist.*, 37(5B):2655–2675, 10 2009.
- [74] Aad van der Vaart and Harry van Zanten. Information rates of nonparametric gaussian process methods. *J. Mach. Learn. Res.*, 12:2095–2119, July 2011.
- [75] Ragav Venkatesan and Baoxin Li. *Convolutional Neural Networks in Visual Computing: A Concise Guide*. CRC Press, 2017.
- [76] Sebastian J Vollmer. Posterior consistency for bayesian inverse problems through stability and regression results. *Inverse Problems*, 29(12):125011, November 2013.
- [77] Zhou Wang, Alan C Bovik, Hamid R Sheikh, and Eero P Simoncelli. Image quality assessment: From error visibility to structural similarity. *IEEE transactions on image processing*, 13(4):600–612, 2004.
- [78] Zhewei Yao, Zixi Hu, and Jinglai Li. A tv-gaussian prior for infinite-dimensional bayesian inverse problems and its numerical implementations. *Inverse Problems*, 32(7):075006, May 2016.

# Appendix

## A Proofs

### A.1 Theorems of BP, STBP Priors

**Theorem 2.1.** *If  $u \sim \mathcal{B}(\kappa, B^{s,q}(\mathcal{X}))$  as in (8), then  $u \in L_{\mathbb{P}}^q(\Omega; B^{s',q}(\mathcal{X}))$  for all  $s' < s - \frac{d}{q}$ .*

*Proof of Theorem 2.1.* Based on (6), it is straightforward to verify

$$\mathbb{E}[\|u\|_{s',q}^q] = \sum_{\ell=1}^{\infty} \ell^{\tau_q(s')q} \mathbb{E}|u_{\ell}|^q = \kappa^{-1} \mathbb{E}[|\xi_1|^q] \sum_{\ell=1}^{\infty} \ell^{(\tau_q(s') - \tau_q(s))q} < \infty$$

if  $(\tau_q(s') - \tau_q(s))q = \frac{s'-s}{d}q < -1$ , i.e.  $s' < s - \frac{d}{q}$ .  $\square$

**Theorem 3.3.** *If  $\xi(\cdot) \sim \mathfrak{q} - \mathcal{EP}(0, \mathcal{C})$  with a trace-class HS operator  $T_{\mathcal{C}}$  satisfying Assumption 1-(i), then  $\xi(\cdot) \in L_{\mathbb{P}}^q(\Omega, B^{s',q}(\mathcal{T}))$ . If Assumption 1-(ii) holds instead, then  $\xi(\cdot) \in L_{\mathbb{P}}^q(\Omega, L^q(\mathcal{T}))$  and in particular  $\mathbb{E}[\|\xi(\cdot)\|_q^q] = \|\lambda\|_{\frac{q}{2}} < \infty$ .*

*Proof of Theorem 3.3.* Note  $r(\xi_{\ell})^{\frac{q}{2}} = \lambda_{\ell}^{-\frac{q}{2}} |\xi_{\ell}|^q \sim \chi^2(1)$  for all  $\ell \in \mathbb{N}$  by Proposition 3.1. Denote  $\chi_{\ell}^2 := \lambda_{\ell}^{-\frac{q}{2}} |\xi_{\ell}|^q \stackrel{iid}{\sim} \chi^2(1)$ . Hence  $\|\xi\|_{s',q}^q = \sum_{\ell=1}^{\infty} \ell^{\tau_q(s')q} \lambda_{\ell}^{\frac{q}{2}} \chi_{\ell}^2$  becomes an infinite mixture of chi-squared random variables whose density is analytically intractable. Yet we have

$$\mathbb{E}[\|\xi(\cdot)\|_{s',q}^q] = \sum_{\ell=1}^{\infty} \ell^{\tau_q(s')q} \lambda_{\ell}^{\frac{q}{2}} \mathbb{E}[\chi_{\ell}^2] = \sum_{\ell=1}^{\infty} \ell^{\tau_q(s')q} \lambda_{\ell}^{\frac{q}{2}} < \infty$$

if Assumption 1-(i) holds. From above we have  $\mathbb{E}[\|\xi(\cdot)\|_q^q] = \|\lambda\|_{\frac{q}{2}} < \infty$  if Assumption 1-(ii) holds.  $\square$

**Theorem 4.2.** *Let  $u \sim \mathcal{STBP}(\mathcal{C}, B^{s,q}(\mathcal{Z}))$  as in (21) satisfy both Assumptions 1-(ii) and 2. The following statements are equivalent:*

- (i)  $u \in B^{s',q}(\mathcal{Z})$   $\Pi$ -a.s.
- (ii)  $\mathbb{E}[\exp(\alpha \|u\|_{s',q}^q)] < \infty$  for any  $\alpha \in (0, (\sup_{\ell} \lambda_{\ell})^{-\frac{q}{2}}/2)$ .
- (iii)  $s' < s - \frac{d}{q}$ .

*Proof of Theorem 4.2.* First, by Assumption-2 and the proof of Theorem 3.3 we have

$$\|u\|_{s',q}^q = \sum_{\ell=1}^{\infty} \ell^{\tau_q(s')q} \|u_{\ell}(\cdot)\|_q^q = \sum_{\ell=1}^{\infty} \ell^{(\tau_q(s') - \tau_q(s))q} \|\xi_{\ell}(\cdot)\|_q^q = \sum_{\ell=1}^{\infty} \ell^{\frac{s'-s}{d}q} \sum_{\ell'=1}^{\infty} \lambda_{\ell'}^{\frac{q}{2}} \chi_{\ell\ell'}^2$$

where  $\chi_{\ell\ell'}^2 \stackrel{iid}{\sim} \chi^2(1)$ . Denote  $\alpha_{\ell\ell'} = \alpha \ell^{\frac{s'-s}{d}q} \lambda_{\ell'}^{\frac{q}{2}}$ . Then we have

$$\mathbb{E}[\exp(\alpha_{\ell\ell'} \chi_{\ell\ell'}^2)] = M_{\chi^2(1)}(\alpha_{\ell\ell'}) = [1 - 2\alpha_{\ell\ell'}]^{-\frac{1}{2}}, \quad \text{for } \alpha_{\ell\ell'} < \frac{1}{2}$$

(iii)  $\implies$  (ii). Now that

$$\mathbb{E}[\exp(\alpha \|u\|_{s',q}^q)] = \mathbb{E} \left[ \exp \left( \sum_{\ell=1}^{\infty} \sum_{\ell'=1}^{\infty} \alpha_{\ell\ell'} \chi_{\ell\ell'}^2 \right) \right] = \prod_{\ell=1}^{\infty} \prod_{\ell'=1}^{\infty} [1 - 2\alpha_{\ell\ell'}]^{-\frac{1}{2}}$$

Assume  $\alpha > 0$ , we have each item in the product bigger than 1. To bound such infinite product, it suffices to bound the following infinite sum

$$\sum_{\ell=1}^{\infty} \sum_{\ell'=1}^{\infty} \left( [1 - 2\alpha_{\ell\ell'}]^{-\frac{1}{2}} - 1 \right) = \sum_{\ell=1}^{\infty} \sum_{\ell'=1}^{\infty} \frac{2\alpha_{\ell\ell'}}{\sqrt{1 - 2\alpha_{\ell\ell'}} + 1 - 2\alpha_{\ell\ell'}} \leq \frac{2\alpha \sum_{\ell=1}^{\infty} \ell^{\frac{s'-s}{d}q} \|\lambda\|_{\infty}^{\frac{q}{2}}}{\sqrt{1 - 2\alpha \|\lambda\|_{\infty}^{\frac{q}{2}} + 1 - 2\alpha \|\lambda\|_{\infty}^{\frac{q}{2}}}}$$

By Assumptions 1-(ii), it is finite provided that  $\frac{s'-s}{d}q < -1$  and  $1 - 2\alpha \|\lambda\|_{\infty}^{\frac{q}{2}} > 0$ , that is,  $s' < s - \frac{d}{q}$  and  $\alpha < \frac{1}{2} \|\lambda\|_{\infty}^{-\frac{q}{2}}$  where  $\|\lambda\|_{\infty} = \sup_{\ell} \lambda_{\ell}$ .

(ii)  $\implies$  (i)  $\implies$  (iii). The proof remains the same as in [42, 15].  $\square$

**Proposition 4.1.** For  $q, q^{\dagger} \in [1, 2]$  and  $s' < s^{\dagger} - \left(\frac{d}{q^{\dagger}} - \frac{d}{q}\right)_+$  with  $x_+ := \max\{x, 0\}$ , we have  $B^{s^{\dagger}, q^{\dagger} \wedge q, q}(\mathcal{Z}) \hookrightarrow B^{s', q}$ , where  $q^{\dagger} \wedge q := \min\{q^{\dagger}, q\}$ .

*Proof of Proposition 4.1.* If  $q^{\dagger} = q$ , we have  $B^{s^{\dagger}, q^{\dagger}}(\mathcal{Z}) \subset B^{s', q}(\mathcal{Z})$  when  $s' < s^{\dagger}$ ; if  $q^{\dagger} > q$ , for  $u \in B^{s^{\dagger}, q^{\dagger}}(\mathcal{Z})$  by Hölder inequality with  $(\frac{q^{\dagger}}{q}, \frac{q^{\dagger}}{q^{\dagger}-q})$ ,

$$\begin{aligned} \|u\|_{s',q}^q &= \sum_{\ell=1}^{\infty} \ell^{\tau_q(s')q} \|u_{\ell}(\cdot)\|_q^q \leq \sum_{\ell=1}^{\infty} \ell^{\tau_{q^{\dagger}}(s^{\dagger})q} \|u_{\ell}(\cdot)\|_{q^{\dagger}}^q \ell^{(\tau_q(s') - \tau_{q^{\dagger}}(s^{\dagger}))q} \\ &\leq \|u\|_{s^{\dagger}, q^{\dagger}}^q \left[ \sum_{\ell=1}^{\infty} \ell^{(\tau_q(s') - \tau_{q^{\dagger}}(s^{\dagger}))qq^{\dagger}/(q^{\dagger}-q)} \right]^{1 - \frac{q}{q^{\dagger}}} < \infty \end{aligned} \quad (38)$$

holds when  $(\tau_q(s') - \tau_{q^{\dagger}}(s^{\dagger}))qq^{\dagger}/(q^{\dagger} - q) = \frac{(s'-s^{\dagger})/d}{\frac{1}{q} - \frac{1}{q^{\dagger}}} - 1 < -1$ , i.e.,  $s' < s^{\dagger}$ ; if  $q^{\dagger} < q$ , for  $u \in B^{s^{\dagger}, q^{\dagger}, q}(\mathcal{Z})$ , we have

$$\begin{aligned} \|u\|_{s',q}^q &= \sum_{\ell} \ell^{\tau_q(s')q} \|u_{\ell}(\cdot)\|_q^q = \sum_{\ell} \ell^{\tau_{q^{\dagger}}(s^{\dagger})q^{\dagger}} \|u_{\ell}(\cdot)\|_{q^{\dagger}}^{q^{\dagger}} \ell^{(\tau_q(s')q - \tau_{q^{\dagger}}(s^{\dagger})q^{\dagger})} \|u_{\ell}(\cdot)\|_q^{(q-q^{\dagger})} \\ &\leq \sum_{\ell} \ell^{\tau_{q^{\dagger}}(s^{\dagger})q^{\dagger}} \|u_{\ell}(\cdot)\|_{q^{\dagger}}^{q^{\dagger}} \ell^{(\tau_q(s')q - \tau_{q^{\dagger}}(s^{\dagger})q^{\dagger})} \|u\|_{s^{\dagger}, q^{\dagger}, q}^{(q-q^{\dagger})} \\ &= \|u\|_{s^{\dagger}, q^{\dagger}, q}^{(q-q^{\dagger})} \sum_{\ell} \ell^{\tau_{q^{\dagger}}(s^{\dagger})q^{\dagger}} \|u_{\ell}(\cdot)\|_{q^{\dagger}}^{q^{\dagger}} \ell^{(\tau_q(s') - \tau_{q^{\dagger}}(s^{\dagger}))q} \lesssim \|u\|_{s^{\dagger}, q^{\dagger}, q}^q \end{aligned} \quad (39)$$

holds when  $(\tau_q(s') - \tau_{q^{\dagger}}(s^{\dagger}))q = \left(\frac{s'-s^{\dagger}}{d} - \frac{1}{q} + \frac{1}{q^{\dagger}}\right)q < 0$ , i.e.,  $s' < s^{\dagger} + \frac{d}{q} - \frac{d}{q^{\dagger}}$ .  $\square$

**Theorem 4.3.** [Karhunen-Loève] If  $u \sim \mathcal{STBP}(\mathcal{C}, B^{s,q}(\mathcal{Z}))$  as in (21) with a trace-class HS operator  $T_{\mathcal{C}}$  having eigen-pairs  $\{\lambda_{\ell}, \psi_{\ell}(\cdot)\}_{\ell=1}^{\infty}$ , then we have the following series representation for  $u(\mathbf{z})$ :

$$u(\mathbf{z}) = \sum_{\ell=1}^{\infty} \sum_{\ell'=1}^{\infty} u_{\ell\ell'} \phi_{\ell}(\mathbf{x}) \psi_{\ell'}(t), \quad u_{\ell\ell'} := \int_{\mathcal{T}} u_{\ell}(t) \psi_{\ell'}(t) dt \sim \mathfrak{q}\text{-ED}(0, \gamma_{\ell}^2 \lambda_{\ell'}). \quad (22)$$

Moreover, the spatiotemporal covariance of STBP bears a separable structure, i.e.,

$$\text{Cov}(u(\mathbf{z}), u(\mathbf{z}')) = \sum_{\ell=1}^{\infty} \gamma_{\ell}^2 \phi_{\ell}(\mathbf{x}) \phi_{\ell}(\mathbf{x}') \mathcal{C}(t, t'). \quad (23)$$

*Proof of Theorem 4.3.* The series expansion (22) is the result of applying Theorem 3.2 to each  $\xi_\ell(\cdot) \stackrel{iid}{\sim} \mathcal{q}\text{-}\mathcal{EP}(0, \mathcal{C})$  and the convergence is in  $L^2_{\mathbb{P}}(\Omega, B^{s,2}(\mathcal{Z}))$ . We then directly compute the spatiotemporal covariance

$$\begin{aligned} & \text{Cov}(u(\mathbf{z}), u(\mathbf{z}')) \\ &= \mathbb{E}(u(\mathbf{z})u(\mathbf{z}')) = \mathbb{E} \left[ \sum_{\ell=1}^{\infty} \gamma_\ell \xi_\ell(t) \phi_\ell(\mathbf{x}) \sum_{\ell'=1}^{\infty} \gamma_{\ell'} \xi_{\ell'}(t') \phi_{\ell'}(\mathbf{x}') \right] \\ &= \sum_{\ell, \ell'=1}^{\infty} \gamma_\ell \gamma_{\ell'} \phi_\ell(\mathbf{x}) \phi_{\ell'}(\mathbf{x}') \mathbb{E}[\xi_\ell(t) \xi_{\ell'}(t')] = \sum_{\ell=1}^{\infty} \gamma_\ell^2 \phi_\ell(\mathbf{x}) \phi_\ell(\mathbf{x}') \mathbb{E}[\xi_\ell(t) \xi_\ell(t')] \\ &= \sum_{\ell=1}^{\infty} \gamma_\ell^2 \phi_\ell(\mathbf{x}) \phi_\ell(\mathbf{x}') \mathcal{C}(t, t') \end{aligned}$$

where we use the iid assumption of  $\xi_\ell(\cdot)$  so that  $\mathbb{E}[\xi_\ell(t) \xi_{\ell'}(t')] = \mathbb{E}[\xi_\ell(t) \xi_\ell(t')] \delta_{\ell\ell'}$ .  $\square$

**Theorem 4.4.** [*Hölder Continuity*] *Let  $u \sim \text{STBP}(\mathcal{C}, B^{s,q}(\mathcal{Z}))$  as in (21) satisfy both Assumptions 1-(ii) and 2. Suppose the spatial  $(\{\phi_\ell\}_{\ell=1}^{\infty})$  and temporal  $(\{\psi_{\ell'}\}_{\ell'=1}^{\infty})$  bases in the series representation (22) satisfy Assumption 3. Then for any  $\beta < \alpha$ , there exists a version  $\tilde{u}(\mathbf{z})$  of  $u(\mathbf{z})$  in  $C^{0,\beta}(\mathcal{Z}, B^{s,q}(\mathcal{Z}))$ .*

*Proof of Theorem 4.4.* Based on the series representation of  $u(\cdot)$  in (21), we have by Jensen's inequality

$$\begin{aligned} \mathbb{E}[\|u(\mathbf{z}) - u(\mathbf{z}')\|_{\tau_q(s'),q}^q] &\leq \sum_{\ell=1}^{\infty} \mathbb{E}[\ell^{(\tau_q(s') - \tau_q(s))q} |\phi_\ell(\mathbf{x}) \xi_\ell(t) - \phi_\ell(\mathbf{x}') \xi_\ell(t')|^q] \\ &\lesssim \sum_{\ell=1}^{\infty} \ell^{\frac{s'-s}{d}q} \mathbb{E}[|\Delta\phi_\ell|^q |\xi_\ell(t)|^q + |\phi_\ell(\mathbf{x}')|^q |\Delta\xi_\ell|^q] \quad (\text{convexity of } |\cdot|^q) \\ &\lesssim \sum_{\ell=1}^{\infty} \ell^{\frac{s'-s}{d}q} [L(\phi_\ell) |\mathbf{x} - \mathbf{x}'|^{q\alpha+d} + \|\phi_\ell(\cdot)\|_\infty^q \mathbb{E}|\Delta\xi_\ell|^q] \end{aligned}$$

where  $\Delta\phi = \phi(\mathbf{x}) - \phi(\mathbf{x}')$  and  $\Delta\xi = \xi(t) - \xi(t')$ . Now based on the series representation  $\xi(\cdot)$  in (12), by Jensen's inequality and the proof of Theorem 3.3 we have further for  $\forall \ell \in \mathbb{N}$  (due to the iid assumption of  $\xi_\ell(\cdot)$  in Assumption 2)

$$\mathbb{E}[|\Delta\xi_\ell|^q] \leq \sum_{\ell'=1}^{\infty} \mathbb{E}[|\xi_{\ell'}|^q |\psi_{\ell'}(t) - \psi_{\ell'}(t')|^q] \leq \sum_{\ell'=1}^{\infty} \lambda_{\ell'}^{\frac{q}{2}} L(\psi_{\ell'}) |t - t'|^{q\alpha+d}$$

Therefore by Assumption 3 we have

$$\begin{aligned} & \mathbb{E}[\|u(\mathbf{z}) - u(\mathbf{z}')\|_{\tau_q(s'),q}^q] \\ & \lesssim |\mathbf{x} - \mathbf{x}'|^{q\alpha+d} \sum_{\ell=1}^{\infty} \ell^{\frac{s'-s}{d}q} L(\phi_\ell) + |t - t'|^{q\alpha+d} \sum_{\ell=1}^{\infty} \ell^{\frac{s'-s}{d}q} \|\phi_\ell(\cdot)\|_\infty^q \sum_{\ell'=1}^{\infty} \lambda_{\ell'}^{\frac{q}{2}} L(\psi_{\ell'}) \lesssim |\mathbf{z} - \mathbf{z}'|^{q\alpha+d} \end{aligned}$$

The conclusion follows by the Kolmogorov continuity theorem [15].  $\square$

<sup>2</sup>A version of stochastic process  $u(\mathbf{z})$  is  $\tilde{u}(\mathbf{z})$  such that  $\mathbb{P}[\tilde{u}(\mathbf{z}) = u(\mathbf{z})] = 1$  for  $\forall \mathbf{z} \in \mathcal{Z}$ .

## A.2 Posterior Theorems of Inverse Problems with STBP Priors

**Theorem 4.5.** *[Well-definedness of Posterior] Let the potential function  $\Phi$  in (2) satisfy Assumption 4 (i)-(iii). If  $\Pi$  is an  $\mathcal{STBP}(\mathcal{C}, B^{s',q}(\mathcal{Z}))$  measure with  $s > s' + \frac{d}{q}$ , then  $\Pi^y \ll \Pi$  and satisfies*

$$\frac{d\Pi^y}{d\Pi}(u) = \frac{1}{Z(y)} \exp(-\Phi(u; y)), \quad (24)$$

with the normalizing factor  $0 < Z(y) = \int_{B^{s',q}(\mathcal{Z})} \exp(-\Phi(u; y)) \Pi(du) < \infty$ .

*Proof of Theorem 4.5.* The proof is based on [Theorem 3.2 of 14] and [Theorem 14 15] and we include it here for the completeness. Define  $\pi_0(du, dy) = \Pi(du) \otimes \mathbb{Q}_0(dy)$  and  $\pi(du, dy) = \Pi(du) \otimes \mathbb{Q}_u(dy)$ . We assume  $\mathbb{Q}_0 \ll \mathbb{Q}$  and the Radon-Nikodym derivative (2) holds for  $\Pi$ -a.s.. Thus, for fixed  $u$ ,  $\Phi(u; \cdot) : \mathbb{Y} \rightarrow \mathbb{R}$  is  $\mathbb{Q}_0$ -measurable and  $\int_{\mathbb{Y}} \exp(-\Phi(u; y)) \mathbb{Q}_0(dy) = 1$ . On other hand, by Assumption 4-(iii), we have  $\Phi(\cdot; y) : B^{s',q}(\mathcal{Z}) \rightarrow \mathbb{R}$  is continuous on  $B^{s',q}(\mathcal{Z})$ . By Corollary 4.1  $\Pi(B^{s',q}(\mathcal{Z})) = 1$ . Hence  $\Phi(\cdot; y)$  is  $\Pi$ -measurable. Therefore,  $\Phi$  is  $\pi_0$ -measurable and  $\pi \ll \pi_0$  with

$$\frac{d\pi}{d\pi_0}(u; y) = \exp(-\Phi(u; y)), \quad \int_{B^{s',q}(\mathcal{Z}) \times \mathbb{Y}} \exp(-\Phi(u; y)) \pi_0(du, dy) = 1$$

Then by [Lemma 5.3 of 25] (also [Theorem 13 of 15]), the conditional distribution  $\Pi^y(du) := \pi(du, dy' | y' = y) \ll \Pi(du) = \pi_0(du, dy' | y' = y)$  due to the definition of  $\pi_0$ . The same Lemma/Theorem implies (24) if the normalizing constant  $Z(y) > 0$ .

First, by Assumption 4-(i), we have

$$Z(y) = \int_{B^{s',q}(\mathcal{Z})} \exp(-\Phi(u; y)) \Pi(du) \leq \int_{B^{s',q}(\mathcal{Z})} \exp(-M + \alpha_1 \|u\|_{s',q}) \Pi(du) < \infty$$

where the boundedness is the result of Theorem 4.2-(ii). Now we show  $Z(y) > 0$ . By Theorem 4.1, we have  $R = \mathbb{E}\|u\|_{s',q} < \infty$ . Since  $\|u\|_{s',q}$  is nonnegative, we have  $\Pi(\|u\|_{s',q} < R) > 0$ . Let  $r = \max\{\|y\|_{\mathbb{Y}}, R\}$ . By Assumption 4-(ii), we have

$$Z(y) = \int_{B^{s',q}(\mathcal{Z})} \exp(-\Phi(u; y)) \Pi(du) \geq \int_{\|u\|_{s',q} < R} \exp(-K) \Pi(du) = \exp(-K) \Pi(\|u\|_{s',q} < R) > 0$$

□

**Theorem 4.6.** *[Well-posedness of Posterior] Let the potential function  $\Phi$  in (2) satisfy Assumption 4 (i)-(iv). If  $\Pi$  is an  $\mathcal{STBP}(\mathcal{C}, B^{s,q}(\mathcal{Z}))$  measure with  $s > s' + \frac{d}{q}$ , then*

$$d_H(\Pi^y, \Pi^{y'}) \leq C \|y - y'\|_{\mathbb{Y}},$$

where  $C = C(r)$  is a constant depending on  $r$  such that  $\max\{\|y\|_{\mathbb{Y}}, \|y'\|_{\mathbb{Y}}\} \leq r$ .

*Proof of Theorem 4.6.* The proof is based on [Theorem 3.3 of 14] and [Theorem 16 of 15] and included for the completeness. As in Theorem 4.5,  $Z(y), Z(y') \in (0, \infty)$ . We directly compute

$$\begin{aligned} 2d_H^2(\Pi^y, \Pi^{y'}) &= \int_{B^{s',q}(\mathcal{Z})} \left[ Z(y)^{-\frac{1}{2}} \exp\left(-\frac{1}{2}\Phi(u; y)\right) - Z(y')^{-\frac{1}{2}} \exp\left(-\frac{1}{2}\Phi(u; y')\right) \right]^2 \Pi(du) \\ &\leq \frac{2}{Z(y)} \int_{B^{s',q}(\mathcal{Z})} \left[ \exp\left(-\frac{1}{2}\Phi(u; y)\right) - \exp\left(-\frac{1}{2}\Phi(u; y')\right) \right]^2 \Pi(du) \\ &\quad + 2|Z(y)^{-\frac{1}{2}} - Z(y')^{-\frac{1}{2}}|^2 Z(y') \end{aligned}$$

By the mean value theorem and Assumptions 4 (i) and (iv), we have

$$\begin{aligned} & \int_{B^{s',q}(\mathcal{Z})} \left[ \exp\left(-\frac{1}{2}\Phi(u; y)\right) - \exp\left(-\frac{1}{2}\Phi(u; y')\right) \right]^2 \Pi(du) \\ & \leq \int_{B^{s',q}(\mathcal{Z})} \frac{1}{4} \exp(\alpha_1 \|u\|_{s',q} - M) \exp(2\alpha_2 \|u\|_{s',q} + 2C) \|y_1 - y_2\|_{\mathbb{Y}}^2 \Pi(du) \leq C \|y_1 - y_2\|_{\mathbb{Y}}^2 \end{aligned}$$

where the boundedness is the result of Theorem 4.2-(ii). By the mean value theorem, Jensen's inequality and Assumptions 4 (i) and (iv) we have

$$\begin{aligned} & 2|Z(y)^{-\frac{1}{2}} - Z(y')^{-\frac{1}{2}}|^2 Z(y') \leq C |Z(y) - Z(y')|^2 \\ & \leq C \left[ \int_{B^{s',q}(\mathcal{Z})} |\exp(-\Phi(u; y)) - \exp(-\Phi(u; y'))| \Pi(du) \right]^2 \\ & \leq C \int_{B^{s',q}(\mathcal{Z})} |\exp(-\Phi(u; y)) - \exp(-\Phi(u; y'))|^2 \Pi(du) \leq C \|y_1 - y_2\|_{\mathbb{Y}}^2 \end{aligned}$$

where we used the above result.  $\square$

**Theorem 4.7.** [Posterior Contraction] *Let  $u$  be an  $STBP(\mathcal{C}, B^{s,q}(\mathcal{Z}))$  random element as in (21) satisfying both Assumptions 1-(ii) and 2 in  $\Theta := B^{s',q}(\mathcal{Z})$  with  $s' < s - \frac{d}{q}$  and  $P_u^{(n)} := \bigotimes_{j=1}^n P_{u,j}$  be the product measure of  $Y^{(n)}$  parameterized by  $u$  with the potential function  $\Phi$  (2) satisfying Assumption 4 (i)-(iii). If the true value  $u^\dagger \in \Theta$  is in the support of  $u$ , and  $\varepsilon_n$  satisfies the rate equation  $\varphi_{u^\dagger}(\varepsilon_n) \leq n\varepsilon_n^2$  with  $\varepsilon_n \geq n^{-\frac{1}{2}}$ , then there exists  $\Theta_n \subset \Theta$  such that  $\Pi_n(u \in \Theta_n : d_{n,H}(u, u^\dagger) \geq M_n \varepsilon |Y^{(n)}) \rightarrow 0$  in  $P_{u^\dagger}^{(n)}$ -probability for every  $M_n \rightarrow \infty$ .*

Before we proceed with the proof, we need the following lemma to bound the Hellinger distance, Kullback-Leibler (K-L) divergence and K-L variation.

**Lemma A.1.** *Suppose the inverse model (1) has the potential function  $\Phi$  (2) satisfy Assumption 4-(iii). Then we have*

- $d_H(p_u, p_{u'}) \lesssim \|u - u'\|_{s',q}$
- $K(p_u, p_{u'}) \lesssim \|u - u'\|_{s',q}$
- $V(p_u, p_{u'}) \lesssim \|u - u'\|_{s',q}^2$

*Proof.* First, we consider K-L divergence:

$$K(p_u, p_{u'}) = \int \log \frac{p_u}{p_{u'}} p_u d\mu = \int (\Phi(u'; y) - \Phi(u; y)) p_u d\mu(y) \leq L \|u - u'\|_{s',q}$$

by Assumption 4-(iii). Similarly, we have for K-L variation:

$$V(p_u, p_{u'}) = \int \left( \log \frac{p_u}{p_{u'}} \right)^2 p_u d\mu = \int |\Phi(u'; y) - \Phi(u; y)|^2 p_u d\mu(y) \leq L^2 \|u - u'\|_{s',q}^2$$

Lastly, we bound the Hellinger distance:

$$\begin{aligned} 2d_H^2(p_u, p_{u'}) &= \int (\sqrt{p_u} - \sqrt{p_{u'}})^2 d\mu = \int \left[ 1 - \exp\left(\frac{1}{2}\Phi(u; y) - \frac{1}{2}\Phi(u'; y)\right) \right]^2 p_u d\mu(y) \\ &\leq \int \frac{C}{4} |\Phi(u'; y) - \Phi(u; y)|^2 p_u d\mu(y) \leq \frac{CL^2}{4} \|u - u'\|_{s',q}^2 \end{aligned}$$

where the inequality holds for  $\|u - u'\|_{s',q}^2$  small enough.  $\square$

*Proof of Theorem 4.7.* Based on [Theorem 1 of 21], it suffices to verify the following two conditions (the entropy condition (2.4), and the prior mass condition (2.5)) for some universal constants  $\eta, K > 0$  and sufficiently large  $k \in \mathbb{N}$ ,

$$\sup_{\varepsilon > \varepsilon_n} \log N(\eta\varepsilon/2, \{u \in \Theta_n : d_{n,H}(u, u^\dagger) < \varepsilon\}, d_{n,H}) \leq n\varepsilon_n^2 \quad (40)$$

$$\frac{\Pi_n(u \in \Theta_n : k\varepsilon_n < d_{n,H}(u, u^\dagger) \leq 2k\varepsilon_n)}{\Pi_n(B_n(u^\dagger, \varepsilon_n))} \leq e^{Kn\varepsilon_n^2 k^2/2} \quad (41)$$

where the left side of (40) is called *Le Cam dimension* [44], logarithm of the minimal number of  $d_{n,H}$ -balls of radius  $\xi\varepsilon/2$  needed to cover a ball of radius  $\varepsilon$  around the true value  $u^\dagger = \sum_{\ell=1}^{\infty} \gamma_\ell \xi_\ell^\dagger(t) \phi_\ell(\mathbf{x})$ ;  $B_n(u^\dagger, \varepsilon_n) = \{u \in \Theta : \frac{1}{n} K_j(u^\dagger, u) \leq \varepsilon^2, \frac{1}{n} V_j(u^\dagger, u) \leq \varepsilon^2\}$  with  $K_j(u^\dagger, u) = K(P_{u^\dagger, j}, P_{u, j})$  and  $V_j(u^\dagger, u) = V(P_{u^\dagger, j}, P_{u, j})$ .

We adopt the argument for infinite sequence of functions in [Theorem 4 of 41]. For each  $1 \leq \ell \leq n$ ,  $\xi_\ell(\cdot) \in B^{s', q}(\mathcal{T}) \subset L^q(\mathcal{T})$  satisfy conditions for Theorem 3.4. Therefore, there exists  $B_{n, \ell} \subset B^{s', q}(\mathcal{T})$  such that (15)-(17) hold for each  $\ell$  with  $B_n$  replaced by  $B_{n, \ell}$ , and  $\varepsilon_n$  replaced by  $\varepsilon_{n, \ell} = c2^{-\ell} \ell^{-\frac{s'-s}{d}} \varepsilon_n^2$  for some constant  $c > 0$ . Note, for given spatial basis  $\{\phi_\ell(\mathbf{x})\}_{\ell=1}^{\infty}$  and  $\gamma = \{\gamma_\ell\}_{\ell=1}^{\infty}$  in (21),  $u \in \Theta = B^{s', q}(\mathcal{Z})$  can be identified with  $\xi_{\mathcal{T}} = \{\xi_\ell(\cdot)\}_{\ell=1}^{\infty} \in \ell^{q, \tau_q(s')}(L^q(\mathcal{T}))$  through  $f_\gamma$  in Definition 4, i.e.  $\Theta \cong \ell^{q, \tau_q(s')}(L^q(\mathcal{T}))$ . Now we set

$$\Theta_n = \{u = f_\gamma(\xi_{\mathcal{T}}) \in \Theta \mid \xi_\ell(\cdot) \in B_{n, \ell}, \text{ for } \ell = 1, \dots, n\} \subset \Theta$$

For  $\forall u, u' \in \Theta_n$  such that  $\|\xi_\ell(\cdot) - \xi'_\ell(\cdot)\|_{s', q} \leq \varepsilon_{n, \ell}$  for  $\ell = 1, \dots, n$ , we have  $d_{n,H}(u, u') \lesssim \|u - u'\|_{s', q} \leq \varepsilon_n$  by Lemma A.1 and (15). Therefore  $N(\varepsilon_n, \Theta_n, d_{n,H}) = \max_{1 \leq \ell \leq n} N(4\varepsilon_{n, \ell}, B_{n, \ell}, \|\cdot\|_{s', q})$  and we have the following global entropy bound holds

$$\log N(\varepsilon_n, \Theta_n, d_{n,H}) \leq Rn(c2^{-\ell} \ell^{-\frac{s'-s}{d}} \varepsilon_n^2)^2 \leq n\varepsilon_n^2$$

for some  $1 \leq \ell \leq n$  and  $c > 0$ , which is stronger than the local entropy condition (40).

Now by Lemma A.1 and (17), we have

$$\begin{aligned} \Pi_n(B_n(u^\dagger, \varepsilon_n)) &\geq \Pi_n(\|u^\dagger - u\|_{s', q} \leq \varepsilon_n^2, \|u^\dagger - u\|_{s', q}^2 \leq \varepsilon_n^2) \\ &= \Pi_n(\|u^\dagger - u\|_{s', q}^q \leq \varepsilon_n^{2q}) \geq \exp \left\{ \sum_{\ell=1}^n \log \mu(\|\xi_\ell(\cdot) - \xi'_\ell(\cdot)\|_{s', q} < 2\varepsilon_{n, \ell}) \right\} \\ &\geq e^{-n \sum_{\ell=1}^n \varepsilon_{n, \ell}^2} = e^{-Knk^2 \varepsilon_n^4/2}, \quad \text{with } K = 2, k^2 = \sum_{\ell=1}^n 2^{-2\ell} \ell^{-2\frac{s'-s}{d}} \end{aligned}$$

Then the prior mass condition (41) is satisfied because the numerator is bounded by 1. The proof is hence completed.  $\square$

**Theorem 4.8.** [*Posterior Contraction Rate*] Let  $u$  be an  $\mathcal{STBP}(\mathcal{C}, B^{s, q}(\mathcal{Z}))$  random element in  $\Theta := B^{s', q}(\mathcal{Z})$  with  $s' < s - \frac{d}{q}$ . The rest of the settings are the same as in Theorem 4.7. If the true value  $u^\dagger \in B^{s^\dagger, q^\dagger}(\mathcal{Z})$  with  $s^\dagger > s' + \left(\frac{d}{q^\dagger} - \frac{d}{q}\right)_+$  and  $q^\dagger, q \in [1, 2]$ , then we have the rate of the posterior contraction as  $\varepsilon_n = n^{-\frac{\sigma(s, q, s^\dagger, q^\dagger) - s'}{2(\sigma(s, q, s^\dagger, q^\dagger) - s') + q(s - \sigma(s, q, s^\dagger, q^\dagger))}}$ , where  $\sigma(s, q, s^\dagger, q^\dagger) = \left(s - \frac{d}{q}\right) \wedge \left(s^\dagger - \left(\frac{d}{q^\dagger} - \frac{d}{q}\right)_+\right)$ .

The following lemma studies the small ball probability in the concentration function (25).

**Lemma A.2** (Small ball probability). *Let  $\Pi$  be an  $\mathcal{STBP}(\mathcal{C}, B^{s,q}(\mathcal{Z}))$  prior on  $B^{s',q}(\mathcal{Z})$  with  $s' < s - \frac{d}{q}$ . Then as  $\varepsilon \rightarrow 0$ , we have*

$$-\log \Pi(\|u\|_{s',q} \leq \varepsilon) \asymp \varepsilon^{-\frac{1}{\frac{s-s'}{d}-\frac{1}{q}}}$$

*Proof.* We can compute

$$\Pi(\|u\|_{s',q} \leq \varepsilon) = \mathbb{P} \left[ \sum_{\ell=1}^{\infty} (\ell^{\tau_q(s')-\tau_q(s)} \|\xi_\ell(\cdot)\|_q)^q \leq \varepsilon^q \right]$$

where  $\mathbb{P}$  is the probability measure on the infinite product space  $\Omega = (L^q(\mathcal{T}))^\infty$  as in Definition 4. From the proof of Theorem 3.3 we know  $\|\xi\|_q^q = \sum_{\ell=1}^{\infty} \lambda_\ell^{\frac{2}{q}} \chi_\ell^2$  is an infinite mixture of  $\chi^2(1)$  random variables, so the condition of [Theorem 4.2 of 4] is trivially met and we have

$$\log \mathbb{P} \left[ \sum_{\ell=1}^{\infty} (\ell^{\tau_q(s')-\tau_q(s)} \|\xi_\ell(\cdot)\|_q)^q \leq \varepsilon^q \right] \asymp \varepsilon^{-\frac{1}{\tau_q(s)-\tau_q(s')-\frac{1}{q}}}$$

□

The second lemma gives an upper bound of the first term of the concentration function (25).

**Lemma A.3** (Decentering function). *Assume  $u^\dagger \in B^{s^\dagger, q^\dagger}(\mathcal{Z})$  for some  $s^\dagger > s'$  and  $q^\dagger \in [1, 2]$ . Then as  $\varepsilon \rightarrow 0$ , we have the following bounds*

(i) *If  $q^\dagger \geq q$ , we require  $s^\dagger > s'$ :*

$$\inf_{h \in B^{s,q}(\mathcal{Z}) : \|h - u^\dagger\|_{s',q} \leq \varepsilon} \|h\|_{s,q}^q \lesssim \begin{cases} 1, & \text{if } s < s^\dagger \\ (-\log \varepsilon)^{1-\frac{q}{q^\dagger}}, & \text{if } s = s^\dagger \\ \varepsilon^{-\frac{s-s^\dagger}{s^\dagger-s'}(q \wedge q^\dagger)}, & \text{if } s > s^\dagger \end{cases}$$

(ii) *If  $q^\dagger < q$ , we restrict  $u^\dagger \in B^{s^\dagger, q^\dagger, q}(\mathcal{Z}) \subsetneq B^{s^\dagger, q^\dagger}(\mathcal{Z})$  and require  $s^\dagger > s' - \frac{d}{q} + \frac{d}{q^\dagger}$ :*

$$\inf_{h \in B^{s,q}(\mathcal{Z}) : \|h - u^\dagger\|_{s',q} \leq \varepsilon} \|h\|_{s,q}^q \lesssim \begin{cases} 1, & \text{if } s \leq s^\dagger + \frac{d}{q} - \frac{d}{q^\dagger} \\ \varepsilon^{-\frac{\frac{s-s^\dagger}{d}-\frac{1}{q}+\frac{1}{q^\dagger}}{\frac{s^\dagger-s'}{d}+\frac{1}{q}-\frac{1}{q^\dagger}} q}, & \text{if } s > s^\dagger + \frac{d}{q} - \frac{d}{q^\dagger} \end{cases}$$

*Proof.* First of all, by Proposition 4.1 we have  $B^{s^\dagger, q^\dagger \wedge q, q}(\mathcal{Z}) \subset B^{s', q}$  for  $s' < s^\dagger - \left(\frac{d}{q^\dagger} - \frac{d}{q}\right)_+$ .

Next, for given spatial basis  $\{\phi_\ell\}_{\ell=1}^\infty$  in Definition 4, we identify  $u^\dagger \in B^{s^\dagger, q^\dagger}$  with  $u_{\mathcal{T}}^\dagger = \{u_\ell^\dagger(\cdot)\}_{\ell=1}^\infty \in \ell^{q^\dagger, \tau_{q^\dagger}(s^\dagger)}(L^{q^\dagger}(\mathcal{T}))$ . Then we follow [1] to approximate  $u_{\mathcal{T}}^\dagger$  with  $h_{1:L} = \{u_\ell^\dagger(\cdot)\}_{\ell=1}^\infty$  where  $u_\ell^\dagger(\cdot) \equiv 0$  for all  $\ell > L$ . Note  $h_{1:L} \in \ell^{q, \tau_q(s)}(L^q(\mathcal{T}))$  for any finite  $L \in \mathbb{N}$ . Identifying  $h_{1:L}$  with  $h \in B^{s,q}(\mathcal{Z})$ , we use the similar argument as above to get

$$\|h - u^\dagger\|_{s',q}^q = \sum_{\ell=L+1}^{\infty} \ell^{\tau_q(s')q} \|u_\ell^\dagger(\cdot)\|_q^q \leq \begin{cases} \|u^\dagger\|_{s^\dagger, q^\dagger}^{q^\dagger} L^{\frac{s'-s^\dagger}{d} q^\dagger}, & \text{if } q^\dagger = q \\ \|u^\dagger\|_{s^\dagger, q^\dagger}^q L^{\frac{s'-s^\dagger}{d} q}, & \text{if } q^\dagger > q \\ \|u^\dagger\|_{s^\dagger, q^\dagger, q}^q L^{\left(\frac{s'-s^\dagger}{d}-\frac{1}{q}+\frac{1}{q^\dagger}\right)q}, & \text{if } q^\dagger < q \end{cases}$$

Therefore, to have  $\|h - u^\dagger\|_{s',q} \leq \varepsilon$  we let

$$L \gtrsim \begin{cases} \varepsilon^{-\frac{d}{s^\dagger - s'}}, & \text{if } q^\dagger \geq q \\ \varepsilon^{-\frac{1}{\frac{s^\dagger - s'}{d} + \frac{1}{q} - \frac{1}{q^\dagger}}}, & \text{if } q^\dagger < q \end{cases} \quad (42)$$

On the other hand, the infimum is less than  $\|h\|_{s,q}^q$  with above  $h$ , which can be bounded as follows. If  $q^\dagger = q$ ,

$$\|h\|_{s,q}^q = \sum_{\ell=1}^L \ell^{\tau_{q^\dagger}(s)q^\dagger} \|u_\ell^\dagger(\cdot)\|_{q^\dagger}^{q^\dagger} \leq \begin{cases} \|u^\dagger\|_{s^\dagger, q^\dagger}^{q^\dagger}, & \text{if } s \leq s^\dagger \\ \|u^\dagger\|_{s^\dagger, q^\dagger}^{q^\dagger} L^{\frac{s-s^\dagger}{d}q^\dagger}, & \text{if } s > s^\dagger \end{cases}$$

While if  $q^\dagger > q$ , by similar argument using Hölder inequality as in (38),

$$\|h\|_{s,q}^q = \sum_{\ell=1}^L \ell^{\tau_q(s)q} \|u_\ell^\dagger(\cdot)\|_q^q \leq \begin{cases} C \|u^\dagger\|_{s^\dagger, q^\dagger}^q, & \text{if } s < s^\dagger \\ \|u^\dagger\|_{s^\dagger, q^\dagger}^q (\log L)^{1-\frac{q}{q^\dagger}}, & \text{if } s = s^\dagger \\ \|u^\dagger\|_{s^\dagger, q^\dagger}^q L^{\frac{s-s^\dagger}{d}q}, & \text{if } s > s^\dagger \end{cases}$$

And if  $q^\dagger < q$ , by similar argument as in (39),

$$\|h\|_{s,q}^q = \sum_{\ell=1}^L \ell^{\tau_q(s)q} \|u_\ell^\dagger(\cdot)\|_q^q \leq \begin{cases} \|u^\dagger\|_{s^\dagger, q^\dagger}^q, & \text{if } s \leq s^\dagger + \frac{d}{q} - \frac{d}{q^\dagger} \\ \|u^\dagger\|_{s^\dagger, q^\dagger}^q L^{\left(\frac{s-s^\dagger}{d} - \frac{1}{q} + \frac{1}{q^\dagger}\right)q}, & \text{if } s > s^\dagger + \frac{d}{q} - \frac{d}{q^\dagger} \end{cases}$$

Substituting  $L$  in (42) to the above equations yields the conclusion.  $\square$

*Proof of Theorem 4.8.* By Lemmas A.2 and A.3, we have the following bounds for the concentration function (25) as  $\varepsilon \rightarrow 0$ , if  $q^\dagger \geq q$ ,

$$\varphi_{u^\dagger}(\varepsilon) \lesssim \begin{cases} 1 + \varepsilon^{-\frac{1}{\frac{s-s'}{d} - \frac{1}{q}}}, & \text{if } s < s^\dagger \\ (-\log \varepsilon)^{1-\frac{q}{q^\dagger}} + \varepsilon^{-\frac{1}{\frac{s-s'}{d} - \frac{1}{q}}}, & \text{if } s = s^\dagger \\ \varepsilon^{-\frac{s-s^\dagger}{s^\dagger - s'}(q \wedge q^\dagger)} + \varepsilon^{-\frac{1}{\frac{s-s'}{d} - \frac{1}{q}}}, & \text{if } s > s^\dagger \end{cases}$$

For  $s \leq s^\dagger$ , the bound is dominated by  $\varepsilon^{-\frac{1}{\frac{s-s'}{d} - \frac{1}{q}}}$ . For the last case, we need to determine a balancing point of  $s$  for the two terms by setting their powers equal. The calculation shows that if  $s \leq s^\dagger + \frac{d}{q}$ , the bound is still dominated by  $\varepsilon^{-\frac{1}{\frac{s-s'}{d} - \frac{1}{q}}}$ , but otherwise is dominated by  $\varepsilon^{-\frac{s-s^\dagger}{s^\dagger - s'}q}$ . Therefore, we have

$$\varphi_{u^\dagger}(\varepsilon) \lesssim \begin{cases} \varepsilon^{-\frac{1}{\frac{s-s'}{d} - \frac{1}{q}}}, & \text{if } s \leq s^\dagger + \frac{d}{q} \\ \varepsilon^{-\frac{s-s^\dagger}{s^\dagger - s'}q}, & \text{if } s > s^\dagger + \frac{d}{q} \end{cases}$$

We need to determine minimal  $\varepsilon_n$  such that  $\varphi_{u^\dagger}(\varepsilon_n) \leq n\varepsilon_n^2$ . Hence for  $q^\dagger \geq q$ ,

$$\varepsilon_n \asymp \begin{cases} n^{-\frac{q(s-s')-d}{2q(s-s')+(q-2)d}}, & \text{if } s \leq s^\dagger + \frac{d}{q} \\ n^{-\frac{s^\dagger - s'}{2(s^\dagger - s') + q(s-s^\dagger)}}, & \text{if } s > s^\dagger + \frac{d}{q} \end{cases}$$

Now if  $q^\dagger < q$ , by similar argument we have the concentration function (25) as  $\varepsilon \rightarrow 0$

$$\varphi_{u^\dagger}(\varepsilon) \lesssim \begin{cases} 1 + \varepsilon^{-\frac{1}{\frac{s-s'}{d}-\frac{1}{q}}}, & \text{if } s \leq s^\dagger + \frac{d}{q} - \frac{d}{q^\dagger} \\ \varepsilon^{-\frac{\frac{s-s^\dagger}{d}-\frac{1}{q}+\frac{1}{q^\dagger}}{\frac{s^\dagger-s'}{d}+\frac{1}{q}-\frac{1}{q^\dagger}}} q + \varepsilon^{-\frac{1}{\frac{s-s'}{d}-\frac{1}{q}}}, & \text{if } s > s^\dagger + \frac{d}{q} - \frac{d}{q^\dagger} \end{cases}$$

Thus the contraction rate for  $q^\dagger < q$  becomes

$$\varepsilon_n \asymp \begin{cases} n^{-\frac{q(s-s')-d}{2q(s-s')+(q-2)d}}, & \text{if } s \leq s^\dagger + \frac{2d}{q} - \frac{d}{q^\dagger} \\ n^{-\frac{s^\dagger-s'+\frac{d}{q}-\frac{d}{q^\dagger}}{2(s^\dagger-s')+q(s-s^\dagger)-(q-2)(\frac{d}{q}-\frac{d}{q^\dagger})}}, & \text{if } s > s^\dagger + \frac{2d}{q} - \frac{d}{q^\dagger} \end{cases}$$

Rewriting the equations into one yields the conclusion.  $\square$

**Theorem 4.9.** [Adaptive Posterior Contraction Rate] Let  $u$  be an  $\mathcal{STBP}(\mathcal{C}, B_\kappa^{s,q}(\mathcal{Z}))$  random element in  $\Theta := B_\kappa^{s',q}(\mathcal{Z})$  with  $s' < s - \frac{d}{q}$ . Suppose  $\varepsilon_n$  satisfies the rate equation  $\varphi_{u^\dagger, \kappa}(\varepsilon_n) \leq n\varepsilon_n^2$  with  $\varepsilon_n \geq n^{-\frac{1}{2}}$ . The rest of the settings are the same as in Theorem 4.7. If the true value  $u^\dagger \in B_\kappa^{s^\dagger, q^\dagger}(\mathcal{Z})$  with  $s^\dagger > s' + \left(\frac{d}{q^\dagger} - \frac{d}{q}\right)_+$  and  $1 \leq q^\dagger < q \leq 2$ , then the minimax posterior contraction rate  $\varepsilon_n^\dagger = n^{-\frac{s^\dagger}{2s^\dagger+d}}$  can be attained at  $s = \frac{s^\dagger(s^\dagger-s')}{s^\dagger + \left(\frac{d}{q^\dagger} - \frac{d}{q}\right)} + s'$  with

$$\text{the scaling factor } \kappa_n \asymp n^{-\frac{1}{2s^\dagger+d} \left[ -\frac{s^\dagger(s^\dagger-s')}{s^\dagger + \left(\frac{d}{q^\dagger} - \frac{d}{q}\right)} + \frac{d}{q} + s^\dagger \right]}.$$

*Proof of Theorem 4.9.* Denote the upper bound of the first term in the concentration in Lemma A.3 as  $d(\varepsilon)$ . By re-examining the proof of Theorem 4.8, we have the concentration function (26) bounded as

$$\varphi_{u^\dagger, \kappa}(\varepsilon) \lesssim \kappa^{-q} d(\varepsilon) + (\varepsilon/\kappa)^{-\frac{1}{\frac{s-s'}{d}-\frac{1}{q}}}$$

The optimal choice,  $\kappa \asymp d(\varepsilon)^{\frac{1}{q} - \frac{d}{q^2(s-s')}} \varepsilon^{\frac{d}{q(s-s')}}$ , is made by balancing the above two terms. Hence the concentration function bound becomes  $\varphi_{u^\dagger, \kappa}(\varepsilon) \lesssim d(\varepsilon)^{\frac{d}{q(s-s')}} \varepsilon^{-\frac{d}{s-s'}}$ . Note, most bounds in Lemma A.3 appears in the format of  $d(\varepsilon) \asymp \varepsilon^{-b}$  except when  $q^\dagger \geq q$  and  $s = s^\dagger$ . We substitute in and force the derived rate to be minimax:

$$n^{-\frac{1}{2 + \frac{db}{q(s-s')} + \frac{d}{s-s'}}} \asymp n^{-\frac{1}{2 + \frac{d}{s^\dagger}}}$$

which implies that  $b(s) = q\left(\frac{s-s'}{s^\dagger} - 1\right)$  and the corresponding scaling factor  $\kappa \asymp \varepsilon^{-\frac{s-s'-\frac{d}{q}}{s^\dagger} + 1}$ .

Next we examine whether the bound  $\varepsilon^{-b(s)} = \varepsilon^{-q\left(\frac{s-s'}{s^\dagger} - 1\right)}$  can be achieved as those  $d(\varepsilon)$  in Lemma A.3. If  $q^\dagger \geq q$ , setting  $b(s) = 0$  leads to  $s = s' + s^\dagger$  contradicting with  $s < s^\dagger$ ;  $b(s) = \frac{s-s^\dagger}{s^\dagger-s'}(q \wedge q^\dagger)$  yields  $s = s^\dagger + s' - (s^\dagger)^2/s'$  contradicting with  $s > s^\dagger$ ; Lastly,  $s = s^\dagger$  does not solve  $(-\log \varepsilon)^{\left(1-\frac{q}{q^\dagger}\right)\frac{d}{q(s-s')}} \varepsilon^{-\frac{d}{s-s'}} = \varepsilon^{-\frac{1}{2+\frac{d}{s^\dagger}}}$ . If  $q^\dagger < q$ ,  $s = s' + s^\dagger$  does not satisfy  $s \leq s^\dagger - \left(\frac{d}{q^\dagger} - \frac{d}{q}\right)$ ; solving  $b(s) = \frac{\frac{s-s^\dagger}{d}-\frac{1}{q}+\frac{1}{q^\dagger}}{\frac{s^\dagger-s'}{d}+\frac{1}{q}-\frac{1}{q^\dagger}} q$  gives  $s = \frac{s^\dagger(s^\dagger-s')}{s^\dagger + \left(\frac{d}{q^\dagger} - \frac{d}{q}\right)} + s'$ , which can be shown  $s > s^\dagger - \left(\frac{d}{q^\dagger} - \frac{d}{q}\right)$ . Hence, substitute the only feasible  $s$  and the minimax rate  $\varepsilon_n^\dagger$

into the above expression of  $\kappa$  and the scaling factor becomes  $\kappa_n \asymp (\varepsilon_n^\dagger)^{-\frac{s^\dagger - s'}{s' + \left(\frac{d}{q^\dagger} - \frac{d}{q}\right)} + \frac{d}{qs^\dagger} + 1} \asymp n^{-\frac{1}{2s^\dagger + d} \left[ -\frac{s^\dagger(s^\dagger - s')}{s' + \left(\frac{d}{q^\dagger} - \frac{d}{q}\right)} + \frac{d}{q} + s^\dagger \right]}$ .  $\square$

## B Inference

---

### Algorithm 1 White-noise dimension-independent MCMC (wn- $\infty$ -MCMC)

---

- 1: Initialize current state  $u^{(0)}$  and transform it into the whitened space  $\zeta^{(0)} = T^{-1}(u^{(0)})$
  - 2: Sample velocity  $\eta^{(0)} \sim \mathcal{N}(0, I)$
  - 3: Calculate current energy  $E_0 = \Phi(\zeta^{(0)}) - \frac{\varepsilon^2}{8} \|g(\zeta^{(0)})\|^2 + \frac{1}{2} \log |\mathcal{K}(\zeta^{(0)})|$
  - 4: **for**  $i = 0$  to  $I - 1$  **do**
  - 5:   Run  $\Psi_\varepsilon : (\zeta^{(i)}, \eta^{(i)}) \mapsto (\zeta^{(i+1)}, \eta^{(i+1)})$  according to (33).
  - 6:   Update the energy  $E_0 \leftarrow E_0 + \frac{\varepsilon}{2} (\langle g(\zeta^{(i)}), \eta^{(i)} \rangle + \langle g(\zeta^{(i+1)}), \eta^{(i+1)} \rangle)$
  - 7: **end for**
  - 8: Calculate new energy  $E_1 = \Phi(\zeta^{(I)}) - \frac{\varepsilon^2}{8} \|g(\zeta^{(I)})\|^2 + \frac{1}{2} \log |\mathcal{K}(\zeta^{(I)})|$
  - 9: Calculate acceptance probability  $a = \exp(-E_1 + E_0)$  according to (34).
  - 10: Accept  $\zeta^{(I)}$  with probability  $a$  for the next state  $\zeta'$  or set  $\zeta' = \zeta^{(0)}$ .
  - 11: Record the next state  $u' = T(\zeta')$  in the original space.
- 

**Proposition 5.1.** *If we assume a inverse-gamma hyper-prior for the variance magnitude  $\kappa^{\frac{q}{2}} \sim \Gamma^{-1}(\alpha, \beta)$  such that  $\xi_\ell | \kappa \stackrel{iid}{\sim} \text{q-ED}_J(\mathbf{0}, \mathbf{C})$  in (27), then we have*

$$\kappa^{\frac{q}{2}} | \mathbf{u} \sim \Gamma^{-1}(\alpha', \beta'), \quad \alpha' = \alpha + \frac{JL}{2}, \quad \beta' = \beta + \frac{1}{2} \sum_{\ell=1}^L r_{0,\ell}^{\frac{q}{2}} \quad (36)$$

*Proof of Proposition 5.1.* We can compute the joint density of  $\Xi$  and  $\kappa$

$$\begin{aligned} p(\Xi, \kappa) &= \prod_{\ell=1}^L p(\xi_\ell | \kappa) p(\kappa^q) \\ &= \left(\frac{q}{2}\right)^L (2\pi)^{-\frac{JL}{2}} |\mathbf{C}_0|^{-\frac{L}{2}} \prod_{\ell=1}^L r_{0,\ell}^{\left(\frac{q}{2}-1\right)\frac{J}{2}} \kappa^{-\frac{q}{2} \cdot \frac{JL}{2}} \exp \left\{ -\kappa^{-\frac{q}{2}} \sum_{\ell=1}^L \frac{r_{0,\ell}^{\frac{q}{2}}}{2} \right\} \frac{\beta^\alpha}{\Gamma(\alpha)} \kappa^{-\frac{q}{2}(\alpha+1)} \exp(-\beta \kappa^{-\frac{q}{2}}) \\ &\propto \left(\kappa^{\frac{q}{2}}\right)^{-(\alpha + \frac{JL}{2} + 1)} \exp \left\{ -\kappa^{-\frac{q}{2}} \left( \beta + \frac{1}{2} \sum_{\ell=1}^L r_{0,\ell}^{\frac{q}{2}} \right) \right\} \end{aligned}$$

By identifying the parameters for  $\kappa^{\frac{q}{2}}$  we recognize that  $\kappa^{\frac{q}{2}} | \Xi$  is another inverse-gamma with parameters  $\alpha'$  and  $\beta'$  as given.  $\square$

## C More Numerical Results

### C.1 Simulation

Figure 10 illustrates the regularization effect of parameter  $q > 0$  of STBP priors in the simulated regression problem of a shrinking annulus. When the regularization parameter  $q$  ranges in  $[0, 2]$ , the smaller  $q$  is, the more regularization it imposes hence the sharper MAP

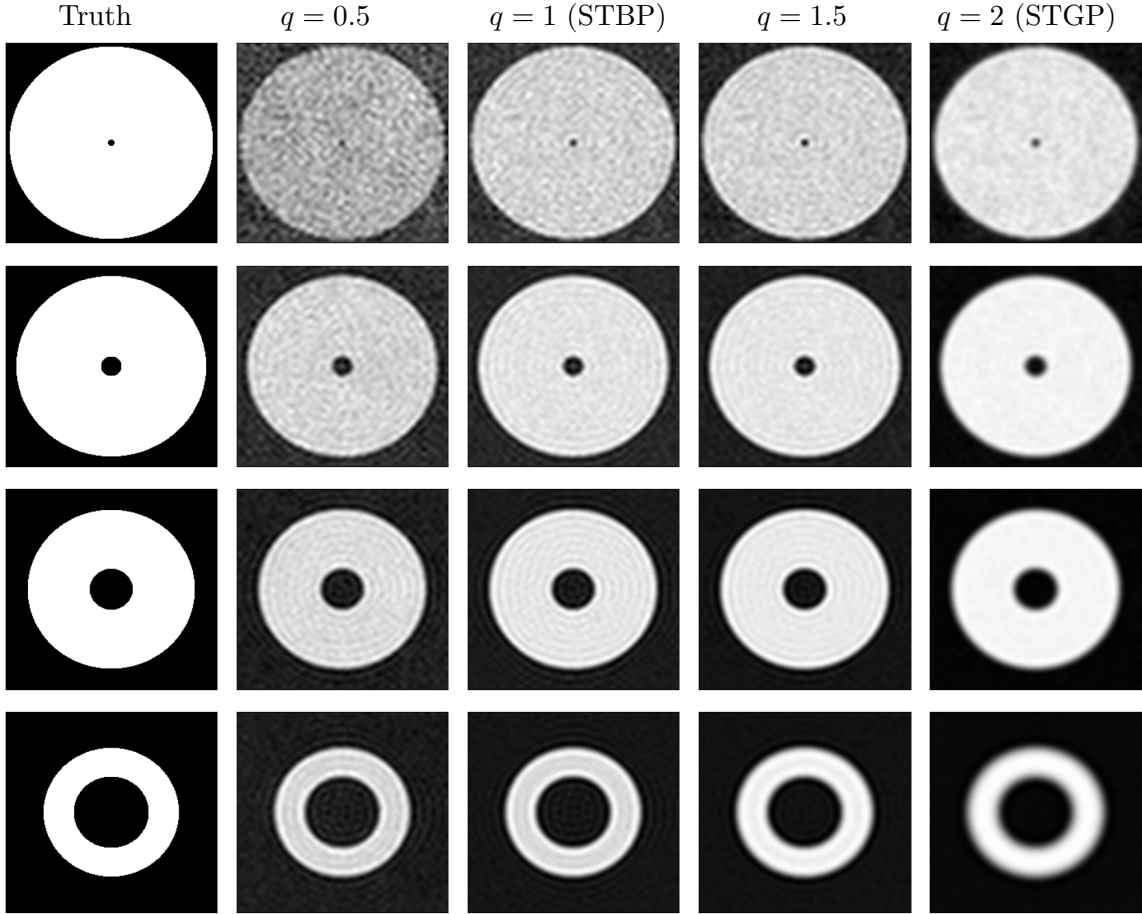


Figure 10: MAP reconstruction of simulated annulus with  $I = 256 \times 256$ ,  $J = 100$ . Columns from left to right: true images, MAP estimates by STBP models with  $q = 0.5, 1, 1.5, 2$  respectively. Rows from top to bottom: time step  $t_j = 0.1, 0.3, 0.6, 0.9$ .

solution the corresponding model renders compared with the truth. When  $q = 2$ , STBP reduces to STGP which returns the smoothest reconstruction with blurring boundaries. Even  $q = 0.5$  is not in the main range of interest  $[1, 2]$  where the associated priors have good properties, e.g. convexity, the resulting prior model still yields a solution (the second column) with the lowest error among the models for selective  $q$ 's.

## C.2 Dynamic Tomography Reconstruction

In Figure 11, MAP estimates of the dynamic STEMPO tomography obtained by optimizing the log-posterior 28 in the original space of  $\Xi$  are compared among STBP, STGP, and time-uncorrelated models. Although we still observe the better reconstruction by STBP (the third column) compared with the other two (the fourth and the last columns), these results are generally more noisy with larger errors compared with those obtained by optimizing (31) in the whitened space of  $\mathbf{Z}$ , as illustrated in Figure 4. Such comparison not only supports the superior performance of STBP, but also highlights the benefit of the white-noise representation (29), which is also verified in Figure 5.

Similarly in the example of dynamic reconstruction of emoji tomography, MAP estimates in the original space shown in Figure 12 demonstrate similar contrast among the three models, STBP, STGP and time-uncorrelated; but are also more blurry compared with those obtain in the whitened space as in Figure 7.

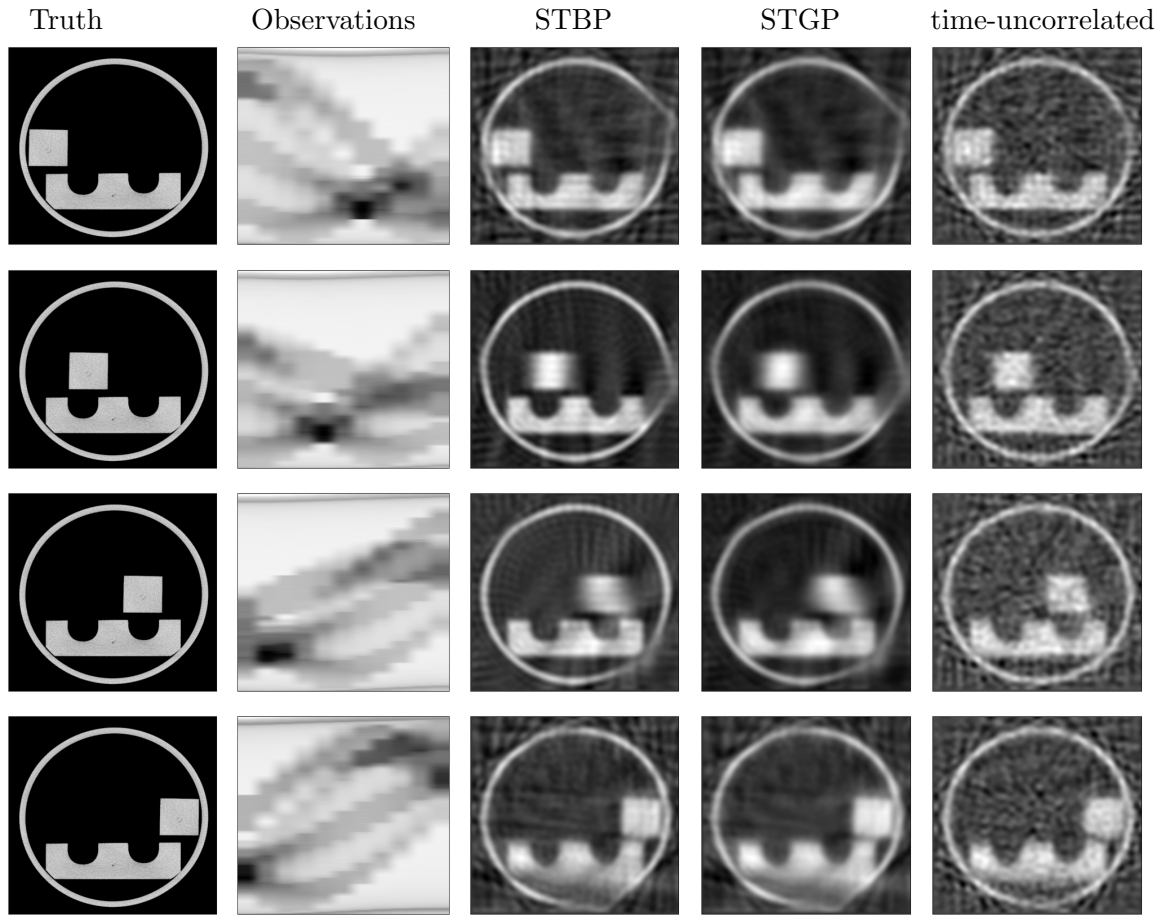


Figure 11: Reconstruction results of dynamic STEMPO tomography in the original space. Columns from left to right: true images, sinograms, MAP estimates by STBP, STGP and time-uncorrelated models respectively. Rows from top to bottom: time step  $j = 0, 6, 13, 19$ .

Finally, Figure 13 compares the MCMC estimates for the emoji tomography reconstruction in the whitened space by STBP and STGP models. They are all more noisy compared with MAP estimates plotted in Figure 7 due to the limited samples. The posterior standard deviations by the STBP model (the fourth column) possess slightly more recognizable spatial feature of smiling faces than these by the STGP model (the last column).

### C.3 Navier-Stokes Inverse Problems

In the inverse problem governed by the Navier-Stokes equation (NSE), Figure 14 compares the true trajectory of the vorticity solved by the classical PDE solver (upper row) for the time window  $(10, 40]$  with the one emulated by FNO network (lower row). The negligible difference indicates that the trained FNO network serves as a very precise emulator of the PDE solver that can facilitate the Bayesian inference, which requires expensive repeated PDE forward solving but it is now replaced by cheap emulation.

Figure 15 compares the MCMC estimates for the first 10 unit time vorticity of NSE obtained in the whitened space by STBP and STGP models. Albeit noisy, the posterior mean estimates by STBP (the second column) manifest spatial features closer to the truth compared with the those by STGP (the third column) model. For the UQ, posterior standard deviation results are not very informative for both models, but a few of them at later time ( $j = 6, 9$ ) show more spatial traits in the STBP model than in the STGP model.

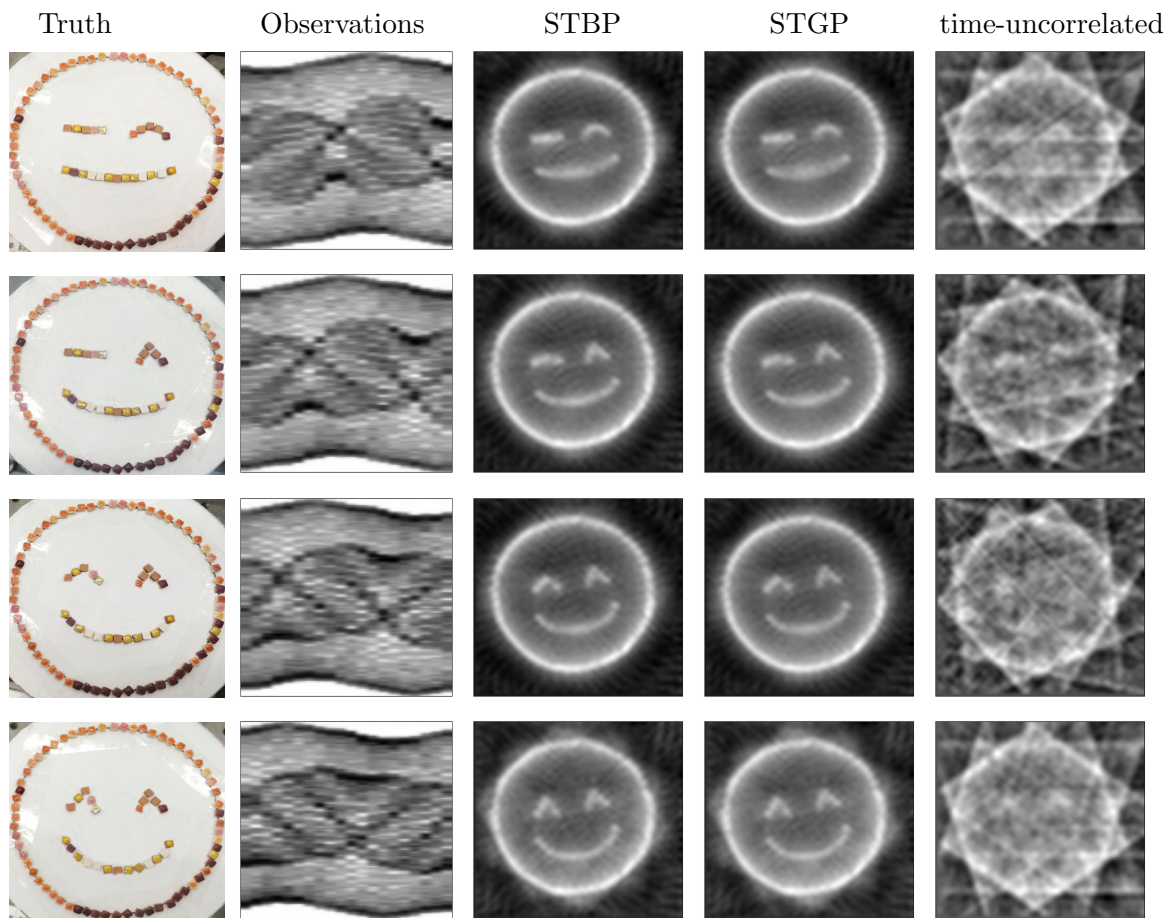


Figure 12: MAP reconstruction for the dynamic emoji tomography in the original space. Columns from left to right: true images, sinograms, MAP estimates by STBP, STGP and time-uncorrelated models respectively. Rows from top to bottom: time step  $j = 6, 14, 22, 30$ .

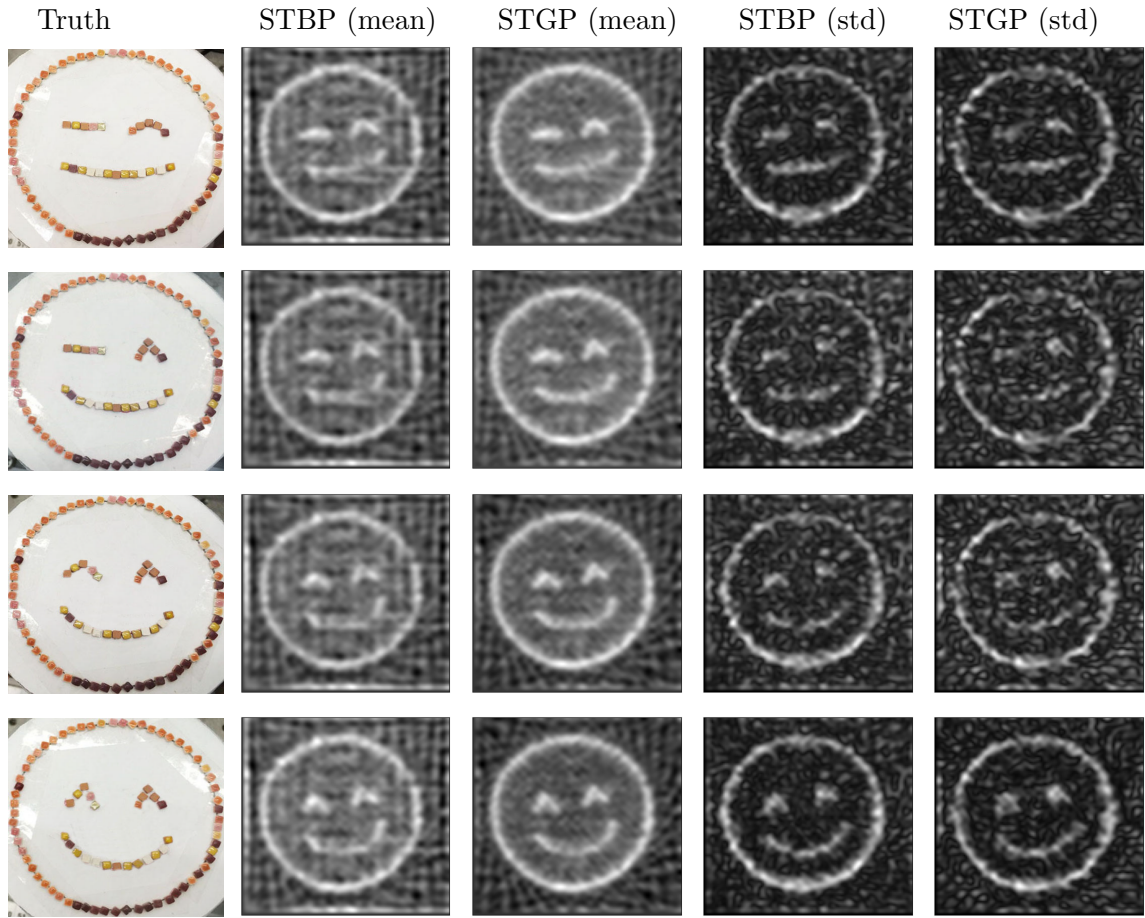


Figure 13: MCMC reconstruction of dynamic emoji tomography in the whitened space. Columns from left to right: true images, posterior mean estimates by STBP and STGP, posterior standard deviation estimates by STBP and STGP models respectively. Rows from top to bottom: time step  $j = 6, 14, 22, 30$ .

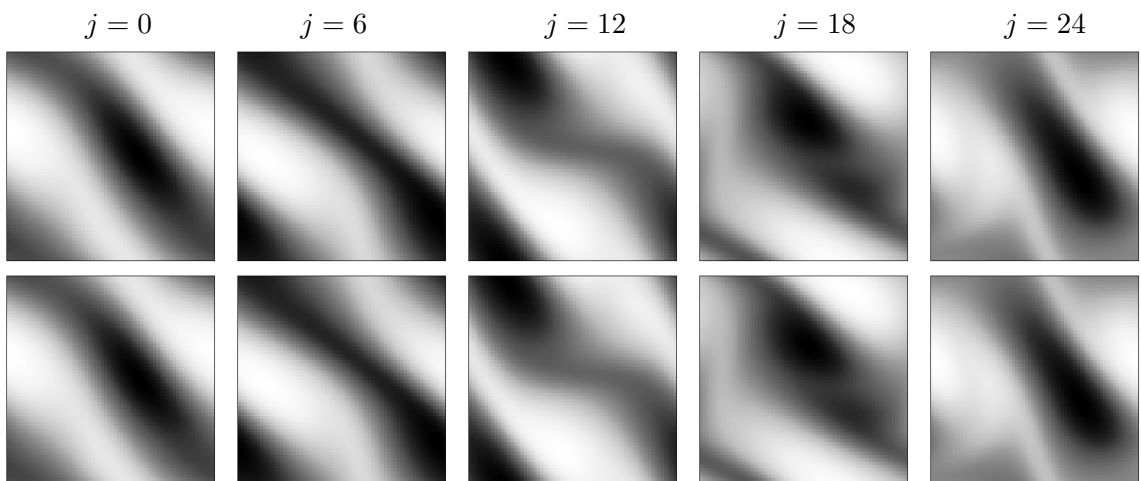


Figure 14: Observed and emulated Navier-Stokes equation solutions. Upper row: true NSE trajectory solved by classical PDE solver; Lower row: emulated NSE trajectory by FNO. Left to right: time step  $j = 0, 6, 12, 18, 24$  ( $t_j \in (10, 40]$ ).

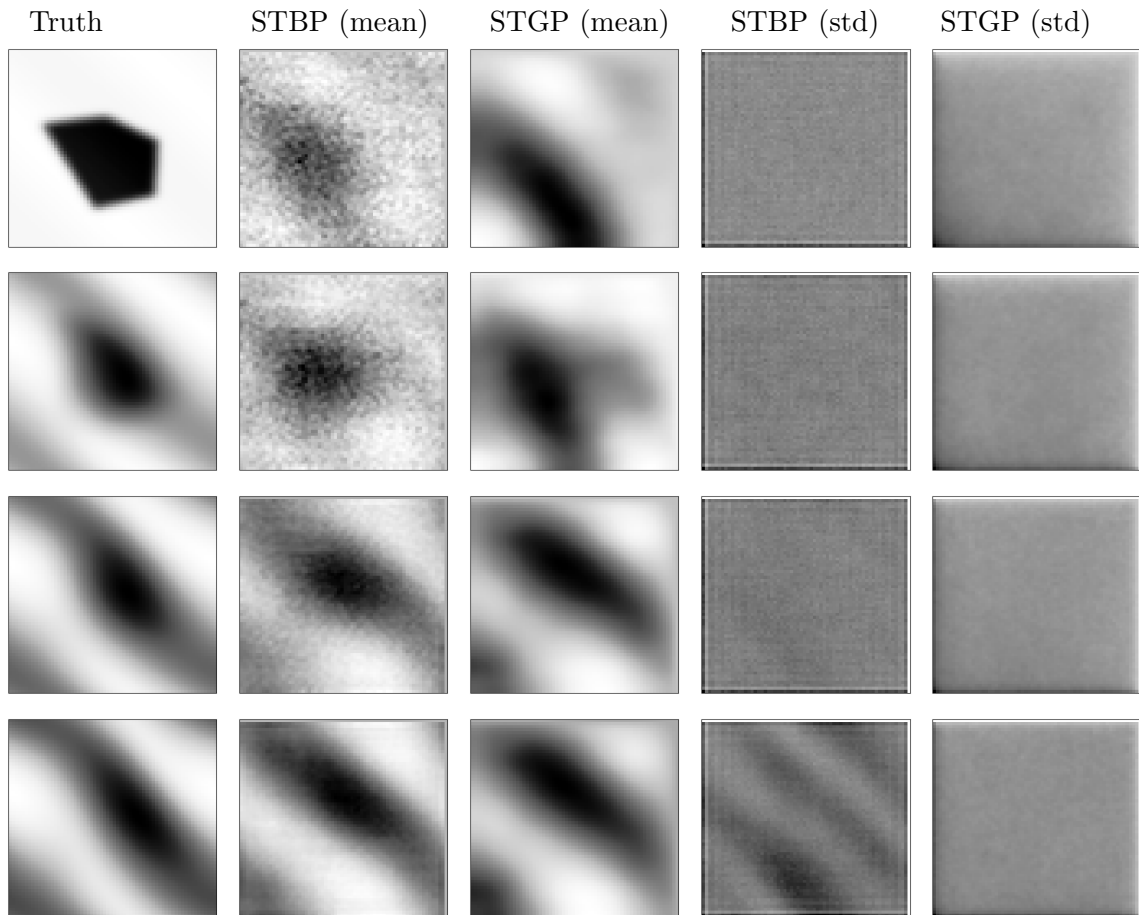


Figure 15: MCMC inverse solutions of Navier-Stokes equation in the whitened space. Columns from left to right: true vorticity, posterior mean estimates by STBP and STGP, posterior standard deviation estimates by STBP and STGP models respectively. Rows from top to bottom: time step  $j = 0, 3, 6, 9$ .